A PHENOMENOLOGICAL THEORY OF MAGNON SIDEBANDS IN THE SPECTRA

OF MAGNETIC INSULATORS
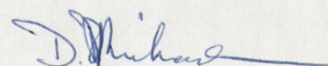
A Thesis submitted to

The Australian National University

for the degree of

Doctor of Philosophy

by

Donald Dalyell Richardson

PREFACE

With the exception of chapter I which is a summary of some concepts involved in the later work, this thesis presents original work carried out by the candidate at the Australian National University. Where it has been appropriate to relate the candidate's work to that of others, proper acknowledgement has been made in the form of specific references.

D.D. Richardson

ACKNOWLEDGEMENTS

ABSTRACT

The work of this thesis presents a simple phenomenological model for calculating properties of magnetic insulators when an exciton-magnon interaction is involved. The advantage of the model is its simplicity while still being able to explain the essential features of observations of the phenomena studied. The model is solved exactly and therefore allows precise physical interpretation of the results.

In chapter I we present a discussion of the forms of the Hamiltonians necessary for the calculation, and discuss the effect of a substitutional spin impurity on the form of the crystal Hamiltonian and therefore on the crystal spectrum. We present a discussion of the means of calculating the optical absorption of a crystal using Green function methods.

Model calculations of magnon sideband lineshapes in pure ferromagnetic and antiferromagnetic insulators are presented in chapter II. The main features of the results are discussed with respect to specific examples of face centred cubic ferromagnetic crystals such as EuO and perovskite anti-ferromagnetic crystals such as $RbMnF_3$. For a wavenumber-independent exciton-magnon interaction strength g it is found that the magnon sideband lineshape is closely approximated by the shape of the corresponding magnon density of states, the sideband being situated on the high-energy side of the parent exciton frequency and of width given by the maximum value of the magnon energy.

The effect of substitutional spin impurities on the magnon sideband have been studied in chapter III using a Koster-Slater type model. Calculations have been given for both ferromagnetic and antiferromagnetic crystals with the changes in the spectrum of the pure crystal examples discussed in chapter II given in some detail. It is found for certain values of an impurity parameter γ that local modes may occur outside the

pure crystal absorption band separated by an amount dependent on the absolute magnitude of γ. For all positive values of γ it is found that a local mode will occur on the high-energy side of the band for both the *fcc* and perovskite crystals studied. When γ is negative there may occur local modes on the low energy side of the band, for certain values of γ.

The possibility of the occurrence of resonance modes within the band has been considered for certain values of γ for which there will be no local modes. It is found that for both the *fcc* and perovskite examples used that the criteria for resonance modes to appear are not all satisfied and it is therefore expected that these will not be observable.

In the appendices we present discussions of the forms of exciton-magnon and perturbation Hamiltonians that have been used in the model; a discussion of how the calculation may be done exactly for a more realistic form of the impurity part of the Hamiltonian; a description of the methods used to perform the numerical calculations which were done using a Monte-Carlo method and also with the help of a Fourier series expansion, and a discussion of some aspects of the model calculation when the crystal has an infinite number of ions in its lattice. It is shown that the form of the results obtained for a finite crystal still applies. An indication of how the model may be solved exactly for the case where the exciton has some dispersion, and the exciton-magnon interaction strength has some k-dependence, is given also.

PUBLICATIONS

The following publication by the candidate is relevant to the work of this thesis:

"Phenomenological Theory of Magnon Sideband Shapes in a Ferromagnet with Impurities", Aust. J. Phys. **27**, 457-470 (1974).

Other publications written wholly or in part, by the candidate are:

Mahanty, J. and Richardson, D.D., "Dispersion contribution to the Binding Energy of a Molecular Crystal", J. Phys. C **8**, 1322-1331 (1975);

Mahanty, J. and Richardson, D.D., "Thermodynamic Properties of a Hindered Rotator", Chem. Phys. Lett. **34**, 307-308 (1975);

Richardson, D.D., "Dispersion Contribution to Two-Atom Interaction Energy: Multipole Interactions", J. Phys. A (in press).

TABLE OF CONTENTS

ERRATA

p.60   eqns. III.19 to III.22

            x should be replaced by X everywhere
            y should be replaced by Y everywhere

p.122   reference to Callaway 1963 should read

            Callaway, J., 1963, Phys.Rev. 132, 2003-2009

p.125   reference to Richards and Brya should read

            Richards, P.M. and Brya, W.J., 1974
              Phys.Rev. B9, 3044-3052

INTRODUCTION

This thesis presents an approach to the calculation of magnon sidebands in magnetic insulators. The method used in the model is basically one of matrix manipulation and the success of the method lies in being able to use a phenomenological model Hamiltonian of the system which is exactly solvable and which describes the essential features of the magnon sidebands observed in the crystal spectra or expected to be observed on physical grounds.

One useful property of the phenomenological Hamiltonian selected is that it allows inclusion of the effect of substitutional spin impurities on the magnon sideband. As expected from the general theory of impurity effects (Callaway 1974; Elliott, Krumhansl and Leath 1974) the inclusion of an impurity may lead to the appearance of "resonances" which modify the crystal density of states, and may also cause the appearance of local modes outside the sideband.

Magnon sidebands are the result of an exciton-magnon interaction in the magnetic crystal. They are characterised by the following properties: (refer also to Sell 1968, McClure 1968)

(1) They almost always occur on the high-energy side of the parent excition line, though "hot bands" are sometimes found on the low energy side. The separation between the parent exciton and the high-energy cut-off of the magnon sideband is typically very close to the maximum magnon band energy.

(2) They are usually of different dipole character to the parent line, e.g. in antiferromagnetic $RbMnF_3$ the ${}^6A_1 \rightarrow {}^4T_1({}^4G)$ exciton line is a weak magnetic dipole transition while the sideband is much stronger and considered to be electric dipole in character (Imbusch and Guggenheim 1968).

The majority of sidebands so far observed are electric dipole with magnetic dipole parent excitons, but magnetic dipole sidebands have been observed, for example, in antiferromagnetic FeF_2 . The character of the transition is determined from the polarisation of the transition and its behaviour in applied magnetic fields.

(3) Sell, Greene and White (1967) have discussed the temperature dependence of spin wave energies and conclude that the dependence is similar to that of sublattice magnetisation $M(T)/M(0)$, so increasing temperature will cause the magnon energy to decrease. Such behaviour should be and is reflected in the temperature dependence of the magnon sideband since the exciton frequency is highly insensitive to temperature.

(4) Since magnons are usually insensitive to stress applied to the crystal, the magnon sideband follows the same behaviour under stress on the crystal as the parent exciton, for stress applied along the direction of crystal magnetisation. For stress along other axes in the crystal, the effect is more complicated since the magnetic ions will be affected due to their different symmetries, especially for an antiferromagnet where the sublattices have different orientations. Dietz, Misetich and Guggenheim (1966), for example, use uniaxial stress along the direction of magnetisation [001] in antiferromagnetic MnF_2 to decide which excitons are the parents of the observed magnon sidebands, but find that the excitons and sidebands split and behave differently to each other in the [110] direction where one sublattice is affected along the x-direction and the other along the y-direction, which are inequivalent for the magnetic ion. Uniaxial stress along the direction of magnetisation may thus be used to determine the parent exciton of a magnon sideband.

(5) Sidebands are typically as broad as the pure magnon transition from which they are derived. That is, the magnon transition has a range of approximately $\epsilon_0 = \epsilon(k)_{max}$, the maximum value of the magnon energy within

the first Brillouin zone which also closely reproduces the range of the magnon sideband. Hence in most cases the effect of the exciton dispersion (which is small) on the sideband is negligible.

(6) Almost all magnon sidebands observed have been found in anti-ferromagnetic insulators. Only two cases of their existence in ferromagnets have been reported (Hulin, Benoit à la Guillaume and Hanus 1971 and Meltzer 1972). This may be merely a result of the rarity of ferromagnetic insulators, though Moriya (1968) states that large nonuniaxial anisotropy energy compared with the exchange energy may be necessary for their observation.

The thesis is organised as follows: in chapter I we discuss various theoretical and phenomenological aspects of magnon sidebands and the Hamiltonians required for their calculation. We include discussion of the effects of a low concentration of substitutional spin impurities on the calculation of magnon sidebands. Chapter II presents sideband calculations for pure crystalline ferro- and antiferromagnetic insulators with examples of sidebands in ferromagnetic EuO and antiferromagnetic $RbMnF_3$ discussed from the viewpoint of the model calculations. In chapter III the calculations are extended to include substitutional spin impurities. Examples of a hypothetical one-dimensional ferromagnet and also EuO and $RbMnF_3$ are discussed with emphasis on the effect of an impurity.

CHAPTER I

I.1 Interacting Excitations in a Crystal: Exciton-Magnon Interaction

There are two basic kinds of interactions between excitations in a crystal. The first is when one type of excitation is scattered due to interaction with another, as it propagates through the crystal. Such interaction is independent of any external field for its existence, though it may effectively be temperature dependent. The other type of interaction arises from the interaction of an applied field with the excitations in the crystal. In such an interaction there may be induced coupling between many types of excitations.

The former type of interaction between excitations will cause a change in the spectrum of the crystal Hamiltonian independent of any applied field. It has been common practice until recently to ignore the change in the crystal Hamiltonian due to an intrinsic exciton-magnon interaction and treat only excitons and magnons interacting together with an applied radiation field as it perturbs the crystal. Eremenko, Novikov and Petrov (1974), however, have obtained an expression for the intrinsic exciton-magnon interaction, as previously used by Parkinson and Loudon (1968) and Moriya and Inoue (1968), who concluded that the intrinsic interaction may have a significant effect on the sideband lineshape.

In the present work we choose a phenomenological intrinsic exciton-magnon interaction Hamiltonian. This allows the crystal Hamiltonian to be diagonalised exactly, and gives exact expressions for the shape and position of magnon sidebands. The problem is thus reduced to what extent our assumed Hamiltonian describes a real crystal. Justification of the form chosen for the Hamiltonian depends on the faithfulness of the result.

The calculations of Parkinson and Loudon (1968), Moriya and Inoue (1968) and Eremenko and others (1974) are rather involved because of the complexity

of their Hamiltonians, and it is necessary to introduce certain approximations during the course of their calculations to make them tractable. These approximations cause some difficulty in physical interpretation of their effect on the final result. The fact that the present model calculation may be done exactly therefore represents some advantage over these theories, and as will be demonstrated, gives a reasonably faithful description of the observed data.

Eremenko, Novikov and Petrov (1974) (see also Petrov 1971) obtain the following exciton-magnon Hamiltonian for an antiferromagnet with two sublattices represented by $\mu = 1, 2$, N ions per sublattice,

$$H_{ex-mag} = \frac{1}{N} \sum_{k_1 \cdots k_4} \sum_{\mu_1 \cdots \mu_4} V \begin{pmatrix} k_1\mu_1 & | & k_3\mu_3 \\ k_2\mu_2 & | & k_4\mu_4 \end{pmatrix} B^+_{\mu_1}(k_1, f) B_{\mu_2}(k_2, f)$$
$$\cdot \, b^+_{\mu_3}(k_3) b_{\mu_4}(k_4) \qquad \text{I.1}$$

where V represents the magnitude of the interaction (the values of V are given by the authors), the sums over $k_1 \ldots k_4$ are over the first Brillouin zone corresponding to the lattice whose unit cell has an ion from both sublattices, and $B^+_\mu(k, f)$ is the creation operator of an exciton in the fth optical state with wavenumber k, on the μth branch, and $b^+_\mu(k)$ is the creation operator of a magnon with wavenumber k in the μth branch. (Note that if there are two sublattices, there will in general be two branches of excitons and magnons.) A Hamiltonian with interaction term like I.1 cannot be diagonalised exactly, and the most commonly used approximation is to "decouple" the desired Green function obtained from the Hamiltonian in some way.

The form of exciton-magnon interaction given by eqn. I.1 is the only form given in the literature for the interaction apart from one given by Dietz and Misetich (1968) to describe the effect of coupling between excitons and magnons as the result of localisation of states around

substitutional impurities. These authors present an exciton-magnon
Hamiltonian of the form

$$H_{\text{ex-mag}} = \sum_{i,j} c_{ij} \left(A_i^+ b_j^+ + A_i b_j \right) \qquad \text{I.1a}$$

for an antiferromagnetic crystal. On Fourier transforming this equation and
making the appropriate Bogoliubov transformation (section I.2) we obtain a
form very similar to that chosen for the present work for the antiferro-
magnetic case. The ferromagnetic crystal Hamiltonian is related to this by
using an equivalent form for the combination of exciton and magnon operators.

The following phenomenological forms for the ferro- and antiferro-
magnetic crystal exciton-magnon interaction are taken in the present work:

$$H_{\text{ex-mag}}^{(F)} = g \sum_k \left(a_k^+ b_k + a_k b_k^+ \right) \qquad \text{I.2}$$

$$H_{\text{ex-mag}}^{(AF)} = g \sum_k \left(\alpha_k^+ A_k + A_k^+ \alpha_k + \beta_k^+ B_k + B_k^+ \beta_k \right) , \qquad \text{I.3}$$

where in I.2, a_k^+, b_k^+ are the creation operators of a magnon and exciton
respectively of wavenumber k and in I.3, α_k^+, A_k^+ and β_k^+, B_k^+ are **obtained
from**
∧ creation operators of magnons and excitons on sublattices A and B
respectively. We take the interaction g as independent of wavenumber.
The sums over k are over the first Brillouin zone, and for I.3 taken as
for eqn. I.1 for a Brillouin zone with a unit cell having an ion from each
sublattice. We have assumed further that there is only a single orbital
excited state involved, and drop the excited state notation (f) from I.2
and I.3. In appendix 1 we relate eqn. I.3 to eqn. I.1.

As pointed out earlier, the usefulness of the forms eqns. I.2 and I.3
would be in their ability to give an adequate description of a real crystal.
This point will be discussed further in chapters II and III where we compare
the present model calculation with observations on a real crystal.

The form of the perturbation of the crystal by an external electro-
magnetic field has been discussed in the literature more widely. Two

different mechanisms were presented for describing the perturbation coupling an external field with both excitons and magnons (Sugano and Tanabe 1963, Tanabe, Moriya and Sugano 1965 and Halley and Silvera 1965). Though the two mechanisms are quite different in the magnitude of the interaction, the functional form of the two Hamiltonians is similar. Both mechanisms involve two-ion interaction, Tanabe, Moriya and Sugano (1965) proposing an exchange interaction resulting from overlap of the neighbouring ion wavefunctions, while Halley and Silvera (1965) and Halley (1966) ascribe the interaction to a spin-orbit induced electric quadrupole moment on one atom interacting with an electric dipole moment, created by interaction with the radiation field, on a neighbour. Allen, Loudon and Richards (1966) have pointed out that both two-ion interactions are cases of a general theory of Dexter (1962) describing electric-dipole induced two-ion transitions in a solid. We will present a discussion of the two electric field induced exciton-magnon transitions in more detail.

We will firstly describe the exchange mechanism proposed by Sugano and Tanabe (1963) and elaborated on by Tanabe, Moriya and Sugano (1965). Moriya (1968, 1970) and McClure (1968) have given good reviews of the interaction. The exchange mechanism has also been used to describe the magnon-magnon interaction leading to two-magnon and n-magnon absorption $(n > 2)$ (Moriya and Inoue 1968).

McClure (1968) has depicted the exchange interaction between ions as shown in fig. I.1. The crystal is a two-sublattice antiferromagnet with sublattice A having spin up and sublattice B spin down. The spin projection of the pair is conserved in the interaction and there is an intermediate state of odd parity on one ion $\left(B^{u}$ in fig. I.1$\right)$. In the figure, the ion on sublattice A exchanges an electron with a neighbouring ion on sublattice B, the electron from the ground state B^{o} moving to state A' and that from A^{o} going to the intermediate state B^{u} where it then undergoes an electric dipole transition to its final state B^{g}.
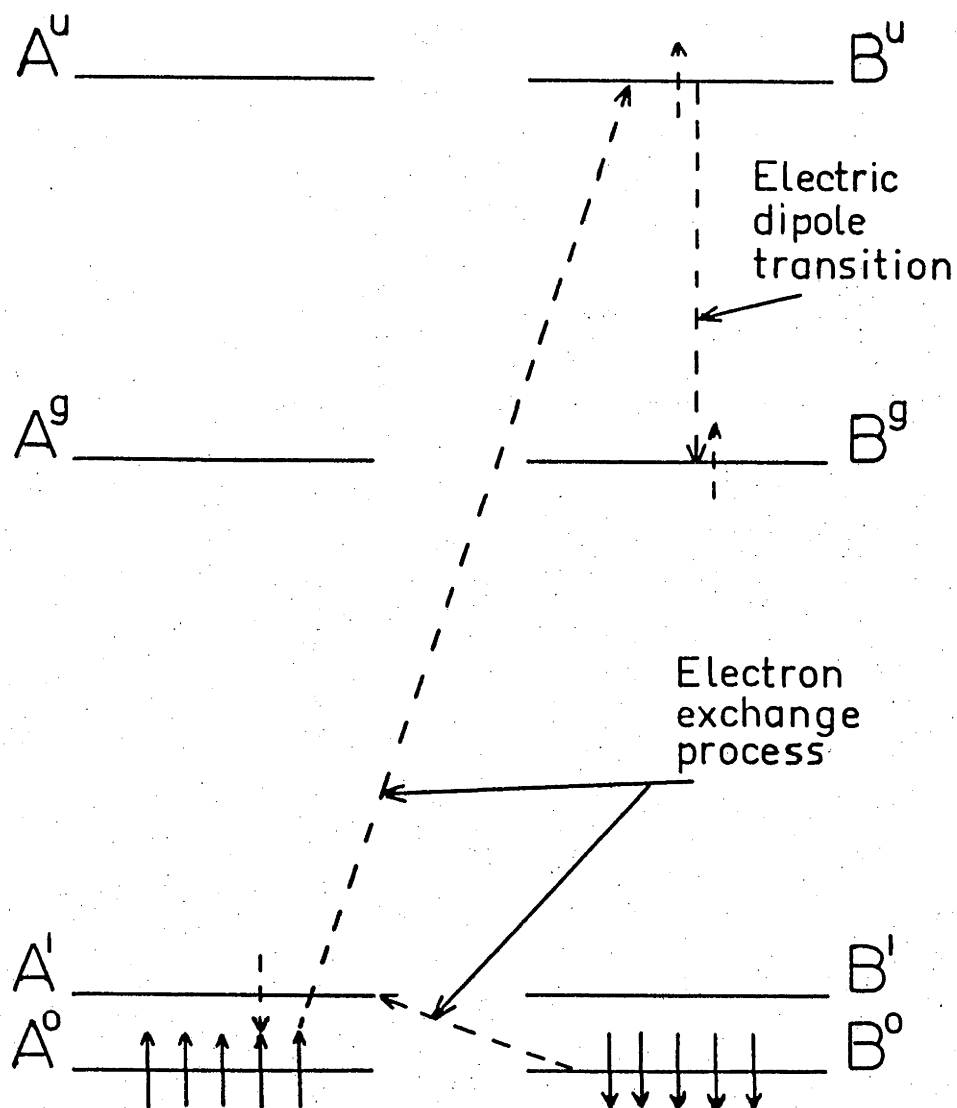
FIGURE I.1. Illustration of the two-ion exchange interaction induced by an external electric field (after McClure 1968).

The transition moment in the crystal as a result of the interaction shown in fig. I.1 is (McClure 1968)

$$M = \sum_{\delta} e^{i k \cdot \delta} P_{\delta}$$
I.4

where δ are the locations of the nearest neighbour ions and P_{δ} is the effective electric dipole moment due to the exchange interaction (Tanabe, Moriya and Sugano 1965). Summing over all wavenumbers in the first Brillouin zone, we obtain the sideband lineshape in the form

$$\alpha_{p}(\omega) = \text{const.} \sum_{k} |M_{p}(k)|^2 \delta\left(\omega - \omega_{k}^{e} - \omega_{k}^{m}\right)$$
I.5

for a polarisation p. In eqn. I.5, ω is the frequency of the line, ω_{k}^{e} and ω_{k}^{m} represent the dispersion frequencies of the exciton and magnon, respectively.

Eqn. I.5 for the sideband lineshape ignores any intrinsic exciton-magnon interaction as discussed earlier in this section.

Petrov and Gaididei (1971) and Eremenko, Novikov and Petrov (1974) have given a derivation of the form of the crystal-radiation field Hamiltonian in second quantised form. The result is

$$H_{\text{cry-field}} = E\, P_{\text{eff}}\, e^{-i \omega t} + \text{Herm.conj.}$$
I.6

where

$$P_{\text{eff}} = \sqrt{2} \sum_{k, \mu} \Pi(k)(-)^{\mu+1} u_{\mu}(k) B_{\mu}^{+}(k, f) b_{\mu}^{+}(-k) .$$
I.7

$B_{\mu}^{+}(k, f)$ and $b_{\mu}^{+}(-k)$ are the creation operators for excitons and magnons of wavenumber k, the exciton being in excited state f. The sublattice is represented by $\mu = 1, 2$ (as in eqn. I.1). $\Pi(k)$ may be determined from the symmetry of the ion site and is related to the dipolar moment of the transition in the pair of magnetic ions from opposite sublattices (Eremenko, Novikov and Petrov 1974). Values for the coefficient have been given for several crystals (Meltzer, Lowe and McClure 1969,

Parkinson and Loudon 1968, Tanabe, Moriya and Sugano 1965, Gondiara and

Tanabe 1966, Loudon 1968). The functions $u_\mu(k)$ are the coefficients of

the Bogoliubov transformation (e.g. Kittel 1963) and correspond to the

functions $l_1(k)$ and $l_2(k)$ of eqns. I.25. They are used to diagonalise

the antiferromagnetic magnon Hamiltonian.

The other proposed mechanism for interaction of the crystal with the

radiation field was first put forward by Halley and Silvera (1965). It

involves a direct interaction between neighbouring ions via a dipole-

quadrupole interaction (Halley 1966). The interaction is illustrated

schematically in fig. I.2. An ion on one sublattice is excited through an

electric dipole transition while a neighbouring ion $(j+\delta)$ has a magnon

localised on it so that the spin on the ion precesses. Such spins then

interact with the ionic charge cloud via the spin-orbit coupling term

$(\lambda L.S)$ to create a quadrupole moment on the ion. The inter-ion interaction

is then that between the quadrupole (Q) on ion $j + \delta$ with the dipole

(T) on ion j . This leads to a coupling between odd and even states 0

and e' which leads to the exciton-magnon interaction. The resultant

Hamiltonian has a form very similar to that of eqn. I.6 for the exchange

interaction.

It has been pointed out by several authors (e.g. Tanabe, Moriya and

Sugano 1965, Allen, Loudon and Richards 1966, Moriya 1968) that the direct

interaction may be very weak compared to the exchange interaction, and for

certain site symmetries of the ions, may actually be identically zero. In

systems where the exchange interaction is weak, however, the direct inter-

action may be important, e.g. in CoF_2 (Moriya 1968).

For the present phenomenological model, it is sufficient to choose a

suitable form for the interaction between the crystal and radiation. Since

the dependence of both the direct and exchange interaction Hamiltonians on

the creation and annihilation operators is identical we will use a Hamiltonian
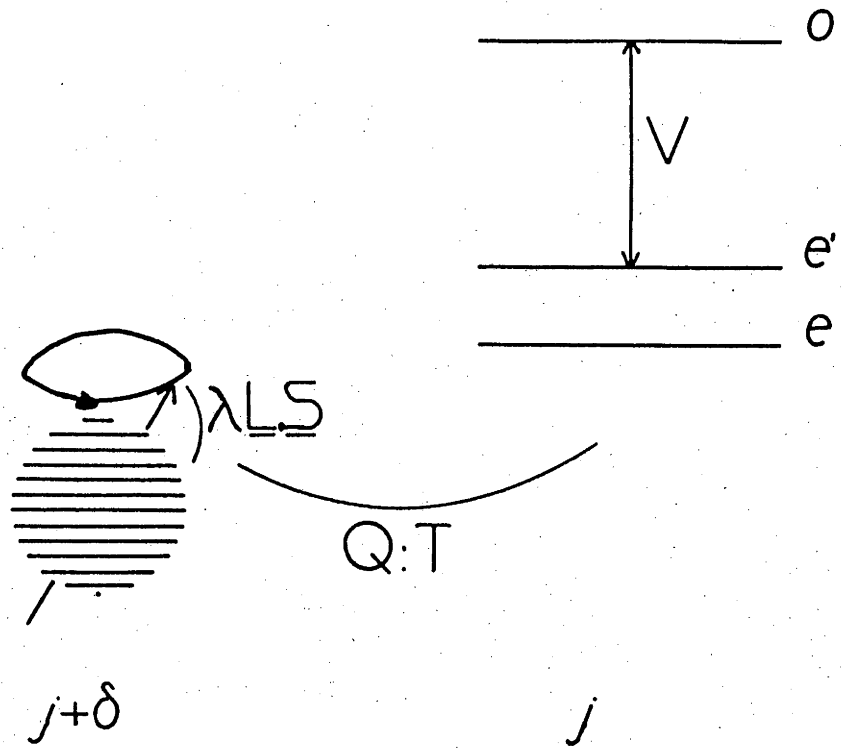
FIGURE I.2.   Illustration of the direct interaction between ions in a

radiation field (after Halley 1966).   States labelled 0

and *e*, *e'* have odd and even parity respectively.

of that form. The Hamiltonians for the ferro- and antiferromagnetic crystals are taken respectively as follows:

$$H_{pert}^{(F)} = l \sum_k \left(a_k^+ b_k^+ + a_k b_k\right) ,$$ I.8

$$H_{pert}^{(AF)} = l \sum_k \left(\alpha_k^+ A_k^+ + \alpha_k A_k + \beta_k^+ B_k^+ + \beta_k B_k\right)$$ I.9

where the symbols are explained after eqn. (I.3). We choose for convenience that the interaction energy l is independent of wavenumber but time dependent, including the time dependence of the applied field. The Hamiltonians I.8 and I.9 are treated as perturbations on the full crystal Hamiltonian (Chapter II). It is shown in appendix 1 that eqn. I.8, for example, may also be justified from time-dependent perturbation and consideration of the matrix elements involved.

Halley (1967) has considered a third mechanism for interaction of the crystal with an applied field. The process involves the interaction of a photon with a (virtual) phonon which in turn interacts with an exciton (or magnon) via exchange striction and dipole-dipole interactions. The interaction has not, however, been popular in explaining the absorption sideband.

I.2 The Ideal Crystal Hamiltonian

Apart from the exciton-magnon interaction term considered in section I.1, the crystal Hamiltonian must include terms representing the creation and annihilation of both excitons and magnons individually. In the present section we shall discuss each of these terms.

We begin with a discussion of excitons in the crystal. Good reviews of exciton theory are given by Knox (1963), Callaway (1974). Experiments on crystals exhibiting magnon sidebands reveal that the exciton and magnon involved are both strongly localised on particular adjacent ion sites (McClure 1968). We may thus consider the excitons in the crystal to be well

represented as Frenkel excitons (Heller and Marcus 1951).

The forms of the exciton Hamiltonians we have chosen for the present work are as follows

$$H_{ex}^{(F)} = \varepsilon_2 \sum_k b_k^+ b_k ,$$

$$H_{ex}^{(AF)} = \varepsilon_2 \sum_k A_k^+ A_k + B_k^+ B_k$$

where b_k^+, b_k are the creation and annihilation operators of excitons in a ferromagnetic crystal and A_k^+, A_k and B_k^+, B_k are creation and annihilation operators of excitons on sublattices A and B of an anti-ferromagnetic crystal. The exciton energy ε_2 (*not* necessarily the same for ferro- as for antiferromagnetic crystals) is taken to be independent of wavenumber k in both cases, i.e. the excitons are assumed to have no dispersion. This assumption is generally valid (Parkinson 1969b) compared to the dispersion of other quantities (e.g. magnons)*, though there are exceptions, where exciton dispersion may be quite large (McClure 1968). The sum over wavenumber k in I.10 and I.11 is over the first Brillouin zone, which, for the antiferromagnet, has a unit cell with one atom from each sublattice. This means that for the simple Hamiltonian I.11 the exciton line is doubly degenerate, i.e. there is no Davydov splitting of the exciton (Eremenko and Belyaeva 1969, Loudon 1968).

Frenkel excitons are commonly observed to have both electric dipole and magnetic dipole orbital transitions of individual crystal ions associated with them. Magnetic dipole transitions are generally much weaker than electric dipole ones, because of the factor $\left(\dfrac{v}{c}\right)^2$ in the interaction, where v is the orbital velocity of the electron making the transition, c the

---

* The splitting is roughly $(a/d)^2$ where a = Bohr radius, d is separation between ions. Since $d \gtrsim 10a$ the splitting will be $\sim 10^{-2}$ of the transition energy.

speed of light (Sobel'man 1972). This factor is typically of order 10^{-5}.
Hence even parity magnetic dipole (forbidden) transitions are much reduced
in intensity over electric dipole odd parity (allowed) transitions. Apart
from the magnitude and dispersion of the exciton, however, the excitons may
be described by a Hamiltonian of identical form for both electric and
magnetic dipole transitions. Thus our choice of eqns. I.10 and I.11 for
exciton Hamiltonians would apply to both electric and magnetic dipole
transitions, the latter being much reduced in intensity over the former.
The dipole nature of the exciton in a phenomenological model such as the
present case will be determined from the interaction between excitons and
the radiation field. We will treat the case of magnetic dipole excitons and
hence ignore any interactions with an applied electric field. It would be
possible to treat the absorption of the exciton separately by inclusion of
the magnetic field component of the radiation, which, as just mentioned,
would give a weak exciton line at the energy ϵ_2.

We also ignore in our model any crystal field effects on further
splitting of the exciton line. Tanabe and Gondiara (1967) have presented a
detailed discussion of such effects in relation to the magnon-sideband
problem. Our model may be considered as treating a single polarisation
direction in the crystal (see section I.4). As illustrated by the absorption
eqn. I.5, the problem may be decomposed into a separate treatment of
polarisation directions in a quite general manner.

We now turn to the magnon part of the Hamiltonian and will present a
detailed calculation of the ferromagnetic crystal Hamiltonian we have used
in our model.

We begin with the assumption that the magnetic system is adequately
described by a Heisenberg Hamiltonian with only nearest neighbour interactions.
That is, we assume that the exchange integral J is short range, and also
that its value is independent of the position of the interacting ions

in the crystal.   The Hamiltonian is then written

$$H_M = J \sum_{[n]} \sum_{[\Delta]} S_n \cdot S_{n+\Delta} \qquad\qquad \text{I.12}$$

where S_n is the spin of the nth ion in the crystal and the sum over n

is over all magnetic ion sites in the crystal.   The sum over Δ is over all

nearest neighbours of the site n , $S_{n+\Delta}$ being the spins of the nearest

neighbours.   Eqn. I.12 applies equally well to antiferromagnets and ferro-

magnets, with $J > 0$ in the former case, and $J < 0$ in the latter.   For

the present ferromagnetic calculation we rewrite J as $-|J|$.

Consider the Hamiltonian I.12 written in terms of spin raising and

lowering operators $S_n^{(\pm)} = S_n^{(x)} \pm i S_n^{(y)}$ which satisfy the commutation rules

$$\left[S_n^{(+)}, S_{n'}^{(-)} \right] = 2S_n^{(z)} \Delta(n,\, n') \, ,$$

$$\left[S_n^{(z)}, S_{n'}^{(\pm)} \right] = \pm S_n^{(\pm)} \Delta(n,\, n') \qquad\qquad \text{I.13}$$

where $S_n^{(x)}$, $S_n^{(y)}$ and $S_n^{(z)}$ are the $x,$ y and z components of S_n and

$\Delta(n,\, n')$ is the Kronecker delta function which is unity when $n = n'$ and

zero otherwise.

Then eqn. I.12 for the magnon Hamiltonian becomes

$$H_M^{(F)} = -|J| \sum_n \sum_\Delta \left[\tfrac{1}{2}\left(S_{n+\Delta}^{(-)}S_n^{(+)} + S_n^{(-)} S_{n+\Delta}^{(+)} \right) + S_{n+\Delta}^{(z)}S_n^{(z)} \right] \, . \qquad \text{I.14}$$

We now assume that the temperature of the system is sufficiently low

that only a unit spin deviation from the ground state is possible at any

site, and define a single unit spin deviation state at site l as

$$|l\rangle = \frac{1}{\sqrt{2S}} S_l^{(-)} |0\rangle \qquad\qquad \text{I.15}$$

where the ground state is $|0\rangle = |\downarrow\downarrow \ldots \downarrow\rangle$, the state in which all spins

are pointing down.   We also assume that any eigenfunction for the entire

crystal is separable into a product of single-ion site wavefunctions such as

eqn. I.15, i.e. we assume Heitler-London wavefunctions.

We now consider a "magnon" wavefunction as the space Fourier transform of wavefunctions eqn. I.15,

$$\Psi_k = \sum_{[l]} e^{ik.l} |l\rangle$$

$$= \sum_{[l]} e^{ik.l} \frac{S_l^{(-)}}{\sqrt{2S_l}} |0\rangle$$

$$= a_k |0\rangle \qquad \text{I.16}$$

where l is a crystal lattice vector, and a_k a magnon annihilation operator, defined by eqn. I.16.

The Hamiltonian in second quantised form is then given as follows (Landau and Lifshitz 1958)

$$H_M^{(F)} = \frac{1}{N} \sum_{kk'} \sum_{[l],[l']} a_k^+ a_{k'} e^{-ik.l} \langle l|H_M^{(F)}|l'\rangle e^{ik'.l'} . \qquad \text{I.17}$$

Using the wavefunctions I.15, we obtain after some algebra

$$H_M^{(F)} = \sum_k \varepsilon(k) a_k^+ a_k - |J|NS^2 z \qquad \text{I.18}$$

where the magnon dispersion $\varepsilon(k)$ is given by

$$\varepsilon(k) = \sum_{l-l'} \langle l|H_M^{(F)}|l'\rangle e^{ik.(l-l')}$$

$$= 2|J|Sz(1-\gamma_k) \qquad \text{I.19}$$

for

$$\gamma_k = \frac{1}{z} \sum_{[\Delta]} e^{ik.\Delta} \qquad \text{I.20}$$

where z is the number of nearest neighbours of any ion (co-ordination number). Note that $\gamma_k = \gamma_{-k}$ for crystals with orthogonal primitive lattice vectors.

In this and what follows we always assume cyclic (Born-Von Kármán 1912) boundary conditions so that $|l\rangle = |l+Na\rangle$ for N atoms in the crystal, and lattice parameter a . The sum in I.19 over $l - l'$ results from the fact

that $H_M^{(F)}$ in the lattice-space representation is circulant (cyclic) and

has eigenvalues given by $\sum_{[l]} H_l\, e^{ik.l}$ where $H_{l-l'} = \langle l|H|l'\rangle$ and

eigenvectors with components of the form $u_k(l) = N^{-\frac{1}{2}}e^{ik.l}$ (Berlin and Kac

1952). Use has been made of the relations

$$\langle 0|S_l^{(+)}S_{n+\Delta}^{(-)}|0\rangle = \Delta(l,\ n+\Delta)\ ,$$

$$S_n^{(z)}|l\rangle = \big(-S+\Delta(n,\ l)\big)|l\rangle\ ,$$

$$S_l^{(+)}, S_n^{(-)}|0\rangle = 2S_n^z\Delta(n,\ l')|0\rangle$$

where $\Delta(n,\ l)$ is a Kronecker delta function.

The magnon Hamiltonian I.18 may also be obtained by means of the

Holstein-Primakoff approximation, writing

$$S_n^{(+)} = \sqrt{2S_n}\ f_n a_n\ ,$$

$$S_n^{(-)} = \sqrt{2S_n}\ f_n a_n^+\ ,$$

$$S_n^{(z)} = -S + a_n^+ a_n\ ,$$

where one assumes $f_n = \left[1 - \dfrac{a_n^+ a_n}{2S}\right]^{\frac{1}{2}} \approx 1$, ignoring terms with products of

more than two operators. Keffer (1966) in a review article on spin waves

has discussed the implications of the Holstein-Primakoff approximation in

detail. The magnon creation and annihilation operators are obtained as the

space Fourier transforms

$$a_k^+ = \frac{1}{\sqrt{N}} \sum_{[n]} e^{+ik.n} a_n^+\ ,$$

$$a_k = \frac{1}{\sqrt{N}} \sum_{[n]} e^{-ik.n} a_n\ . \hspace{3cm} \text{I.21}$$

The magnon operators a_k^+ and a_k can be shown to satisfy the boson

commutation rules

$$[a_k, a_{k'}^+] = \delta(k, k') ,$$

$$[a_k, a_{k'}] = [a_k^+, a_{k'}^+] = 0 \qquad\qquad \text{I.22}$$

where $\delta(k, k')$ is the Dirac delta function.

The term $-|J|NS^2 z$ occurring in eqn. I.18 is the exchange energy when all spins are aligned (Keffer 1966). Its effect is to determine the spin Hamiltonian ground state and, because it is a constant, will be ignored in the present calculation as it will merely cause a shift of the entire spectrum, without altering its other properties.

In a similar manner to the above ferromagnetic magnon calculation, it is possible to obtain the antiferromagnetic magnon Hamiltonian as

$$H_M^{(AF)} = 2JSz \sum_k \gamma_k \left(a_k^+ b_k^+ + a_k b_k\right) + 2JSz \sum_k \left(a_k^+ a_k + b_k^+ b_k\right) - 2zJN_0 S^2 \qquad \text{I.23}$$

where a_k^+, b_k^+ are creation operators for magnons localised on sublattices A and B, N_0 is the number of atoms on each sublattice and γ_k is given by eqn. I.20.

The Hamiltonian I.23 is not yet diagonal and may be diagonalised by a canonical Bogoliubov transformation (Kittel 1963)

$$a_k^+ = l_1 \alpha_k^+ + l_2 \beta_k ,$$

$$b_k^+ = l_2 \alpha_k + l_1 \beta_k^+ \qquad\qquad \text{I.24}$$

where

$$l_1 = \left[\frac{1 - \left(1 - \gamma_k^2\right)^{\frac{1}{2}}}{2\left(1 - \gamma_k^2\right)^{\frac{1}{2}}}\right]^{\frac{1}{2}} ,$$

$$l_2 = -\left[\frac{1 + \left(1 - \gamma_k^2\right)^{\frac{1}{2}}}{2\left(1 - \gamma_k^2\right)^{\frac{1}{2}}}\right]^{\frac{1}{2}}$$

$$l_1^2 - l_2^2 = 1 ; \quad 2l_1 l_2 = \frac{-\gamma_k}{2\left(1 - \gamma_k^2\right)^{\frac{1}{2}}} ;$$

$$l_1^2 + l_2^2 = \left(1-\gamma_k^2\right)^{-\frac{1}{2}} . \qquad \text{I.25}$$

The antiferromagnetic magnon Hamiltonian in diagonal form, is then

$$H_M^{(AF)} = \sum_k \epsilon(k)\left(\alpha_k^+\alpha_k + \beta_k^+\beta_k\right) \qquad \text{I.26}$$

where

$$\epsilon(k) = 2JSz\left[1-\gamma_k^2\right]^{\frac{1}{2}} . \qquad \text{I.27}$$

In a review article on spin waves by Keffer (1966) is presented a more general expression for the magnon dispersion than I.27. In our derivation we have neglected anisotropy and external magnetic fields. The effect of an applied magnetic field is to split the two degenerate bands represented by α_k and β_k, with splitting of $2g\mu_B H_0$ for splitting factor g, Bohr magneton μ_B and applied field H_0 (Zeeman effect). The effect of an anisotropy field H_A is the same for both bands and is expressed by replacing $1 - \gamma_k^2$ by $\left(1 + \frac{g\mu_B H_A}{2JSz}\right)^2 - \gamma_k^2$ in I.27. Similar modifications of the ferromagnetic dispersion eqn. I.19 are possible also.

At this point it should be stated that magnon Hamiltonians have been calculated more precisely than the above. A more exact Hamiltonian is of value, for example, when temperature-dependent effects are to be studied. Hone, Callen and Walker (1966) have presented a temperature dependent calculation for a Heisenberg ferromagnet while Ghosh (1973) and Swendsen (1975) have discussed the antiferromagnet problem. These calculations make use of the Green function method (Zubarev 1960, Mahanty 1974, Abrikosov, Gorkov and Dzyaloshinski 1963) and involve decoupling the equation of motion of the crystal Green function at some stage, the method of decoupling affecting the degree of accuracy of the calculation. Shah, Umezawa and Vitiello (1974) have discussed the derivation of the magnon operators which avoids the use of the Holstein-Primakoff approximation. Though their work is

of value in imposing restraints on any model calculation, the method used
does not allow the direct calculation of specific model-dependent quantities.

Another interesting aspect of magnon (spin-wave) calculations is a
determination of the ground state of ferro- and antiferromagnets described
by a Heisenberg Hamiltonian. Bloch (1930) has calculated the ferromagnetic
ground state, but, as discussed by Ghosh (1973), the antiferromagnetic
ground state has still not been calculated, although some special cases have
been given. Mermin and Wagner (1966) have proved that, at finite
temperatures, no ferro- or antiferromagnetic order exists in one- or two-
dimensional crystals which have a finite range exchange integral, and which
are isotropic. The theorem does not apply to absolute zero of temperature.
Glass and Lawson (1973) have shown that dipolar ferromagnetism cannot exist
in a simple cubic array of infinite volume, and Reeh (1973) has discussed
the possible degeneracy of the antiferromagnetic ground state. Swendsen
(1973) has discussed the effects of crystal geometry, for cubic crystals,
on antiferromagnetic order.

In summary, then, including the exciton-magnon interaction terms, eqns.
I.2, I.3, the pure crystal Hamiltonians which we have chosen for our model
calculation of magnon sidebands for ferromagnets and antiferromagnets are
respectively

$$H^{(F)} = \sum_k \varepsilon(k) a_k^+ a_k + \varepsilon_2 \sum_k b_k^+ b_k + g \sum_k \left(a_k^+ b_k + b_k^+ a_k \right) \, , \qquad \text{I.28}$$

$$H^{(AF)} = \sum_k \varepsilon(k) \left(\alpha_k^+ \alpha_k + \beta_k^+ \beta_k \right) + \varepsilon_2 \sum_k \left(A_k^+ A_k + B_k^+ B_k \right)$$

$$+ g \sum_k \left(\alpha_k^+ A_k + A_k^+ \alpha_k + \beta_k^+ B_k + B_k^+ \beta_k \right) \, . \quad \text{I.29}$$

Use will be made of these Hamiltonians in chapter II.

As pointed out, for example, by Parkinson (1969a), the effect of an
exciton-magnon interaction is very similar to that of a substitutional
magnetic impurity in the crystal. As will be shown below, one effect of the

latter is to add a constant term to the magnon energy $\varepsilon(k)$, thus effectively shifting the magnon line. Parkinson and Loudon (1968) have shown that one effect of the exciton-magnon interaction is to add a constant term to the exciton energy, ε_2. In our phenomenological theory, we would thus expect the exciton line to be shifted by an adjustable parameter depending in some manner on the strength g of the exciton-magnon interaction. As shown below or as is evident from the delta function in eqn. I.5, one would also expect a shift in the magnon sideband due to g as a result of the term added to ε_2, though this may be small.

I.3 Substitutional Magnetic Impurity

We now consider how the pure crystal Hamiltonians I.28 and I.29 will be modified by the inclusion of a substitutional defect whose sole difference from the host atoms is a difference in spin and exchange interaction with its neighbours. We assume that the excitons will be unaffected.

An excellent review of defects in solids has been given by Elliott, Krumhansl and Leath (1974), and Cowley and Buyers (1972) have given a review of the effects of impurities on magnetic crystals. We begin by obtaining an expression for one impurity in a ferromagnet, extend the result to an antiferromagnet, and finally discuss the implications of the magnetic impurity as it might affect the crystal spectrum.

The Heisenberg Hamiltonian for a ferromagnet with an impurity at site l, with spin S'_l and exchange integral J' with nearest neighbours is given by (White 1970)

$$H_{M+I}^{(F)} = -|J| \sum_{[n]} \sum_{[\Delta]} S_n \cdot S_{n+\Delta} + 2\left(|J|S_l - |J'|S'_l\right) \cdot \sum_{[\Delta]} S_{l+\Delta} \qquad \text{I.30}$$

We write I.30 in second quantised form using the same methods outlined in section I.2. The result is

$$H_{M+I}^{(F)} = H_M^{(F)} + \frac{1}{N} \sum_{k,k'} \gamma(k, k') a_k^+ a_{k'} - JS^2 z\rho \sum_k a_k^+ a_k \qquad \text{I.31}$$

where $H_M^{(F)}$ is the pure crystal Hamiltonian given by eqn. I.28 and

$$\gamma(k, k') = 2|J|Sz\, e^{i(k'-k).1} \left[\epsilon + \rho\gamma_{k'-k} - \gamma\left(\gamma_{k'} + \gamma_k\right)\right] , \qquad \text{I.32}$$

$$\epsilon = (J'-J)/J ,$$

$$\rho = (J'S'-JS)/JS ,$$

$$\gamma = \frac{J'}{J} \sqrt{\frac{S'}{S}} - 1 . \qquad \text{I.33}$$

γ_k is given by eqn. I.20. Eqns. I.33 conform with the notation of

Lovesey (1968a) and others. The expression for $\gamma(k, k')$, eqn. I.32 has

been obtained previously by Callaway (1963).

For the model used in this work, we assume that we are able to write

$\gamma(k, k')$ as independent of wavenumber, i.e. we put $\gamma(k, k') = \gamma$. Our

problem then reduces to treating the impurity along the lines of the Koster-

Slater model (Callaway 1964, 1974, Wolfram and Callaway 1963). In

appendix 2 we discuss the model calculation using the crystal Hamiltonian

I.31 with the full expression I.32 for $\gamma(k, k')$ and show that the model

calculation is still possible without the assumption on $\gamma(k, k')$, though

mathematically more complicated.

Impurities in a Heisenberg ferromagnet have also been studied by

Takeno (1963a, 1963b) and Ishii, Kanamori and Nakamura (1965). Takeno (1963a,

1963b) has discussed a Koster-Slater type model for an impurity with ferro-

magnetic interaction with its neighbours $(J' < 0)$, as we have assumed

above. He has discussed in detail the nature of the localised spin-waves

which occur in the vicinity of the impurity. Ishii and others (1965) have

treated in depth the case of antiferromagnetic coupling of the impurity with

the host. We need not discuss the details of such work here, but will

present the essential effects of a ferromagnetically coupled impurity towards

the end of the present section.

The antiferromagnetic crystal with impurity has a Hamiltonian corresponding to the ferromagnetic one (eqn. I.30) which is more conveniently written in matrix notation as follows:

$$H_{M+I}^{(AF)} = [\alpha^+ \beta] \begin{bmatrix} \hat{M}_1 & \vdots & \hat{M}_2 \\ \cdots & \vdots & \cdots \\ \hat{M}_3 & \vdots & \hat{M}_4 \end{bmatrix} \begin{bmatrix} \alpha \\ \beta^+ \end{bmatrix}$$

I.34

where

$$\alpha^+ = [\alpha_{k_1}^+, \ldots, \alpha_{k_{N_0}}^+] \ ; \quad \beta^+ = [\beta_{k_1}^+, \ldots, \beta_{k_{N_0}}^+] \ ,$$

$$(M_{1,4})_{ij} = \gamma_{ij}^{(1),(4)} + \left[JS^2 z \rho + \epsilon(k_i) \right] \delta(i, j) \ ,$$

$$(M_{2,3})_{ij} = \gamma_{ij}^{(2),(3)}$$

I.35

and

$$\frac{\gamma_{ij}^{(1)}}{2JSz} = \frac{\gamma^{(1)}(k_i, k_j)}{2JSz} = (l_1(k_i) l_2(k_j) \gamma_{k_j} + l_2(k_i) l_1(k_j) \gamma_{k_i}) \gamma$$

$$+ \epsilon \, l_1(k_i) l_1(k_j) + \rho \gamma_{k_i - k_j} l_2(k_i) l_2(k_j) \ ,$$

$$\frac{\gamma_{ij}^{(2)}}{2JSz} = \frac{\gamma_{ij}^{(3)}}{2JSz} = \frac{\gamma^{(2)}(k_i, k_j)}{2JSz} = (l_1(k_i) l_1(k_j) \gamma_{k_j} + l_2(k_i) l_2(k_j) \gamma_{k_i}) \gamma$$

$$+ \epsilon \, l_2(k_i) l_1(k_j) + \rho \gamma_{k_i - k_j} l_1(k_i) l_2(k_j) \quad \text{I.36}$$

where γ, ϵ and ρ are given by eqns. I.33 and $l_1(k)$, $l_2(k)$ are given by eqns. I.25. $\gamma_{ij}^{(4)}$ is the same as $\gamma_{ij}^{(1)}$ with l_1 replaced by l_2 and vice versa, everywhere. We have considered the impurity to be situated at the origin, and on sublattice A , for convenience.

For the present phenomenological model Hamiltonian we assume that points close to the edge of the Brillouin zone contribute most to the regions where the density of states of the magnon system is large (as is true for cubic crystals, for example). These points of the Brillouin zone correspond to small values of γ_k for the antiferromagnetic dispersion, eqn. I.27. We

also consider that the impurity may lie on either sublattice and so to first

approximation $\gamma_{ij}^{(1)} = \gamma_{ij}^{(4)} = \gamma_{ij}$ where γ_{ij} is the average of $\gamma_{ij}^{(1)}$ of

eqn. I.36 and $\gamma_{ij}^{(4)}$ resulting from the interchange of $l_1(k)$ and $l_2(k)$,

and similarly for $\gamma_{ij}^{(2)} = \gamma_{ji}^{(3)}$ as the average of $\gamma_{ij}^{(2)}$ of eqns. I.36 and

the version with l_1 replaced by l_2 . Then for points in the Brillouin

zone near its boundary, it is readily shown from equations I.25 that

$$l_1^2 \to 0 \ ,$$

$$l_2^2 \to 1 \ ,$$

and hence from equations I.36 it follows that

$$\gamma_{ij} \simeq 2JSz\epsilon = \gamma$$

and

$$\gamma_{ij}^{(2)} = \gamma_{ji}^{(3)} \simeq 0 \ . \qquad\qquad \text{I.36a}$$

We therefore assume that sub-matrices $\hat{M}_2$ and $\hat{M}_3$ of eqn. I.34 may be

ignored, and that sub-matrices $\hat{M}_1$ and $\hat{M}_4$ are identical and independent

of wavenumber k . With these assumptions, the antiferromagnetic magnon

Hamiltonian with spin impurity eqn. I.34, is taken as

$$H_{M+I}^{(AF)} = [\alpha^+ \beta^+] \begin{bmatrix} \hat{M} & \hat{0} \\ \hat{0} & \hat{M} \end{bmatrix} \begin{bmatrix} \alpha \\ \beta \end{bmatrix} \qquad\qquad \text{I.37}$$

where

$$(M)_{ij} = \gamma + \left[JS^2\rho z + \epsilon(k_i) \right] \delta(k_i, k_j) \ . \qquad\qquad \text{I.38}$$

Note that γ in eqn. I.38 is *not* the same as γ in eqn. I.33, but is a

free parameter in our phenomenological model which has to be chosen to best

represent the effect of an impurity in the crystal. The severity of the

assumptions made to obtain the impurity Hamiltonian I.37 (and I.31) will be

decided by its ability to describe real crystals with impurities.

Note in the impurity Hamiltonians the presence of a term which is
diagonal in the magnon operators, of magnitude $JS^2 \rho z$. This term amounts
to a correction to the pure magnon term of the full crystal Hamiltonian, in
each case, and represents a shift in the magnon band due to the impurity, as
pointed out earlier. For later calculations, this term will be assumed to
be included in the expression for the magnon energy $\epsilon(k)$ (eqns. I.27 and
I.19).

Note also that the terms with operators like $a_k^+ a_k'$ will lead to
scattering of magnons with different wavenumbers, thus leading to modification
of the magnon density of states due to the impurity.

Magnetic impurities in antiferromagnets have been studied by Tonegawa
and Kanamori (1966), Tonegawa (1968), and Lovesey (1968a, 1968b). These
authors have studied, in particular, the local modes which will occur outside
the pure crystal magnon band due to the impurity, and consider criterion
for the existence of such local modes and their dependence on various para-
meters of the calculation. Both calculations treat the impurity effects in
much more detail than will be done in the present work, though it is felt
that our simplified model will bring out the essential effects of an impurity
in the crystal.

It is expected that all the effects that an impurity in a crystal will
cause may also be found in the perturbed magnon sidebands in a crystal.
The general effects of any impurity are listed as follows (Elliott,
Krumhansl and Leath 1974):

(1) shifting of the pure spectrum line or lines affected, e.g. for
     a spin impurity the pure magnon band will be shifted by the
     last term of eqn. I.31.

(2) modification of the pure density of states, and hence of the
     observed spectrum line. This effect is considered to be the
     result of "resonances" or "virtual states" which result from

the scattering of magnons due to the impurity (Wolfram and Callaway 1963, see also chapter III). Resonances can only occur if there are no local modes outside the band of pure crystal states.

(3) the appearance of local modes, sharp lines which occur outside the pure crystal band, whose intensity is a function of the concentration of impurity and whose separation from the band as modified by (1) and (2) is characteristic of the impurity involved. The existence of local modes in general is a result of the relative strength of the impurity scattering over the bandwidth of the host pure band. (In the present case, γ vs $\varepsilon_0 = \varepsilon(k)_{max}$.)

All or some of the above phenomena are expected to occur whenever there is an impurity in a crystal. The conditions for their appearances depend on the magnitudes of the energies involved. Because of the dependence of the magnon sideband on the magnon dispersion $\varepsilon(k)$, it is expected that these phenomena will effect the magnon sideband, as well as the magnons themselves. Parkinson (1969a, 1969b) has discussed the effects of impurities on magnon sidebands in antiferromagnetic perovskites, stressing the appearance of local modes, confirming their appearance under certain conditions.

The total crystal Hamiltonians to be used in our phenomenological model are, with the inclusion of an impurity term, now given by

$$H^{(F)} = \sum_k \varepsilon(k) a_k^+ a_k + \varepsilon_2 \sum_k b_k^+ b_k + g \sum_k \left(a_k^+ b_k + b_k^+ a_k \right) + \frac{\gamma}{N} \sum_{k,k'} a_k^+ a_{k'} , \qquad \text{I.39}$$

$$H^{(AF)} = \sum_k \varepsilon(k) \left(\alpha_k^+ \alpha_k + \beta_k^+ \beta_k \right) + \varepsilon_2 \sum_k \left(A_k^+ A_k + B_k^+ B_k \right)$$

$$+ g \sum_k \left(\alpha_k^+ A_k + A_k^+ \alpha_k + \beta_k^+ B_k + B_k^+ \beta_k \right) + \frac{\gamma}{N_0} \sum_{k,k'} \left(\alpha_k^+ \alpha_{k'} + \beta_k^+ \beta_{k'} \right) . \quad \text{I.40}$$

Use will be made of these Hamiltonians in chapter III where we calculate the effect of an impurity on the magnon sideband in detail.

I.4 Optical Absorption

Although the calculation of the optical absorption of a crystal with an exciton-magnon interaction will not be given until Chapter II, we give here an indication of how the optical absorption may be obtained. We make use of the Green function method in solid state physics (Zubarev 1960, Mahanty 1974).

Consider a system which is perturbed by a time dependent Hamiltonian H_1 , which may be resolved into time-dependent and time independent parts, as

$$H_1 = Bf(t) .$$

I.41

For dielectric response of a system to an external electric field this will have the form

$$H_1 = -p.E^{(0)} \cos \omega t$$

I.42

where ω is the frequency of the applied field, p is the dipole moment of the crystal, $E^{(0)}$ the time independent part of the applied field.

The change of the ηth component of a physical qualtity A is given as the time integral (for linear response, Kubo 1957)

$$A_\eta(t) = \sum_\nu \int_{-\infty}^{\infty} G_{\eta,\nu}(t-t') E_\nu^{(0)} f(t') dt'$$

$$= \sum_\nu \int_{-\infty}^{\infty} \langle\langle A_\eta(t-t'), p_\nu \rangle\rangle E_\nu^{(0)} f(t') dt'$$

I.43

where $A(t)$ on the right hand side of eqn. I.43 is an operator with time dependence given according to the Heisenberg formula

$$A(t) = e^{iH_0 t/\hbar} A e^{-iH_0 t/\hbar} .$$

I.44

The Green function $\langle\langle \ ... \ \rangle\rangle$ in eqn. I.43 is defined as

$$G_{\eta\nu}(t-t') = \langle\langle A_\eta(t-t'), p_\nu(0) \rangle\rangle$$

$$= \frac{-i}{\hbar Z(\beta)} \text{Tr}\{\exp(-\beta H_0) [A_\eta(t-t'), p_\nu(0)]\}\theta(t)$$

$$= \frac{-i}{\hbar} \langle [A_\eta(t-t'), p_\nu(0)]\rangle \theta(t)$$

I.45

where $Z(\beta)$ is the canonical partition function, $\beta = 1/k_B T$ with

Boltzmann's constant k_B and temperature T. $\theta(t)$ is a step function which

is unity for $t > 0$ and zero for $t < 0$. $[A_\eta, p_\nu]$ represents the

commutator of A_η and p_ν.

For the dielectric response we are interested in the change in dipole

moment of the system due to the perturbation, that is, from eqn. I.43,

$$p_\eta(t) = - \sum_\nu \int_{-\infty}^\infty \langle\langle p_\eta(t-t'), p_\nu(0) \rangle\rangle E_\nu^{(0)} \cos \omega t' dt' . \qquad \text{I.46}$$

Thus the dielectric susceptibility for a linear response to the

perturbation is given by

$$\chi_{\eta\nu}(t) = - \int_{-\infty}^\infty \langle\langle p_\eta(t-t'), p_\nu(0) \rangle\rangle \cos \omega t' dt' . \qquad \text{I.47}$$

Defining the time Fourier transform of the Green function, eqn. I.45 as

$$G(\omega) = \int_{-\infty}^\infty G(t) e^{-i\omega t} dt , \qquad \text{I.48}$$

$\chi_{\eta\nu}(t)$ may be written as

$$\chi_{\eta\nu}(t) = -\left[\cos \omega t \; \text{Re} \; G_{\eta\nu}(\omega) - \sin \omega t \; \text{Im} \; G_{\eta\nu}(\omega)\right] , \qquad \text{I.49}$$

writing G in its real and imaginary parts, using the fact that

$G(-\omega) = G^*(\omega)$, the complex conjugate of $G(\omega)$.

Then

$$p_\eta(t) = \sum_\nu \chi_{\eta\nu}(t) E_\nu^{(0)} . \qquad \text{I.50}$$

The power absorbed by the system is given by the time average

$$P = \left(\sum_\nu \dot{p}_\nu(t) E_\nu^{(0)} \cos \omega t\right)_{\text{time av.}} \qquad \text{I.51}$$

where $\dot{p}$ is the time derivative of p. This gives

$$P = -\tfrac{1}{2}\omega \sum_{\eta,\nu} \text{Im} \; G_{\eta\nu}(\omega) E_\eta^{(0)} E_\nu^{(0)} \qquad \text{I.52}$$

making use of the fact that the time average of $\sin \omega t \cos \omega t$ and $\cos^2 \omega t$

are zero and $\frac{1}{2}$ respectively.

What is normally observed is the value of power absorbed for a particular orientation of the crystal and of the field, that is, a component of the optical absorption tensor

$$\alpha_{\eta\nu}(\omega) = -\tfrac{1}{2}\omega \text{ Im } G'_{\eta\nu}(\omega) \ . \qquad\qquad \text{I.53}$$

In the model calculations presented in this work, no consideration is specifically taken of polarisation of either the crystal or the applied field. The results that are obtained may, however, be considered as the absorption for one particular component of the optical absorption tensor, eqn. I.53.

The problem of calculating optical absorption is thus reduced to evaluating the Green function $G(\omega)$. This is done by solving the (time Fourier transformed) equation of motion

$$\hbar\omega\langle\!\langle p_\eta(t-t'), \ p_\nu(0)\rangle\!\rangle_\omega = \langle\, [p_\eta(0), \ p_\nu(0)]\,\rangle + \langle\!\langle\, [p_\eta, \ H_0], \ p_\nu\rangle\!\rangle_\omega \qquad \text{I.54}$$

where the first term on the right hand side of eqn. I.54 is the equal time average of the commutator of p_η and p_ν . The commutator of the second term is taken at time t . We have made use of the fact that

$$\int_{-\infty}^{\infty} \delta(t)e^{-i\omega t}dt = 1 \ . \qquad\qquad \text{I.55}$$

In chapter II it will be shown that the Green function on the right hand side of eqn. I.54 may be written, for the present model, as proportional to $G_{\eta\nu}(\omega)$ of the left hand side, thus enabling the Green function to be obtained directly and exactly.

It should be pointed out that many physical properties of the dielectric system may be obtained from the dielectric susceptibility tensor, eqn. I.49, not just the optical absorption. For example, the dielectric constant tensor will be given by

$$\varepsilon_{\eta\nu}(\omega) = \delta(\eta, \ \nu) + 4\pi \chi_{\eta\nu}(\omega) \ . \qquad\qquad \text{I.56}$$

Hence the Green function

$$G_{\eta\nu}(\omega) = \langle\langle p_\eta(t-t'), p_\nu(0)\rangle\rangle \qquad \text{I.57}$$

contains all the information required to calculate the linear response of

the system to an external perturbation of the sort given by eqn. I.42.

CHAPTER II

In this section we present calculations of the magnon sideband in pure crystals, making use of the Hamiltonians I.28 and I.29. We attempt to diagonalise these Hamiltonians written in matrix form. Diagonalisation is easy because of the form of the phenomenological Hamiltonian chosen. We treat the ferromagnetic crystal first, and then the antiferromagnet, presenting some numerical calculations of lineshape at each stage.

II.1 Magnon Sidebands in a Pure Ferromagnet

Very few ferromagnetic insulators exist in nature and there have been only a couple of reports of magnon sidebands occurring in ferromagnetic insulators. Because of this there has been little interest to date in calculating magnon sidebands in ferromagnets. One exception is the early work of Wortis (1963) who, while not calculating sideband effects, did calculate the two-magnon bound state in a ferromagnet. Wortis (1963) used a Heisenberg Hamiltonian, and the Green function method with decoupling to solve the problem. Hulin, Benoit à la Guillaume and Hanus (1971) have discussed a theory of magnon sidebands in ferromagnets in their paper which reports sidebands in EuO . Meltzer (1972) presented an alternative mechanism to that of Tanabe, Moriya and Sugano (1965) to describe the magnon sideband found in $GdCl_3$.

In these models leading to the magnon sideband, some approximations are made during the course of the calculation which make it difficult to interpret the results strictly in physical terms. The calculations we present in this work use Hamiltonians which allow the calculation to be made exactly while being sufficiently realistic to give a reasonable description of the observed phenomena.

From eqn. I.28, the pure crystal Hamiltonian is given by

$$H^{(F)} = \sum_k \varepsilon(k) a_k^+ a_k + \varepsilon_2 \sum_k b_k^+ b_k + g \sum_k \left(a_k^+ b_k + b_k^+ a_k \right) \qquad \text{II.1}$$

where

$$\varepsilon(k) = 2|J| Sz \left(1 - \gamma_k \right) , \qquad \text{II.2}$$

$$\gamma_k = \frac{1}{z} \sum_{[\Delta]} e^{ik.\Delta} . \qquad \text{II.3}$$

The perturbation on the crystal due to the external field is given from I.8 as

$$H_{\text{pert}}^{(F)} = l \sum_k \left(a_k^+ b_k^+ + a_k b_k \right) . \qquad \text{II.4}$$

As indicated in section I.4, we require to evaluate the Green function

$$G(\omega) = \sum_{k\underline{k}'} \langle\langle a_k^+ b_k^+ + a_k b_k, \; a_{\underline{k}'}^+ b_{\underline{k}'}^+ + a_{\underline{k}'} b_{\underline{k}'} \rangle\rangle_\omega . \qquad \text{II.5}$$

To do this, we first diagonalise $H^{(F)}$ eqn. II.1 and then obtain $G(\omega)$ from its equation of motion. We consider only the case of close to absolute zero of temperature in all the calculations of this work, so the spin-wave approximation holds (section I.2).

Writing $H^{(F)}$ in matrix form as

$$H^{(F)} = [\mathbf{a}^+ ; \mathbf{b}^+] \begin{bmatrix} \hat{A} & \hat{B} \\ \hat{B} & \hat{D} \end{bmatrix} \begin{bmatrix} \mathbf{a} \\ \mathbf{b} \end{bmatrix} \qquad \text{II.6}$$

where

$$\mathbf{a}^+ = \left[a_{k_1}^+, \; \ldots, \; a_{k_N}^+ \right] ; \quad \mathbf{b}^+ = \left[b_{k_1}^+, \; \ldots, \; b_{k_N}^+ \right]$$

for magnon and exciton creation operators a_k^+ and b_k^+, N atoms in the crystal and

$$(A)_{ij} = \varepsilon \left(k_i \right) \delta(i, j) , \qquad \text{II.7}$$

$$(B)_{ij} = g \delta(i, j) , \qquad \text{II.8}$$

$$(D)_{ij} = \varepsilon_2 \delta(i, j) \qquad \text{II.9}$$

we see that all submatrices are diagonal, and commute with each other. We may thus diagonalise $H^{(F)}$ by treating it as a 2×2 matrix. The

eigenvalues are given by

$$\lambda^{\pm}(k) = \frac{\varepsilon(k)+\varepsilon_2}{2} \pm \left[\left[\frac{\varepsilon_2-\varepsilon(k)}{2}\right]^2 + g^2\right]^{\frac{1}{2}} . \qquad \text{II.10}$$

Defining the functions

$$x(k) = \frac{\varepsilon_2-\varepsilon(k)}{2g} , \qquad \text{II.11}$$

$$y(k) = \left[x(k)^2+1\right]^{\frac{1}{2}} \qquad \text{II.12}$$

the matrix which diagonalises $H^{(F)}$, the matrix of eigenvectors, may be written

$$\hat{S} = \begin{bmatrix} \hat{S}_{11} & \hat{S}_{12} \\ \hat{S}_{21} & \hat{S}_{22} \end{bmatrix} \qquad \text{II.13}$$

where

$$\left(S_{11}\right)_{kk'} = \frac{\delta(k,k')}{\sqrt{2y(k)(y(k)-x(k))}} ,$$

$$\left(S_{12}\right)_{kk'} = \frac{\delta(k,k')}{\sqrt{2y(k)(y(k)+x(k))}} ,$$

$$\left(S_{21}\right)_{kk'} = - \sqrt{\frac{y(k)-x(k)}{2y(k)}} \, \delta(k, k') ,$$

$$\left(S_{22}\right)_{kk'} = \sqrt{\frac{y(k)+x(k)}{2y(k)}} \, \delta(k, k') . \qquad \text{II.14}$$

It is easily shown that $\hat{S}$ is unitary, so $\hat{S}^{-1} = \hat{S}^{+}$ the Hermitian adjoint of $\hat{S}$.

Then the pure crystal Hamiltonian in diagonal form is

$$H^{(F)} = [a^{+};b^{+}]_{\hat{S}\hat{S}^{+}} \begin{bmatrix} \hat{A} & \hat{B} \\ \hat{B} & \hat{D} \end{bmatrix} \hat{S}\hat{S}^{+} \begin{bmatrix} a \\ b \end{bmatrix}$$

$$= \sum_k \lambda^{-}(k)\eta_k^{+}\eta_k + \lambda^{+}(k)\nu_k^{+}\nu_k \qquad \text{II.15}$$

where η_k and ν_k are defined by

$$\begin{bmatrix} \eta \\ \nu \end{bmatrix} = \hat{S}^{+} \begin{bmatrix} a \\ b \end{bmatrix}$$

that is,

$$\eta_k = \frac{a_k}{\sqrt{2y(y-x)}} - \sqrt{\frac{y-x}{2y}}\, b_k \ ,$$

$$\nu_k = \frac{a_k}{\sqrt{2y(y+x)}} + \sqrt{\frac{y+x}{2y}}\, b_k \qquad\qquad\qquad \text{II.16}$$

where we have dropped the k-subscript on x and y . As the exciton-magnon interaction g goes to zero, $\eta_k \rightarrow a_k$ and $\nu_k \rightarrow b_k$ as required, since in this limit $H^{(F)}$ is already diagonal.

From the fact that a_k and b_k both satisfy boson commutation rules, eqn. II.16 may be used to determine the commutation rules for η_k and ν_k . The result is

$$[\eta_k, \eta_{k'}^+] = \delta(k, k') \ ,$$

$$[\nu_k, \nu_{k'}^+] = \delta(k, k') \qquad\qquad\qquad \text{II.17}$$

and all other commutators are zero. Hence η_k and ν_k also satisfy boson commutation rules. Eqn. II.16 plus the limits as $g \rightarrow 0$ indicate that η and ν represent two new types of excitation, with some exciton and some magnon character in each. The limits indicate that η is "magnon-like" and ν is "exciton-like". The diagonalised Hamiltonian, eqn. II.15 thus has two branches. If we expand the square roots in $\lambda^{\pm}(k)$ we obtain the first approximation that $\lambda^+ \sim \varepsilon_2$, $\lambda^- \sim \varepsilon(k)$ confirming the magnon- and exciton-like natures of η and ν .

The optical absorption may be obtained by expressing a_k and b_k in terms of η_k and ν_k , and evaluating the Green functions of the latter. We have

$$a_k = \frac{\eta_k}{\sqrt{2y(y-x)}} + \frac{\nu_k}{\sqrt{2y(y+x)}} \ ,$$

$$b_k = - \sqrt{\frac{y-x}{2y}}\, \eta_k + \sqrt{\frac{y+x}{2y}}\, \nu_k \qquad\qquad\qquad \text{II.18}$$

so

$$a_k^+ b_k^+ + a_k b_k = (\nu_k^+ \nu_k^+ + \nu_k \nu_k)/2y + \frac{x}{y}(\eta_k \nu_k + \eta_k^+ \nu_k^+) - (\eta_k^+ \eta_k^+ + \eta_k \eta_k)/2y \quad . \quad \text{II.19}$$

The non-zero Green functions obtained from using II.19 in eqn. II.5 are

$$\langle\langle \eta_k \eta_k, \; \eta_{k'}^+ \eta_{k'}^+ \rangle\rangle \; , \quad \langle\langle \nu_k \nu_k, \; \nu_{k'}^+ \nu_{k'}^+ \rangle\rangle \quad \text{and} \quad \langle\langle \eta_k \nu_k, \; \eta_{k'}^+ \nu_{k'}^+ \rangle\rangle \; .$$

We will demonstrate how these may be found by calculating the last one.

The equation of motion, from eqn. I.54, is, in time Fourier transform

$$\hbar\omega\langle\langle \eta_k \nu_k, \; \eta_{k'}^+ \nu_{k'}^+ \rangle\rangle = \langle [\eta_k \nu_k, \; \eta_{k'}^+ \nu_{k'}^+] \rangle + \langle\langle [\eta_k \nu_k, \; H_0], \; \eta_{k'}^+ \nu_{k'}^+ \rangle\rangle \quad . \quad \text{II.20}$$

Now the equal time average commutator is

$$\langle [\eta_k \nu_k, \; \eta_{k'}^+ \nu_{k'}^+] \rangle = \langle \eta_k \eta_{k'}^+ \rangle \delta(k, \; k') + \langle \nu_{k'}^+ \nu_k \rangle \delta(k, \; k')$$

$$= \delta(k, \; k') \quad\quad\quad\quad\quad \text{II.21}$$

since $\nu_k|0\rangle = 0$.

The Green function which is the last term on the right hand side of eqn. II.20 is

$$\langle\langle [\eta_k \nu_k, \; H_0], \; \eta_{k'}^+ \nu_{k'}^+ \rangle\rangle = \sum_{k''} \langle\langle [\eta_k \nu_k, \; \lambda^-(k'')\eta_{k''}^+ \eta_{k''} + \lambda^+(k'')\nu_{k''}^+ \nu_{k''}], \; \eta_{k'}^+ \nu_{k'}^+ \rangle\rangle$$

$$= (\lambda^-(k) + \lambda^+(k))\langle\langle \eta_k \nu_k, \; \eta_{k'}^+ \nu_{k'}^+ \rangle\rangle \quad\quad \text{II.22}$$

from standard manipulations of the commutators.

Hence from eqns. II.20-II.22,

$$\langle\langle \eta_k \nu_k, \; \eta_{k'}^+ \nu_{k'}^+ \rangle\rangle = \frac{\delta(k,k')}{\hbar\omega - (\lambda^+(k) + \lambda^-(k))} \quad . \quad \text{II.23}$$

Similarly, the other two Green functions may be calculated to give

$$\langle\langle \eta_k \eta_k, \; \eta_{k'}^+ \eta_{k'}^+ \rangle\rangle = \frac{\delta(k,k')}{\hbar\omega - 2\lambda^-(k)} \quad , \quad \text{II.24}$$

$$\langle\langle \nu_k \nu_k, \; \nu_{k'}^+ \nu_{k'}^+ \rangle\rangle = \frac{\delta(k,k')}{\hbar\omega - 2\lambda^+(k)} \quad . \quad \text{II.25}$$

The optical absorption is then proportional to the imaginary part of the sum of these three Green functions (section I.4):

$$\alpha(\omega) \sim -\frac{\omega}{2} \sum_{k,k'} \text{Im}\left[\frac{x(k)^2}{x(k)^2 + 1} \frac{\delta(k,k')}{\hbar\omega - (\lambda^+(k) + \lambda^-(k))} + \right.$$

$$\left. + \frac{\delta(k,k')}{4(x(k)^2 + 1)} \left(\frac{1}{\hbar\omega - 2\lambda^-(k)} + \frac{1}{\hbar\omega - 2\lambda^+(k)} \right) \right] \quad . \quad \text{II.26}$$

The Green functions II.23-II.25 are considered with the energy $\hbar\omega$ having a small imaginary part, $i\eta$. Use is then made of the relation

$$\text{Im}(x-i\eta)^{-1}\Big|_{\eta\to0^+} = \pi\delta(x) \qquad\qquad \text{II.27}$$

leading to the optical absorption

$$\alpha(\delta) \sim -\frac{\omega}{2}\sum_k\left\{\frac{x(k)^2}{x(k)^2+1}\,\delta\big(\hbar\omega-\big(\lambda^+(k)+\lambda^-(k)\big)\big)\right.$$

$$\left.+ \frac{1}{4\big(x(k)^2+1\big)}\,\big(\delta\big(\hbar\omega-2\lambda^-(k)\big)+\delta\big(\hbar\omega-2\lambda^+(k)\big)\big)\right\} . \quad \text{II.28}$$

It will be seen that the last two terms of eqn. II.28 will contribute to the absorption at frequencies of $2\lambda^-(k)$ and $2\lambda^+(k)$. Hence these represent "two-magnon" and "two exciton" lines in the spectrum. Since λ^- is not exactly $\varepsilon(k)$ and λ^+ not exactly ε_2 , the lines are shifted by the exciton-magnon interaction. The intensity of the lines is also affected, as is the shape, by the factor $\big[4\big(x(k)^2+1\big)\big]^{-1}$ which is also dependent on g ,

$$\big[4\big(x(k)^2+1\big)\big]^{-1} = \frac{g^2}{\big(\varepsilon_2-\varepsilon(k)\big)^2+4g^2} . \qquad\qquad \text{II.29}$$

The first term of II.28 yields the magnon sideband at a frequency of

$$\lambda^+(k) + \lambda^-(k) = \varepsilon_2 + \varepsilon(k) . \qquad\qquad \text{II.30}$$

The sideband lineshape is given from II.28 as

$$\alpha(\omega) \sim -\frac{\omega}{2}\sum_k\frac{\big(\varepsilon_2-\varepsilon(k)\big)^2}{\big(\varepsilon_2-\varepsilon(k)\big)^2+4g^2}\,\delta\big(\hbar\omega-\big(\varepsilon_2+\varepsilon(k)\big)\big)$$

$$\sim -\frac{\omega}{2}\,4\pi\int\frac{\big(\varepsilon_2-\varepsilon\big)^2}{\big(\varepsilon_2-\varepsilon\big)^2+4g^2}\,\delta\big(\hbar\omega-\big(\varepsilon_2+\varepsilon\big)\big)g_0(\varepsilon)d\varepsilon$$

$$\sim -2\pi\omega\,\frac{\big(2\varepsilon_2-\hbar\omega\big)^2}{\big(2\varepsilon_2-\hbar\omega\big)^2+4g^2}\,g_0\big(\hbar\omega-\varepsilon_2\big) \qquad\qquad \text{II.31}$$

where $g_0(\varepsilon)$ is the pure magnon density of states,

$$g_0(\varepsilon) = \frac{1}{N} \sum_{k} \delta\big(\varepsilon - \varepsilon(k)\big) \qquad\qquad \text{II.32}$$

which may be shown to be non-zero only in the range $[0, \varepsilon_0]$ thus giving

the range of the magnon-sideband.

The expression II.31 will be seen from later work to be a characteristic

form for all the magnon-sideband calculations.

From equations II.30, II.31 it is clear that the magnon sideband lies on

the high energy side of the exciton energy ε_2 and has a bandwidth of

$\varepsilon_0 = \varepsilon(k)_{\max}$. So the sideband lies within the range $[\varepsilon_2, \varepsilon_2 + \varepsilon_0]$ and has

the shape of the magnon density of states modified by the function

$$f(\omega, g) = \frac{\big(2\varepsilon_2 - \hbar\omega\big)^2}{\big(2\varepsilon_2 - \hbar\omega\big)^2 + 4g^2} \qquad\qquad \text{II.33}$$

discussed in detail below.

We have indicated in section I.1 that the exciton-magnon interaction

will cause a shift in the value of ε_2 from the non-interacting case, so

the position of the sideband with respect to the magnetic dipole exciton

line (not given in the absorption spectrum here because we have ignored the

magnetic component of the applied field) will be not exactly in the range

$[\varepsilon_2, \varepsilon_2 + \varepsilon_0]$ but shifted to slightly higher energy by a g-dependent

constant, though the bandwidth ε_0 will be unaffected, as also will the

lineshape be unaffected. In the present model such a shift is treated as a

free parameter determined by any observed shift in the sideband. It is

expected any such shift will be small as the high-energy cut-off of the

sideband is often seen to be very close to $\varepsilon_2 + \varepsilon_0$.

The more specific dependence on the strength of the exciton-magnon

interaction g is given by the factor $f(\omega, g)$, eqn. II.33.

It will be shown in subsequent sections that this term is the same for

all cases considered here, and apart from the shift just discussed, will

contain all the dependence on the exciton-magnon interaction strength. It is therefore of interest to consider the effect $f(\omega, g)$ eqn. II.33 has in modifying the expression for the absorption in the region of the magnon sideband (eqn. II.31) from its value as the density of states when g is zero.

In order to ascertain which values of g will have the greatest affect on the sideband consider the function $f(\omega, g)$ as a function of g. It has a maximum at $g = 0$ of unity and a point of inflection at

$$g = \left(\varepsilon_2 - \frac{\hbar\omega}{2} \right) \frac{1}{\sqrt{3}}$$

$$\approx \left(\frac{\varepsilon_2 - \varepsilon_0}{2} \right) \frac{1}{\sqrt{3}}$$

since the absorption band lies in the range $[\varepsilon_2, \varepsilon_2 + \varepsilon_0]$. At this point $f(\omega, g)$ is 0.75. Since $\varepsilon_2 \gg \varepsilon_0$ in general, the point of inflection will lie at a large distance from the origin, and the function $f(\omega)$ will be slowly varying everywhere in both g and ω. Though it will have maximum slope at the point of inflection, in this neighbourhood it will be very close to linear over the range ε_0 of the absorption band. Hence one would expect the density of states to be altered little by $f(\omega, g)$, at most being convoluted with a straight line with a maximum slope of approximately $\frac{3}{8} [(\varepsilon_2 - \varepsilon_0)]^{-1}$ which, in general, will be small as the exciton energy ε_2 is large. This line will tend to reduce the absorption most near the high-energy edge of the band though this effect will still be small, because of the small slope of $f(\omega, g)$. The only case where there may be a large effect is in the far infra-red where ε_2 is much closer to ε_0 than in the more commonly studied near infra-red and visible regions.

We must therefore conclude that the effect of exciton-magnon interaction on the magnon sideband will be small for the model Hamiltonian we have chosen,

and the dominant contribution to the magnon sideband comes from the perturbation Hamiltonian. According to Parkinson and Loudon (1968), Eremenko, Novikov and Petrov (1974) and others, the effect of the exciton-magnon interaction may have an observable effect on the magnon sideband lineshape, though experimental evidence is still not clear on the point. Hence the generally small contribution of the exciton-magnon interaction represents a limitation of the present model.* The effect of the interaction becomes more noticable as one goes to longer wavelengths so ϵ_2 becomes closer in magnitude to ϵ_0.

We will now present some numerical examples of the sideband predicted by eqn. II.31. Unfortunately, probably due to the scarcity of ferromagnetic insulators in nature, very few instances of magnon sidebands in ferromagnets have been reported. Hulin, Benoit à la Guillaume and Hanus (1971) have given a brief interpretation of a line in the luminescence spectrum of ferromagnetic EuO as the result of a coupled exciton-magnon process, while Meltzer (1972) has discussed a possible magnon sideband in the absorption spectrum of $GdCl_3$. Insufficient details are given in either paper to allow very satisfactory comparison with a model calculation.

For the purposes of illustration we will choose to study the face-centred cubic crystal EuO. We do this for several reasons. Firstly Meltzer (1972) indicates that the sideband reported by him may be explained by a single-ion rather than an exchange-coupled mechanism and so it is not

---

* Note that if we give the exciton-magnon interaction strength g some k-dependence the result of the first line of equation II.31 will be unchanged except for g being replaced by $g(k)$. It is then possible to have a significant effect on the sideband shape if $g(k)$ has some large value for particular values of k (e.g. near the edge of the Brillouin zone) and the sideband will look like a weighted density of states function with a form which can give a lineshape similar to that of Parkinson and Loudon (1968) for an appropriate form for g as a function of k. This statement also applies to the pure antiferromagnet magnon sideband lineshape, eqn. II.60. For the impurity case (Chapter III) the form of the Hamiltonian sub-matrices is such that they no longer commute and hence the simple diagonalisation scheme no longer applies, though the Hamiltonian may still be diagonalised. Hence we may also obtain a significant effect from the exciton-magnon interaction if g has some k-dependence, in this case.

clear that the present model is relevant. On the other hand, though the line reported by Hulin and others (1971) was found in luminescence, and may not appear in absorption (Hulin, Hanus, Benoit à la Guillaume and Reed 1970), other sidebands may be so observable. We also choose the *fcc* structured *EuO* because of its apparently small anisotropy and small next nearest neighbour exchange integral (McGuire, Argyle, Shafer and Smart 1963) though Barak, Gabai and Kaplan (1974) have considered the next nearest neighbour case in their study of nuclear spin-lattice relaxation in *EuO* .

We therefore choose to base our example on ferromagnetic *EuO* and neglect any anisotropy or next nearest neighbour exchange interaction in the crystal. For an *fcc* ferromagnet the magnon energy is given by

$$\varepsilon(k) = \tfrac{1}{4}\varepsilon_0 \left[3 - \left(\cos \frac{k_x a}{2} \cos \frac{k_y a}{2} + \cos \frac{k_y a}{2} \cos \frac{k_z a}{2} + \cos \frac{k_z a}{2} \cos \frac{k_x a}{2} \right) \right] ,$$

$$\varepsilon_0 = 32JS .$$

II.34

The magnon density of states for the pure crystal, $g_0(\varepsilon)$, eqn. II.32 was calculated numerically using a Monte-Carlo method (Buchheit and Loly 1972, Loly and Buchheit 1972) and the details of this and other numerical calculations required in later parts of this work are presented in appendix 3. The accuracy of the calculations has not been estimated explicitly but the essential features of the density of states are shown using an accuracy of better than 5% . The details of the *fcc* Brillouin zone, including its symmetry points are well known and will not be given here. The only features we note in passing are the logarithmic singularity in the density of states at the high energy edge of the band, and the cusp point at 0.75 of the bandwidth, the former due to zeros in the group velocity $|\nabla_k \varepsilon(k)|$ along the line joining $k_X = \frac{\pi}{a} (0, 1, 0)$ with $k_W = \frac{\pi}{a} (\tfrac{1}{2}, 1, 0)$ and equivalent lines, and the latter being due to zeros in the group velocity at the point $k_L = \frac{\pi}{a} (\tfrac{1}{2}, \tfrac{1}{2}, \tfrac{1}{2})$ (Loly and Buchheit 1972). The cusp point is a type *I*.

van Hove singularity which behaves like

$$\pm\left(\omega_c - \omega\right)^{\frac{1}{2}} \, , \quad \omega \lesssim \omega_c \, ,$$

$$\left(\omega - \omega_c\right) \, , \quad \omega \gtrsim \omega_c \, ,$$

for ω_c the cusp-point frequency at 0.75 of the bandwidth (Swendsen and

Callen 1972).

For EuO , Barak and others (1974) give a value for the nearest

neighbour exchange integral ranging from 0.37 to 0.52 cm^{-1} giving values

for ε_0 (eqn. II.34) of between 41 and 58 cm^{-1} for a ground state spin

of $\frac{7}{2}$. Using the value of the Curie temperature of 69.4 K for EuO we

may alternatively estimate ε_0 from molecular field theory (McGuire and

others 1963) using

$$T_c = 8S(S+1)J$$

giving a value of 43 cm^{-1} , for a spin of $\frac{7}{2}$ which corresponds to a

possible ground state spin in EuO for an absorption process (Hulin and

others 1971). For this example we choose $\varepsilon_0 = 45$ cm^{-1} . We will also

consider the magnetic dipole parent exciton to have an energy of

$3.36eV = 27100$ cm^{-1}, a value which has no great significance but will serve

to illustrate the behaviour in this region of the spectrum where an

absorption band might occur (though there is no evidence that one will occur).

We will ignore the effect of a shift of the sideband due to the exciton-

magnon interaction strength g which is expected to be small.

The results of the magnon sideband calculation for a ferromagnetic fcc

crystal with $\varepsilon_0 = 45$ cm^{-1} , $\varepsilon_2 = 27100$ cm^{-1} are shown in fig. II.1 for

several values of the ratio g/ε_2 . All the curves were obtained from the

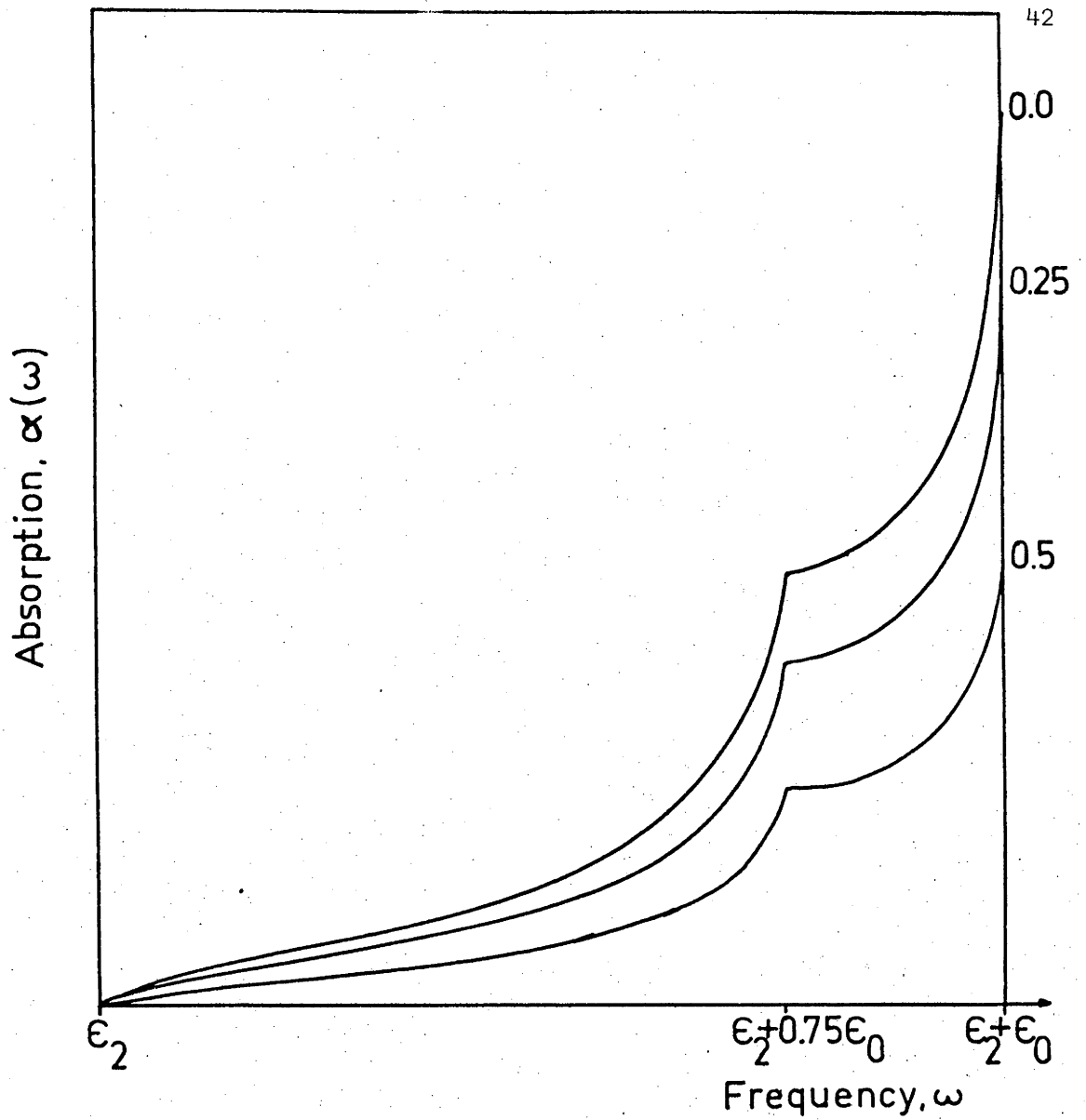same numerical values of the density of states to enable a comparison to be

FIGURE II.1. Curves representing magnon sidebands in the absorption

spectrum of an *fcc* crystal such as *EuO* for various values

of the exciton-magnon interaction strength g , shown in the

figure as the dimensionless quantity g/ε_2 .

made. The logarithmic singularity at the upper band edge is not well described in the calculations where one obtains a finite value at the edge. The pure density of states is very closely approximated by $1/\varepsilon_2$ times the $g/\varepsilon_2 = 0$ curve, since $\varepsilon_2 \gg \varepsilon_0$. Note that the magnon sideband retains the basic shape of the density of states for this model, the effect of increasing g is merely to reduce the intensity in the high-energy region slightly over the lower end, as described earlier in this section. The overall reduction in the absorption shown in fig. II.1 as g is increased will be offset somewhat by an increase in the perturbation strength l (eqn. II.4) which might be expected to be larger as the crystal-field effects (which will affect g) increase. That is, since g and l both involve some form of coupling between excitons and magnons, if one is large the other should also be large.

As no direct observations of absorption magnon sidebands have been made in *EuO* to date, it is not possible to obtain any experimental test of the validity of the forms of the magnon sidebands shown in fig. II.1. We would predict from the present model, however, that the sideband will be skewed to have its maximum very close to the high-energy cut-off of the band, and its width will be approximately given by the separation of the cusp point from that edge, i.e. the band width should be measured at about 0.25 times the separation between the weak magnetic dipole parent exciton and the high-energy cut-off of the band since most of the exciton-magnon states represented by η and ν (eqn. II.16) lie in this region. It would be interesting to see if lines in the absorption spectrum of *EuO* exhibit these properties.

II.2 Magnon Sidebands in a Pure Antiferromagnet

Many more antiferromagnetic insulators occur in nature than ferromagnetic ones, and many of these are found to exhibit magnon sidebands in

their spectra. Several theories have been proposed to describe these sidebands, principally by Sell, Greene and White (1967), Tanabe and Gondiara (1967), Tanabe, Gondiara and Murata (1968), Loudon (1968), Parkinson and Loudon (1968), Moriya (1966, 1968), Moriya and Inoue (1968), Freeman and Hopfield (1968), McClure (1968), Misetich, Dietz and Guggenheim (1968), Dietz, Meixner and Guggenheim (1970), Stokowski, Sell and Guggenhiem (1971), Bhandari and Falicov (1972), Petrov and Gaididei (1971), Gaididei and Loktev (1974), Eremenko, Novikov and Petrov (1974). Some of these theories are very complex. The value of the present model is because of its simplicity and the important fact that the sideband may be calculated exactly from the phenomenological Hamiltonian assumed, thus allowing for a clear physical interpretation of the result.

The calculation of magnon sidebands in a pure antiferromagnet follows similar lines to that of the ferromagnet in the last section. In the present case there are two sublattices, and, using the Hamiltonian I.29, there is no splitting of the consequent twofold degeneracy. In a real crystal, if the exciton parent line has its degeneracy totally, or partially removed, the magnon sideband will also split, with components corresponding to separate exciton lines. The present calculation may be considered to treat only one of the exciton lines, and give its corresponding sideband, with negligible influence from other exciton transitions.

The Hamiltonian, from eqn. I.29 is

$$H^{(AF)} = \sum_k \varepsilon(k) \left(\alpha_k^+ \alpha_k + \beta_k^+ \beta_k\right) + \varepsilon_2 \sum_k \left(A_k^+ A_k + B_k^+ B_k\right)$$

$$+ g \sum_k \left(\alpha_k^+ A_k + A_k^+ \alpha_k + \beta_k^+ B_k + B_k^+ \beta_k\right) \quad \text{II.35}$$

where

$$\varepsilon(k) = 2JSz\left[1 - \gamma_k^2\right]^{\frac{1}{2}}, \quad \text{II.36}$$

$$\gamma_k = \frac{1}{z} \sum_{[\Delta]} e^{ik.\Delta}. \quad \text{II.37}$$

The perturbation on the crystal due to the applied field is given by eqn. I.9 as

$$H_{pert}^{(AF)} = l \sum_k \left(\alpha_k^+ A_k^+ + \alpha_k A_k + \beta_k^+ B_k^+ + \beta_k B_k \right) .$$ II.38

We consider each sublattice to have $N_0 = N/2$ ions on it. Writing $H^{(AF)}$, eqn. II.35 in matrix form, as in section II.1, gives

$$H^{(AF)} = [\alpha^+ \beta^+ A^+ B^+] \begin{bmatrix} \hat{M}_1 & 0 & \hat{M}_2 & 0 \\ 0 & \hat{M}_3 & 0 & \hat{M}_4 \\ \hat{M}_5 & 0 & \hat{M}_6 & 0 \\ 0 & \hat{M}_7 & 0 & \hat{M}_8 \end{bmatrix} \begin{bmatrix} \alpha \\ \beta \\ A \\ B \end{bmatrix}$$ II.39

where

$$\alpha^+ = [\alpha_{k_1}^+, \alpha_{k_2}^+, \dots, \alpha_{k_{N_0}}^+] , \text{ etc.,}$$

$$(M_1)_{ij} = (M_3)_{ij} = \epsilon(k_i) \delta(k_i, k_j) ,$$ II.40

$$(M_2)_{ij} = (M_4)_{ij} = (M_5)_{ij} = (M_7)_{ij} = g \delta(k_i, k_j) ,$$ II.41

$$(M_6)_{ij} = (M_8)_{ij} = \epsilon_2 \delta(k_i, k_j) .$$ II.42

We see again that all submatrices are diagonal. Hence the matrix is diagonalised readily along the same lines as section II.1, giving eigenvalues

$$\lambda^{\pm}(k) = \frac{\epsilon(k) + \epsilon_2}{2} \pm \left[\left(\frac{\epsilon_2 - \epsilon(k)}{2} \right)^2 + g^2 \right]^{\frac{1}{2}}$$ II.43

in direct correspondence with the ferromagnetic case. Because of the sublattice degeneracy, though, there are two states with the same eigenvalue for every wavenumber.

Diagonalisation of $H^{(AF)}$ is achieved by the unitary matrix

$$
\hat{S} = \begin{bmatrix} \hat{S}_1 & 0 & \hat{S}_2 & 0 \\ 0 & \hat{S}_1 & 0 & \hat{S}_2 \\ \hat{S}_3 & 0 & \hat{S}_4 & 0 \\ 0 & \hat{S}_3 & 0 & \hat{S}_4 \end{bmatrix}
$$

II.44

where

$$
\left(S_1\right)_{ij} = [2y(y-x)]^{-\frac{1}{2}} \delta\left(k_i,\ k_j\right) \ ,
$$

II.45

$$
\left(S_2\right)_{ij} = [2y(y+x)]^{-\frac{1}{2}} \delta\left(k_i,\ k_j\right) \ ,
$$

II.46

$$
\left(S_3\right)_{ij} = -\sqrt{\frac{y-x}{2y}}\ \delta\left(k_i,\ k_j\right) \ ,
$$

II.47

$$
\left(S_4\right)_{ij} = \sqrt{\frac{y+x}{2y}}\ \delta\left(k_i,\ k_j\right)
$$

II.48

where $x(k)$ and $y(k)$ are given by eqns. II.11, II.12, as

$$
x(k) = \frac{\varepsilon_2 - \varepsilon(k)}{2g} \ ,
$$

II.49

$$
y(k) = \left[x(k)^2 + 1\right]^{\frac{1}{2}} \ .
$$

II.50

Hence the pure crystal Hamiltonian becomes

$$
H^{(AF)} = \begin{bmatrix} \alpha^+ \beta^+ A^+ B^+ \end{bmatrix} \hat{S}\hat{S}^+ \begin{bmatrix} \hat{M}_1 & 0 & \hat{M}_2 & 0 \\ 0 & \hat{M}_1 & 0 & \hat{M}_2 \\ \hat{M}_5 & 0 & \hat{M}_6 & 0 \\ 0 & \hat{M}_5 & 0 & \hat{M}_6 \end{bmatrix} \hat{S}\hat{S}^+ \begin{bmatrix} \alpha \\ \beta \\ A \\ B \end{bmatrix}
$$

$$
= \sum_k \left[\lambda^-(k)\left(\phi_k^+\phi_k + \chi_k^+\chi_k\right) + \lambda^+(k)\left(\psi_k^+\psi_k + \omega_k^+\omega_k\right)\right]
$$

II.51

where

$$
\begin{bmatrix} \phi \\ \chi \\ \psi \\ \omega \end{bmatrix} = \hat{S}^+ \begin{bmatrix} \alpha \\ \beta \\ A \\ B \end{bmatrix}
$$

II.52

that is,

$$\phi_k = [2y(y-x)]^{-\frac{1}{2}}\alpha_k - \left[\frac{y-x}{2y}\right]^{\frac{1}{2}}A_k , \qquad \text{II.53}$$

$$\chi_k = [2y(y-x)]^{-\frac{1}{2}}\beta_k - \left[\frac{y-x}{2y}\right]^{\frac{1}{2}}B_k , \qquad \text{II.54}$$

$$\psi_k = [2y(y+x)]^{-\frac{1}{2}}\alpha_k + \left[\frac{y+x}{2}\right]^{\frac{1}{2}}A_k , \qquad \text{II.55}$$

$$\omega_k = [2y(y+x)]^{-\frac{1}{2}}\beta_k + \left[\frac{y+x}{2}\right]^{\frac{1}{2}}B_k . \qquad \text{II.56}$$

It is readily shown that as the exciton-magnon interaction goes to zero, $\phi_k \to \alpha_k$, $\chi_k \to \beta_k$, $\psi_k \to A_k$, $\omega_k \to B_k$ while $\lambda^+ \to \varepsilon_2$ and $\lambda^- \to \varepsilon(k)$. Hence we again have two branches of the spectrum, one which is magnon like and one exciton like, both being modified by the exciton-magnon interaction, g . It is readily shown that ϕ, χ, ψ and ω all have boson commutation rules, and commute with each other. This fact follows from the boson commutation rules for α, β, A and B .

Following section II.1 we again write the perturbing Hamiltonian in terms of operators which diagonalise the unperturbed Hamiltonian, giving the result

$$H_{pert}^{(AF)} = l \sum_k \left\{ \frac{1}{2y(k)} \left[\psi_k^+\psi_k^+ + \omega_k^+\omega_k^+ + \psi_k\psi_k + \omega_k\omega_k - \left(\phi_k^+\phi_k^+ + \chi_k^+\chi_k^+ + \phi_k\phi_k + \chi_k\chi_k\right)\right] \right.$$
$$\left. + \frac{x(k)}{y(k)} \left[\phi_k^+\psi_k^+ + \phi_k\psi_k + \chi_k^+\omega_k^+ + \chi_k\omega_k\right] \right\} . \quad \text{II.57}$$

Again only a few of the Green functions obtained from these operators (see eqn. I.54) are non-zero, because of the commutation rules. The non-zero Green functions are obtained in an identical manner to those of section II.1, and are found to be

$$\langle\langle \phi_k\phi_k, \phi_{k'}^+\phi_{k'}^+ \rangle\rangle = \frac{\delta(k,k')}{\hbar\omega - 2\lambda^-(k)}$$
$$= \langle\langle \chi_k\chi_k, \chi_{k'}^+\chi_{k'}^+ \rangle\rangle , \qquad \text{II.58}$$

$$\langle\langle \psi_k\psi_k, \psi_{k'}^+\psi_{k'}^+ \rangle\rangle = \frac{\delta(k,k')}{\hbar\omega - 2\lambda^+(k)}$$
$$= \langle\langle \omega_k\omega_k, \omega_{k'}^+\omega_{k'}^+ \rangle\rangle , \qquad \text{II.59}$$

$$\langle\langle \phi_k\psi_k, \; \phi^+_{k'}\psi^+_{k'} \rangle\rangle = \frac{\delta(k,k')}{\hbar\omega-(\lambda^++\lambda^-)}$$

$$= \langle\langle \chi_k\omega_k, \; \chi^+_{k'}\omega^+_{k'} \rangle\rangle \; . \qquad\qquad \text{II.60}$$

Again the degeneracy caused by the two sublattices is revealed in eqns. II.58-II.60. The two-magnon and two-exciton lines are also obtained as for the ferromagnet, and again the magnon sideband is obtained from the imaginary part of eqn. II.60 as

$$\alpha(\omega) \sim -\omega \sum_k \frac{\left(\varepsilon_2-\varepsilon(k)\right)^2}{\left(\varepsilon_2-\varepsilon(k)\right)^2+4g^2} \; \delta\left(\hbar\omega-\left(\varepsilon_2+\varepsilon(k)\right)\right) \qquad \text{II.61}$$

where we have used eqn. II.27 to take the imaginary part, and

$$\lambda^+(k) + \lambda^-(k) = \varepsilon_2 + \varepsilon(k) \qquad\qquad \text{II.62}$$

from eqn. II.43. The factor of 2 in eqn. II.61 arises from the degeneracy of the sublattices, which is absent from eqn. II.31.

Performing the sum over k, we obtain

$$\alpha(\omega) \sim -4\pi\omega \; \frac{\left(2\varepsilon_2-\hbar\omega\right)^2}{\left(2\varepsilon_2-\hbar\omega\right)^2+4g^2} \; g_0\left(\hbar\omega-\varepsilon_2\right) \qquad \text{II.63}$$

where $g_0(\varepsilon)$ is the pure magnon density of states,

$$g_0(\varepsilon) = \frac{1}{N} \sum_k \delta\left(\varepsilon-\varepsilon(k)\right) \qquad\qquad \text{II.64}$$

for $\varepsilon(k)$ given by eqn. II.36. It can be shown that $g_0(\varepsilon)$ is non-zero only within the range $\left[0, \varepsilon_0\right]$, thus giving the range of the sideband.

The identical nature of the expression for the magnon sideband for the ferromagnet and antiferromagnet is immediately obvious, comparing eqn. II.63 with eqn. II.31. The comments made in section II.1 about the g-dependence of eqn. II.31 apply equally to eqn. II.63, and for these reasons we will ignore the effect of g in what follows.

We will now discuss some observations on a magnon sideband in a real crystal, and compare the results with the magnon sideband calculated using eqn. II.63.

Many antiferromagnetic insulators have been found to exhibit magnon sideband behaviour. A good review of the observations of such crystals is given by Sell (1968), and also by Eremenko and Belyaeva (1969), and studies continue up to the present. The two most popular crystals for these studies are MnF_2 and $RbMnF_3$. We present an analysis of our calculations based on the observations of $RbMnF_3$.

$RbMnF_3$ has a perovskite structure as shown in fig. II.2 with each magnetic ion at the corners of a simple cubic lattice. The lattice parameter is $a = 4.26$ Å (Stokowski, Sell and Guggenheim 1971), the crystal being very highly isotropic, with a negligible anisotropy field (Elliott and others 1968). The magnetic properties of the Mn^{2+} ion are well summarised by Richards and Brya (1974) and Fujiwara, Gebhardt, Petanides and Tanabe (1972) who also discuss the temperature dependence of magnon sidebands. The Néel temperature is $83K$. In fig. II.3 we show the Brillouin zone of the crystal, with some important symmetry points (after Eremenko, Novikov and Petrov 1974).

Richards and Brya (1974) give the value of the nearest neighbour exchange integral in $RbMnF_3$ as $2J = 4.7$ cm^{-1} with an uncertainty of ± 0.25 cm^{-1} at $300K$, a value which agrees well with many other authors. As pointed out by Srivastava and Stevenson (1972), for example, the next nearest neighbour exchange integral is 0 ± 0.14 cm^{-1} (for $2J_2$) and hence negligible. The anisotropy field is also negligible. Using the value of $2J$ given, the maximum magnon energy may be obtained from the expression for the perovskite magnon dispersion of

$$\varepsilon(k) = \varepsilon_0 \left[1 - \frac{1}{9} \left(\cos k_x a + \cos k_y a + \cos k_z a \right)^2 \right]^{\frac{1}{2}},$$

$$\varepsilon_0 = 12JS \qquad\qquad\qquad \text{II.65}$$

which, for a ground state spin of $\frac{5}{2}$ gives a value for ε_0 of 71 cm^{-1}
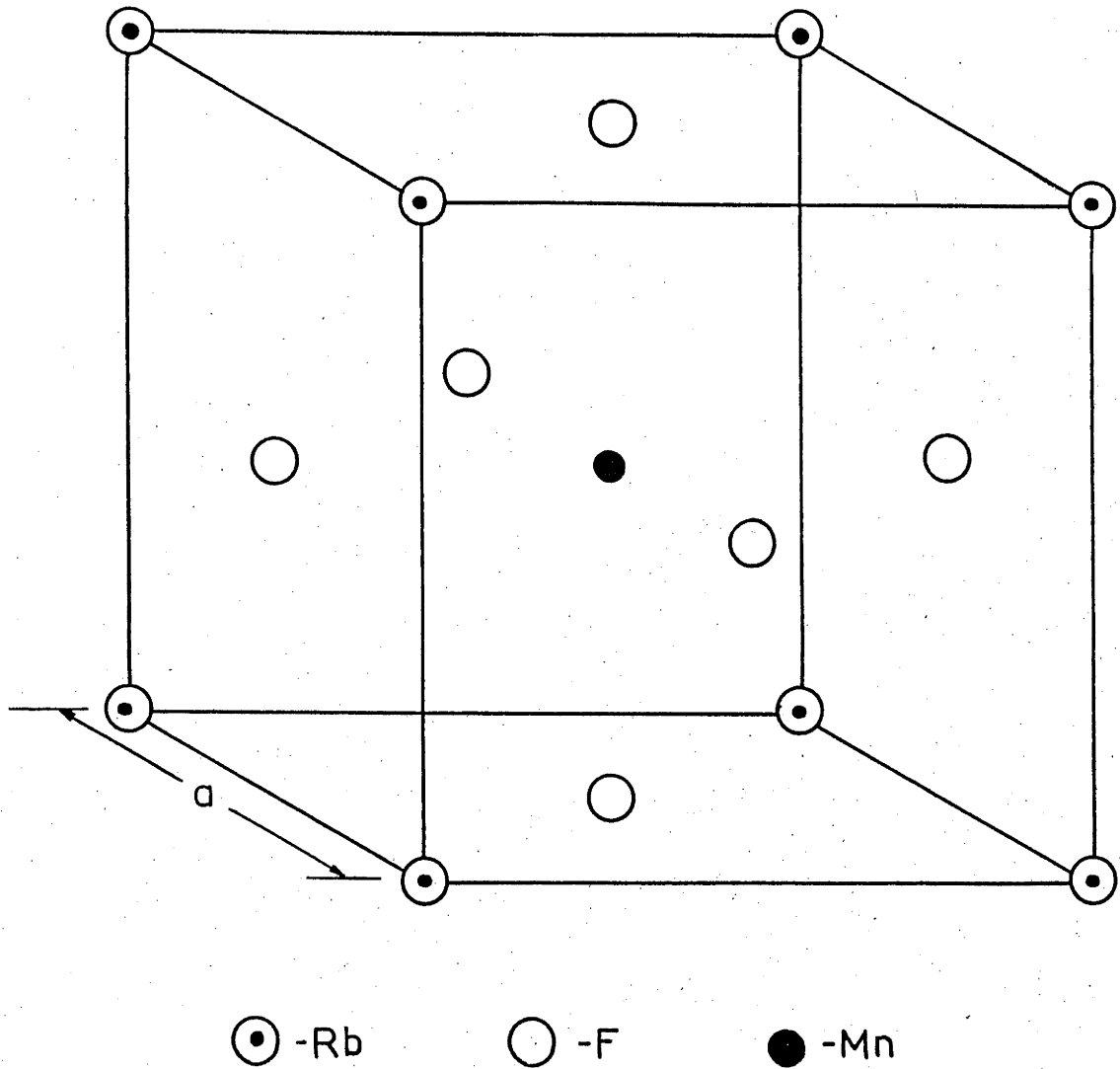
FIGURE II.2. Unit cell of the perovskite $RbMnF_3$. The Rb ions appear at the cube vertices, Mn ions at the body centre of the cube, and F ions at the centre of the cube faces. The magnetic Mn^{2+} ions form a simple cubic structure with lattice parameter a .
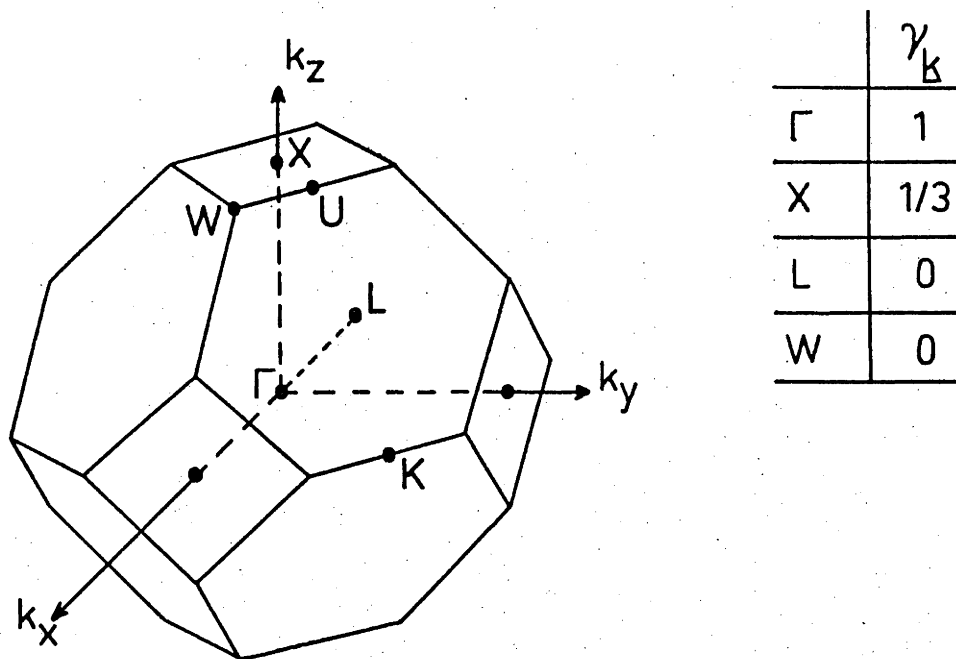
FIGURE II.3. Brillouin zone of antiferromagnetic perovskite $RbMnF_3$, with values of the function γ_k given for some symmetry points of the zone (after Eremenko, Novikov and Petrov 1974).

with the limits on $2J$ giving a range from 67 to 74 cm^{-1} . Hence one

would expect the magnon sideband cut-off to have a value near this, though

Srivastava and Stevenson (1972) point out that the uncertainty in the next

nearest neighbour exchange integral of $2J_2 = \pm.14$ cm^{-1} could allow ε_0 to

lie within the range 55 to 89 cm^{-1} which would account for the variation

in the value of the cut-off observed for various transitions in $RbMnF_3$

with a ground state spin of 5/2 .

From eqn. II.63 the predicted magnon sideband shape for a transition in

$RbMnF_3$ will be given very closely by the pure crystal magnon density of

states. The latter is shown in fig. II.4, for the range normalised to the

interval [0, 1] . Note the cusp point at $\sqrt{\frac{8}{9}}$ due to symmetry point X

of the first Brillouin zone (fig. II.3) and the divergence at the high

energy end of the band, due to the symmetry points L and W in the

Brillouin zone.

From fig. II.4 we would expect the magnon sideband to have its peak at

the cut-off point, and to have a width which is approximately $\left(1 - \sqrt{\frac{8}{9}}\right)$ th

of the distance between the parent exciton frequency and the cut-off

frequency. This sort of behaviour has been measured for example by

Stevenson (1966) for the ${}^6A_{1g}\left({}^6S\right) \rightarrow {}^4E_g\left({}^4G\right)$ transition which has also been

studied in some detail by Srivastava and Stevenson (1972) and Eremenko,

Novikov and Petrov (1974). The relevant curve of Stevenson (1966) is shown

in fig. II.5 with the calculated magnon sideband superimposed for comparison,

with the absorption scale chosen arbitrarily to give a reasonable fit. The

experimental curve has been greatly expanded and so is not considered to be

very accurate, but is merely intended for comparison. It will be seen that

the general shape of the experimental curve is reproduced, though the curve

is much smaller near the top edge of the band. This may be a real effect due
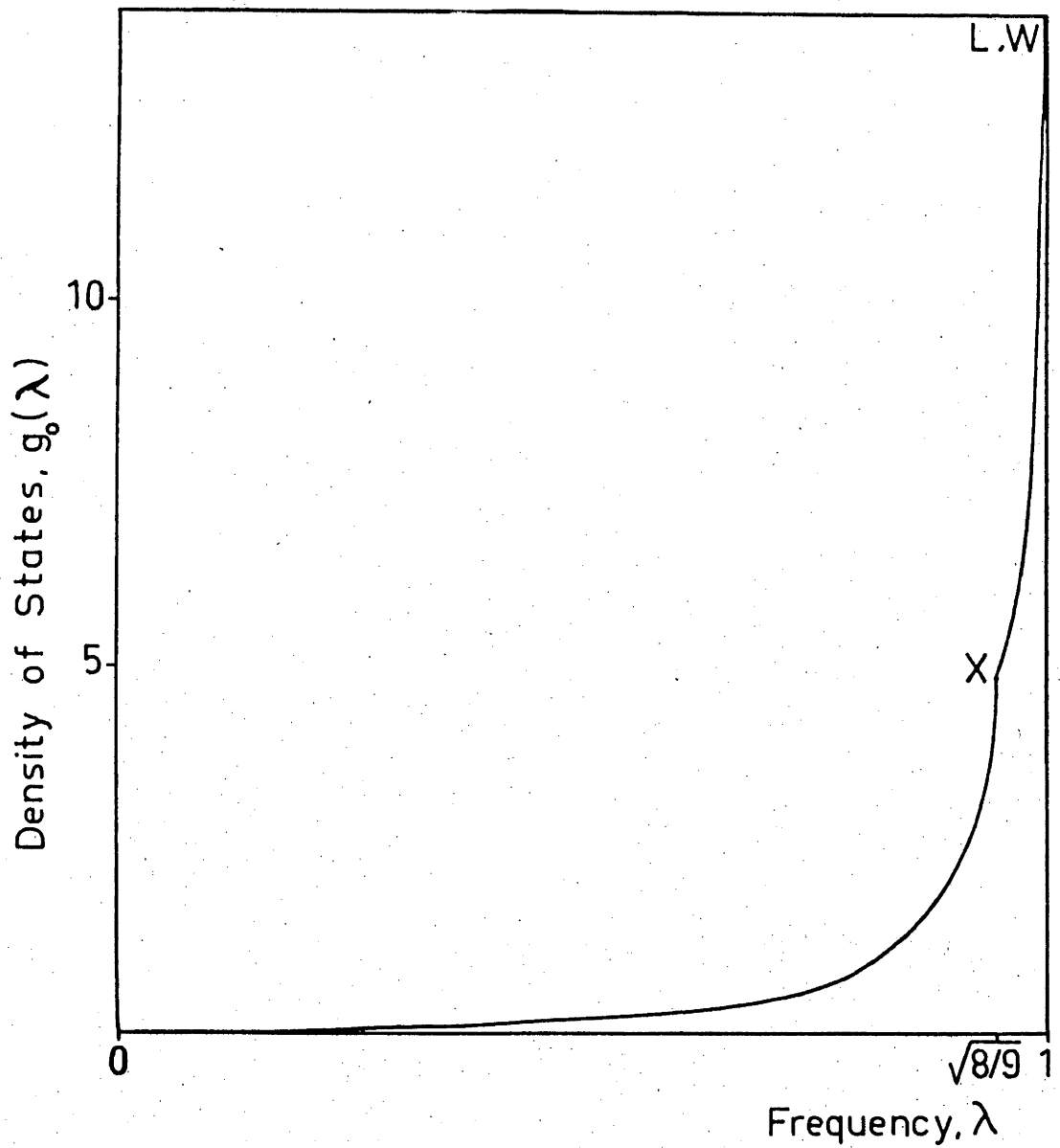
FIGURE II.4. Plot of the pure crystal magnon density of states for an antiferromagnetic perovskite crystal. The frequency has been normalised to the range [0, 1]. The calculated magnon sideband lineshape is a very good approximation to this curve.
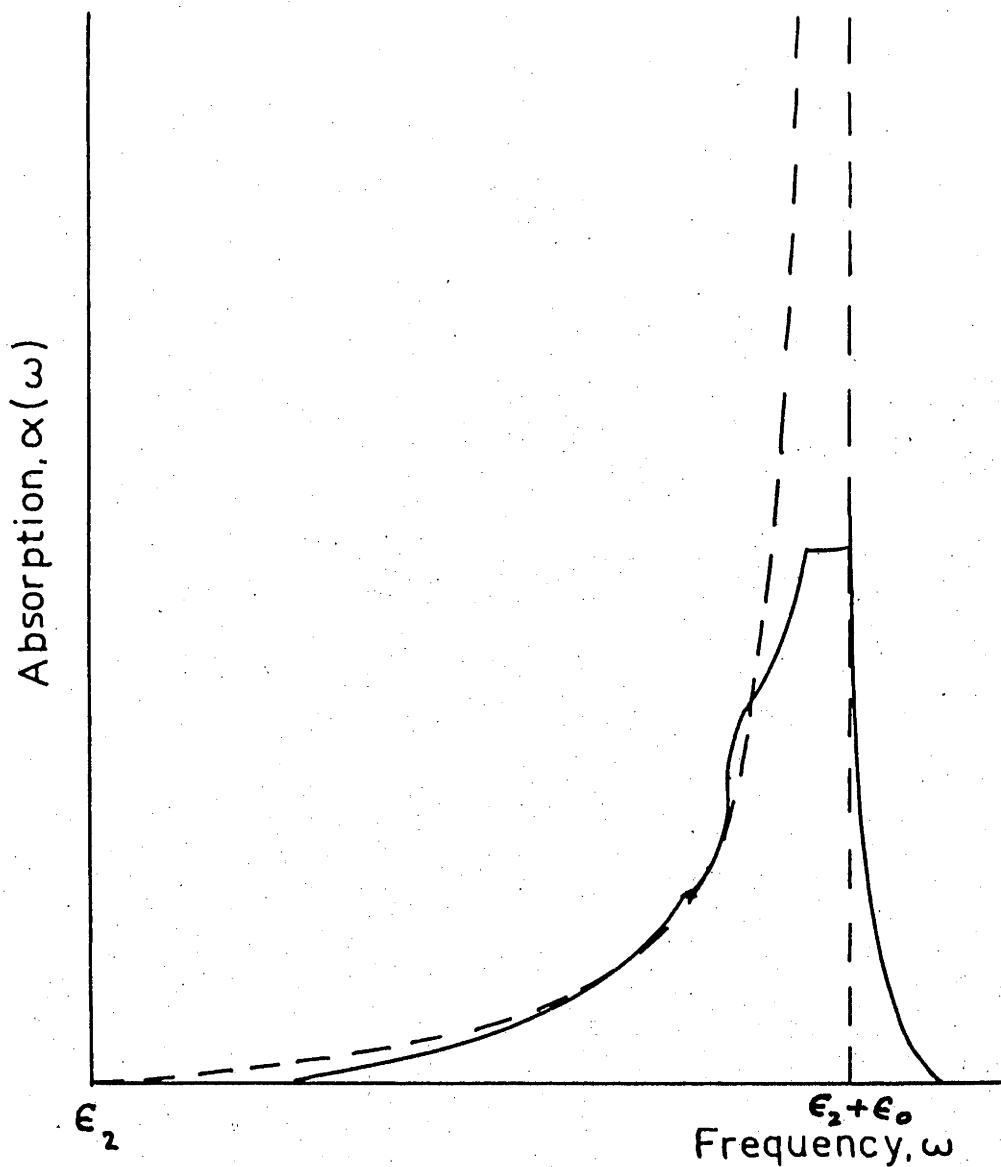
FIGURE II.5. Comparison of the (approximate) observed magnon sideband

lineshape of the $^6A_{1g}(^6S) \rightarrow {}^4E_g(^4G)$ transition in $RbMnF_3$

observed by Stevenson (1966) (solid curve), with the calculated

magnon sideband absorption with parameters chosen to give a

reasonable fit (dashed curve). *Experimentally determined

values of exciton energy and high-energy

cut-off are*

$$\epsilon_2 = 25\ 148\ cm^{-1},$$

$$\epsilon_2 + \epsilon_0 = 25\ 228\ cm^{-1}\ (Srivastava\ \&$$

$$Stevenson,\ 1972)$$

to the imperfection in describing the magnon energy by the form of eqn. II.65, or it may be due to experimental problems of resolution (or both).

It is observed experimentally that as the temperature is increased, the maximum of the sideband moves away from the edge of the band (Srivastava and Stevenson 1972, Srivastava, Stevenson and Linz 1973). Thus one possible explanation for the shift of the maximum of the sideband from the band edge may be due to its temperature dependence, which we have made no attempt to describe here. Parkinson and Loudon (1968) on the other hand state that the shift exists even at temperatures close to zero and is due to the effect of the exciton-magnon interaction. This view is supported by Eremenko, Novikov and Petrov (1974). A further alternative explanation is discussed in chapter IV where we point out that it may be possible to explain the observed shift by taking into account a small second nearest neighbour interaction, or by otherwise making the magnon energy, eqn. II.65 more realistic. See also the footnote on page 39.

CHAPTER III

MAGNON SIDEBANDS IN CRYSTALS WITH SPIN IMPURITIES

We now turn to the problem of the effect of spin impurities on the spectrum of an insulator in the region of its magnon sidebands. The problem has been treated for an antiferromagnet previously by Parkinson (1969a, 1969b) as an extension of the work of Parkinson and Loudon (1968). As noted by Parkinson (1969a) the theory of a substitutional impurity is very similar to that of a magnon sideband. This will be borne out by the great similarity between the results of this chapter and those of chapter II. The theory employed by Parkinson (1969b) is well presented in the review article of Elliott, Krumhansl and Leath (1974).

This chapter is divided up as follows: In the first section we present the model calculation of magnon sidebands of a ferromagnet with impurity, and then give an example for a one-dimensional crystal. We also consider the effects of an impurity on the magnon sideband in EuO which was calculated for the pure crystal in section II.1, after a general discussion of the effects of an impurity on the magnon sideband. Section III.2 contains the corresponding impurity calculation for an antiferromagnetic crystal, and the results are illustrated by a numerical example of a substitutional Ni^{2+} impurity in the $RbMnF_3$ crystal described in section II.2.

III.1 Substitutional Impurity in a Ferromagnet: Magnon Sidebands

There have not been any reported observations of the effects of a substitutional impurity on magnon sidebands in a ferromagnetic insulator. The calculations of this section are entirely predictive. We present the calculations as a preliminary stage to discussing the impure antiferro-magnetic crystal, as an aid to understanding the phenomena involved, and to

demonstrate the adaptability of the method prescribed by the model to several of the magnetically ordered states of a crystal.

The model Hamiltonian for an impure ferromagnet was discussed in section I.3, and is taken as eqn. I.39, that is

$$H^{(F)} = \sum_k \varepsilon(k) a_k^+ a_k + \varepsilon_2 \sum_k b_k^+ b_k + g \sum_k \left(a_k^+ b_k + b_k^+ a_k \right) + \gamma \sum_{k,k'} a_k^+ a_{k'}, \quad \text{III.1}$$

where the magnon dispersion is given by

$$\varepsilon(k) = 2|J|Sz\left(1-\gamma_k\right) + |J|S^2 \rho z , \quad \text{III.2}$$

$$\gamma_k = \frac{1}{z} \sum_{[\Delta]} e^{ik.\Delta} , \quad \text{III.3}$$

$$\rho = (J'S'-JS)/JS \quad \text{III.4}$$

for an impurity with spin S' and nearest neighbour exchange integral J' in a host lattice whose ions have spin S and exchange integral J. The operators a_k^+, b_k^+ represent creation operators of magnons and excitons, respectively, with wavenumber k. The sum over Δ in eqn. III.3 is over the nearest neighbours of any magnetic ion in the crystal. Note the shift in the magnon-energy eqn. III.2 due to the impurity term $|J|S^2\rho z$. This causes a shift in energy of the overall spectrum but will not alter its shape.

The perturbation on the crystal due to the applied field is assumed to couple only to the pure host excitations and is given by eqn. I.8 as

$$H_{\text{pert}}^{(F)} = l \sum_k \left(a_k^+ b_k^+ + a_k b_k \right) . \quad \text{III.5}$$

To calculate the magnon sideband in the absorption spectrum of the crystal, we write the crystal Hamiltonian eqn. III.1 in matrix form as

$$H^{(F)} = [a^+;b^+]\begin{bmatrix} \hat{A} & \hat{B} \\ \hat{B} & \hat{D} \end{bmatrix}\begin{bmatrix} a \\ b \end{bmatrix} \quad \text{III.6}$$

where a^+, b^+ etc. are as given in section II.1, e.g.

$$a^+ = [a_{k_1}^+, \ldots, a_{k_N}^+] .$$

Submatrices $\hat{B}$ and $\hat{D}$ are assumed to be unaffected by the impurity, so

$$(A)_{ij} = \varepsilon(k_i)\delta(k_i, k_j) + \gamma \, , \qquad \qquad \text{III.7}$$

$$(B)_{ij} = g\delta(k_i, k_j) \, , \qquad \qquad \text{III.8}$$

$$(D)_{ij} = \varepsilon_2\delta(k_i, k_j) \, . \qquad \qquad \text{III.9}$$

The matrices $\hat{A}$, $\hat{B}$, and $\hat{D}$ still commute, but $\hat{A}$ is no longer diagonal. We proceed by performing the diagonalisation of $\hat{A}$ and then diagonalising the full matrix of eqn. III.6 by treating it as a 2×2 matrix, as before. The diagonalisation of the Hamiltonian eqn. III.6 is thus a two-stage procedure. We treat here the case of a finite crystal with N atoms, where N is large. The problem of an infinite lattice is discussed in appendix 4.

The secular equation for the eigenvalues λ of $\hat{A}$ is given by the determinant of $\hat{A} - \lambda\hat{I}$ which is

$\det(\hat{A}-\lambda\hat{I}) =$

$$= \prod_i \left(\varepsilon(k_i)-\lambda\right) \begin{vmatrix} 1 + \dfrac{\gamma}{\varepsilon_1-\lambda}, & \dfrac{\gamma}{\varepsilon_1-\lambda} & , \cdots, & \dfrac{\gamma}{\varepsilon_1-\lambda} \\[2ex] \dfrac{\gamma}{\varepsilon_2-\lambda} & , 1 + \dfrac{\gamma}{\varepsilon_2-\lambda}, & \cdots, & \dfrac{\gamma}{\varepsilon_2-\lambda} \\[2ex] \vdots & & & \\[1ex] \dfrac{\gamma}{\varepsilon_N-\lambda} & , & \cdots & , 1 + \dfrac{\gamma}{\varepsilon_N-\lambda} \end{vmatrix}$$

$$= \prod_i \left(\varepsilon(k_i)-\lambda\right)\left(1 + \gamma \sum_i \dfrac{1}{\varepsilon(k_i)-\lambda}\right) \begin{vmatrix} 1 & 1 & \cdots & 1 \\[2ex] \dfrac{\gamma}{\varepsilon_2-\lambda}, & 1 + \dfrac{\gamma}{\varepsilon_2-\lambda}, & \cdots, & \dfrac{\gamma}{\varepsilon_2-\lambda} \\[2ex] \vdots & & & \\[1ex] \dfrac{\gamma}{\varepsilon_N-\lambda}, & & \cdots & , 1 + \dfrac{\gamma}{\varepsilon_N-\lambda} \end{vmatrix}$$

$$= \prod_k \left(\varepsilon(k)-\lambda\right)\left(1 + \gamma \sum_k \dfrac{1}{\varepsilon(k)-\lambda}\right) \qquad \qquad \text{III.10}$$

performing row operations on the determinant. The pure crystal eigenvalues are simply $\varepsilon(k)$, given by the first term of eqn. III.10. Hence the impure crystal eigenvalues satisfy the secular equation

$$\mathcal{D}(\lambda) = 1 + \gamma \sum_k \frac{1}{\varepsilon(k)-\lambda} = 0 \ .$$

The eigenvectors of $\hat{A}$ are obtained in the usual manner from the equation $(\hat{A}-\lambda\hat{I})T = 0$, giving the relation

$$T_\lambda(k_i) = \frac{\varepsilon(k_j)-\lambda}{\varepsilon(k_i)-\lambda} \, T_\lambda(k_j) \ .$$

III.12

When the eigenvectors are properly normalised, one obtains the eigenvector T_λ with k_ith component as

$$T_\lambda(k_i) = \frac{1}{N_\lambda} \frac{1}{\varepsilon(k_i)-\lambda}$$

III.13

where

$$N_\lambda^2 = \sum_k \left(\frac{1}{\varepsilon(k)-\lambda} \right)^2$$

III.14

is the squared normalisation constant. The matrix $\hat{T}$ whose columns are given by T_λ will then diagonalise the matrix $\hat{A}$. The crystal Hamiltonian may then be written

$$H^{(F)} = [a^+;b^+]_{\hat{T}} \begin{bmatrix} \hat{\Lambda} & \hat{B} \\ \hat{B} & \hat{D} \end{bmatrix} \hat{T}^+ \begin{bmatrix} a \\ b \end{bmatrix}$$

III.15

where $\hat{\Lambda}$ is given by

$$(\Lambda)_{ij} = \lambda_i \delta(i, j)$$

III.16

and

$$\hat{T} = \begin{bmatrix} \hat{T} & 0 \\ 0 & \hat{T} \end{bmatrix}$$

for λ_i the ith eigenvalue of matrix $\hat{A}$.

Treating the matrix in eqn. III.15 as a 2×2 matrix one obtains the eigenvalues of $H^{(F)}$ as

$$\lambda^{\pm}(\lambda) = \frac{\varepsilon_2 + \lambda}{2} \pm \left[\left(\frac{\varepsilon_2 - \lambda}{2}\right)^2 + g^2\right]^{\frac{1}{2}} \qquad \text{III.17}$$

and the matrix U which diagonalises the matrix in eqn. III.15 as

$$\hat{U} = \begin{bmatrix} \hat{u}_1 & \hat{u}_2 \\ \hat{u}_3 & \hat{u}_4 \end{bmatrix} \qquad \text{III.18}$$

where

$$(u_1)_{ij} = [2Y(Y-X)]^{-\frac{1}{2}} \delta(i, j) , \qquad \text{III.19}$$

$$(u_2)_{ij} = [2Y(Y+X)]^{-\frac{1}{2}} \delta(i, j) , \qquad \text{III.20}$$

$$(u_3)_{ij} = -[(Y-X)/2Y]^{\frac{1}{2}} \delta(i, j) , \qquad \text{III.21}$$

$$(u_4)_{ij} = [(Y+X)/2Y]^{\frac{1}{2}} \delta(i, j) \qquad \text{III.22}$$

for the λ-dependent functions

$$X = (\varepsilon_2 - \lambda)/2g , \qquad \text{III.23}$$

$$Y = [X(\lambda)^2 + 1]^{\frac{1}{2}} . \qquad \text{III.24}$$

Then the crystal Hamiltonian, fully diagonalised, is given by

$$H = \begin{bmatrix} a;b \end{bmatrix} \hat{T}\hat{U} \begin{bmatrix} \lambda^-(\lambda_1) & & & & & \\ & \ddots & & & 0 & \\ & & \lambda^-(\lambda_N) & & & \\ \hline & & & \lambda^+(\lambda_1) & & \\ & 0 & & & \ddots & \\ & & & & & \lambda^+(\lambda_N) \end{bmatrix} \hat{U}^+\hat{T}^+ \begin{bmatrix} a \\ b \end{bmatrix}$$

$$= \sum_{\lambda} \left(\lambda^-(\lambda) H_{\lambda}^+ H_{\lambda} + \lambda^+(\lambda) N_{\lambda}^+ N_{\lambda}\right) \qquad \text{III.25}$$

where the operators for which the Hamiltonian is diagonal, H_{λ}, N_{λ} , are

defined by

$$\begin{bmatrix} H \\ N \end{bmatrix} = \hat{U}^+\hat{T}^+ \begin{bmatrix} a \\ b \end{bmatrix} \qquad \text{III.26}$$

or

$$H_\lambda = \frac{1}{N_\lambda} [2Y(Y-X)]_\lambda^{-\frac{1}{2}} \sum_k \frac{a_k}{\varepsilon(k)-\lambda} - \frac{1}{N_\lambda} [(Y-X)/2Y]_\lambda^{\frac{1}{2}} \sum_k \frac{b_k}{\varepsilon(k)-\lambda} , \qquad \text{III.27}$$

$$N_\lambda = \frac{1}{N_\lambda} [2Y(Y+X)]_\lambda^{-\frac{1}{2}} \sum_k \frac{a_k}{\varepsilon(k)-\lambda} + \frac{1}{N_\lambda} [(Y+X)/2Y]_\lambda^{\frac{1}{2}} \sum_k \frac{b_k}{\varepsilon(k)-\lambda} . \qquad \text{III.28}$$

Note that in the limit of $g \to 0$, we have that $\lambda^+ \to \varepsilon_2$, $\lambda^- \to \lambda$ so

that again we have an exciton-like branch represented by the operators N_λ

and a magnon-like branch represented by H_λ. The effect of the impurity

is to alter the magnitude of the magnon eigenvalues from $\varepsilon(k)$. We

illustrate this fact by giving in fig. III.1 a schematic plot of the one-

dimensional crystal function $\sum_k \frac{1}{\varepsilon(k)-\lambda}$ as a function of energy, and also

show $-\frac{1}{\gamma}$, the impurity-dependent part. The intersections of the two

curves represent solutions of the secular equation III.11.

It will be seen from fig. III.1 that for the contribution of the

impurity, γ, going to zero the roots of $\mathcal{D}(\lambda)$ correspond to the values of

$\varepsilon(k)$. For a finite γ, however, the roots of the equation are at higher

energies than the values of $\varepsilon(k)$, by an amount which is a function of

$\frac{1}{\gamma}$. Note also that there is a root which lies outside the pure crystal

range of values of $\varepsilon(k)$, i.e. outside the magnon band. For large γ,
this "local mode" may be far removed from the magnon band.* The local mode
will be seen to occur for both positive and negative values of γ being on
the high energy side of the band for $\gamma > 0$ and on the low energy side for
$\gamma < 0$ for $|\gamma|$ sufficiently large. Note also that as $\gamma \to 0$ the local
modes approach the edges of the band.

For an infinite crystal the discrete roots of fig. III.1 merge into a
continuous band, described by the density of states. The density of states
will be perturbed by the impurity as it is in the discrete case. The
behaviour of the local mode will be very similar to that of the discrete

---

* Since it will be shown later in this section that the real part of $\mathcal{D}(\lambda)$
vanishes within the band for a one-dimensional crystal, such a crystal can
have no resonance modes. The existence criteria for resonant modes in three-
dimensional crystals is discussed near the end of this section.
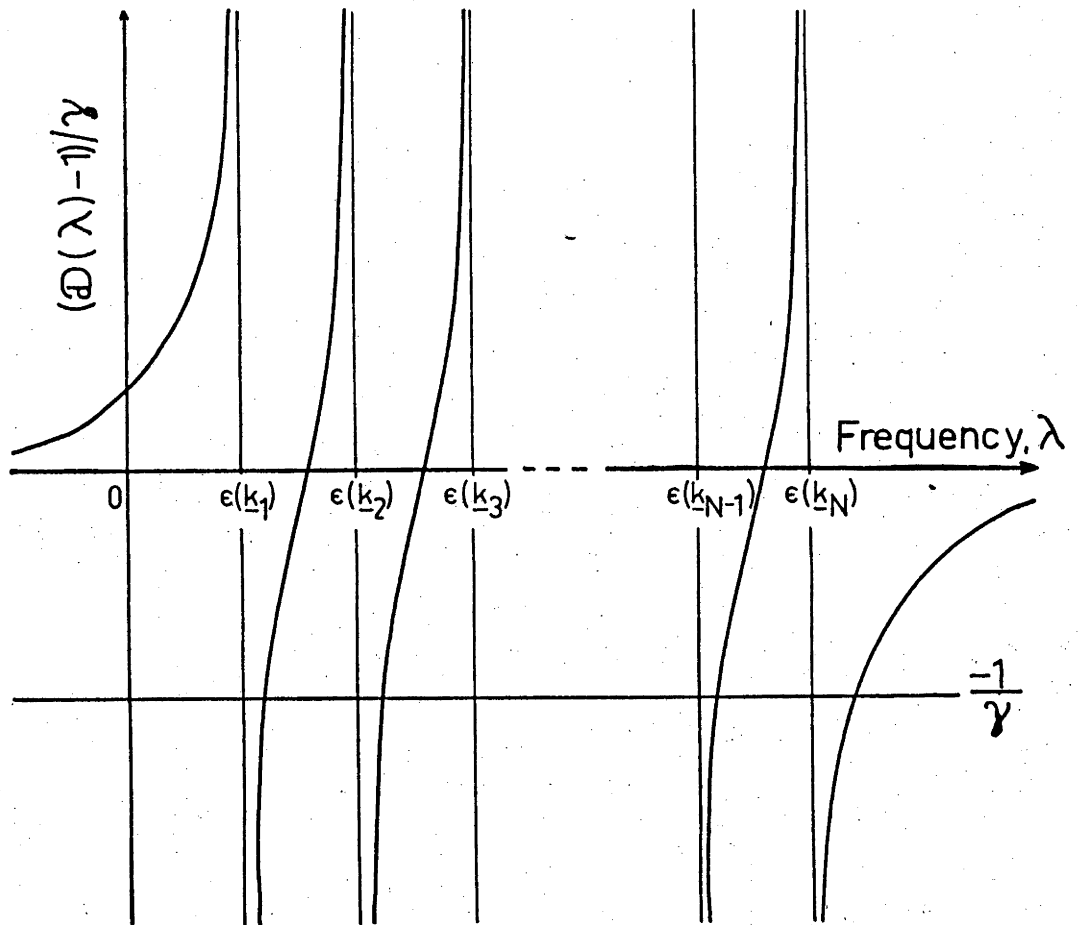
FIGURE III.1. Illustration of the properties of the secular function
$\mathcal{D}(\lambda)$.

crystal case. We discuss the aspects of an infinite crystal calculation in more detail in appendix 4. Maradudin, Montroll and Weiss (1963) have discussed vibrational density of states of the one-dimensional infinite crystal.

The commutation rules for H_λ and N_λ follow from the boson commutation rules of a_k and b_k . For example

$$[H_\lambda, H_{\lambda'}^+] =$$

$$= \frac{1}{N_\lambda N_{\lambda'}} \left\{ \left[4Y(\lambda)Y(\lambda') \left(Y(\lambda)-X(\lambda)\right) \left(Y(\lambda')-X(\lambda')\right) \right]^{-\frac{1}{2}} \sum_{kk'} \frac{\delta(k,k')}{\left(\epsilon(k)-\lambda\right)\left(\epsilon(k')-\lambda'\right)} \right.$$

$$\left. + \left[\left(Y(\lambda)-X(\lambda)\right) \left(Y(\lambda')-X(\lambda')\right) / \left(4Y(\lambda)Y(\lambda')\right) \right]^{\frac{1}{2}} \sum_{kk'} \frac{\delta(k,k')}{\left(\epsilon(k)-\lambda\right)\left(\epsilon(k')-\lambda'\right)} \right\}$$

$$= \delta(\lambda, \lambda') \left[\frac{Y+X}{2Y} + \frac{Y-X}{2Y} \right] = \delta(\lambda, \lambda') \qquad\qquad \text{III.29}$$

since

$$\sum_k \frac{1}{\left(\epsilon(k)-\lambda\right)\left(\epsilon(k)-\lambda'\right)} = \frac{1}{\lambda-\lambda'} \sum_k \left(\frac{1}{\epsilon(k)-\lambda} - \frac{1}{\epsilon(k)-\lambda'} \right) , \quad \lambda \neq \lambda'$$

$$= 0$$

from the secular equation, III.11, and for $\lambda = \lambda'$ we get $N(\lambda)^2$. Similarly,

$$[N_\lambda, N_{\lambda'}^+] = \delta(\lambda, \lambda') \qquad\qquad \text{III.30}$$

and all other commutators are zero. Hence H and N also satisfy boson commutation rules and so may be considered to represent new types of excitations in the crystal.

The perturbation Hamiltonian, eqn. III.5 is now written in terms of H_λ and N_λ , making use of the fact that

$$\frac{1}{N_\lambda N_{\lambda'}} \sum_k \frac{1}{\epsilon(k)-\lambda} \frac{1}{\epsilon(k)-\lambda'} = \delta(\lambda, \lambda') , \qquad\qquad \text{III.31}$$

as

$$H^{(F)}_{\text{pert}} = \iota \sum_\lambda \left\{ \frac{1}{2Y(\lambda)} \left(N^+_\lambda N^+_\lambda + N_\lambda N_\lambda - \left(H^+_\lambda H^+_\lambda + H_\lambda H_\lambda \right) \right) + \frac{X(\lambda)}{Y(\lambda)} \left(H^+_\lambda N^+_\lambda + H_\lambda N_\lambda \right) \right\} . \qquad \text{III.32}$$

Note the similarity of III.32 with the pure crystal form of the perturbation Hamiltonian operators, eqn. II.19.

We may now evaluate the non-zero Green functions which occur in the expression for the optical absorption, section I.4 in a similar manner to those of section II.1, making use of the boson commutation rules for H_λ and N_λ . We obtain

$$\langle\langle H_\lambda H_\lambda , H^+_{\lambda'} H^+_{\lambda'} \rangle\rangle = \frac{\delta(\lambda,\lambda')}{\hbar\omega - 2\lambda^-(\lambda)} , \qquad \text{III.33}$$

$$\langle\langle N_\lambda N_\lambda , N^+_{\lambda'} N^+_{\lambda'} \rangle\rangle = \frac{\delta(\lambda,\lambda')}{\hbar\omega - 2\lambda^+(\lambda)} , \qquad \text{III.34}$$

$$\langle\langle H_\lambda N_\lambda , H^+_{\lambda'} N^+_{\lambda'} \rangle\rangle = \frac{\delta(\lambda,\lambda')}{\hbar\omega - (\lambda^+ + \lambda^-)}$$

$$= \frac{\delta(\lambda,\lambda')}{\hbar\omega - \left(\varepsilon_2 + \lambda\right)} \qquad \text{III.35}$$

which are identical in form to the Green functions obtained in chapter II. Eqns. III.33 and III.34 will again give the absorption due to two-magnon and two-exciton excitations which are perturbed by the exciton-magnon interaction (whose strength is g) while eqn. III.35 gives the absorption of the magnon sideband, that is,

$$\alpha(\omega) \sim - \frac{\omega}{2} \operatorname{Im} \sum_\lambda \left[\frac{X(\lambda)}{Y(\lambda)} \right]^2 \frac{1}{\hbar\omega - \left(\varepsilon_2 + \lambda\right)}$$

$$\sim - \frac{\omega}{2} \sum_\lambda \frac{\left(\varepsilon_2 - \lambda\right)^2}{\left(\varepsilon_2 - \lambda\right)^2 + 4g^2} \, \delta\left(\hbar\omega - \left(\varepsilon_2 + \lambda\right) \right)$$

$$\sim -2\pi\omega \, \frac{\left(2\varepsilon_2 - \hbar\omega\right)^2}{\left(2\varepsilon_2 - \hbar\omega\right)^2 + 4g^2} \, g\left(\hbar\omega - \varepsilon_2\right) \qquad \text{III.36}$$

where we have made use of eqn. II.27 to take the imaginary part, and $g(\lambda)$ is the impure crystal magnon density of states, which is given by

$$g(\lambda) = -\frac{1}{\pi N} \text{ Im } \frac{d}{d\lambda} \ln D(\lambda) \qquad \text{III.37}$$

where N is the number of cells in the crystal. $D(\lambda)$ is the secular determinant of matrix $\hat{A}$, eqn. III.10,

$$D(\lambda) = D_0(\lambda)\mathcal{D}(\lambda) \qquad \text{III.38}$$

where $\mathcal{D}(\lambda)$ is given by eqn. III.11 and

$$D_0(\lambda) = \prod_k \left(\varepsilon(k)-\lambda\right) \qquad \text{III.39}$$

is the pure crystal secular function. Hence eqn. III.37 may be written

$$g(\lambda) = g_0(\lambda) + \Delta g(\lambda) \qquad \text{III.40}$$

for $g_0(\lambda)$ the pure crystal density of states, eqn. II.32. If we define a phase shift δ as

$$\tan \delta = -\frac{\text{Im } \mathcal{D}(\lambda)}{\text{Re } \mathcal{D}(\lambda)} \qquad \text{III.41}$$

it is readily shown (Callaway 1974, appendix 4) that the change in density of states due to the impurity is

$$\Delta g(\lambda) = -\frac{1}{\pi N} \frac{d\delta}{d\lambda} . \qquad \text{III.42}$$

This result is for a single impurity. For the case of n impurities, where n is sufficiently small so that the impurity ions do not interact with each other, the contribution from each impurity may be added, and

$$\Delta g(\lambda) = -\frac{c}{\pi} \frac{d\delta}{d\lambda} \qquad \text{III.43}$$

for concentration $c = \frac{n}{N}$ of impurities.

The g-dependent coefficient of the density of states of eqn. III.36 is identical with that occuring in chapter II. It is thus expected to have little effect on the sideband lineshape, as discussed there. We therefore ignore its effect in what follows.

We will now give a calculation of the magnon sideband in a one-dimensional ferromagnet. This example has been discussed by Richardson (1974) for a model which is somewhat different from that proposed here,

because of the form taken for the coupling of the crystal with the external field. While the model of Richardson (1974) predicts a lineshape due to an exciton-magnon interaction, it suffers from the limitation that it is unable to explain both the width of the sideband and its position with respect to the exciton energy ε_2 , because of the absence of magnon operators in the perturbing Hamiltonian. The present model therefore presents some improvement in describing observed magnon sidebands (see also appendix 1).

For a one-dimensional crystal the magnon energy is

$$\varepsilon(k) = \varepsilon_0(1 - \cos k)/2 + \alpha \qquad\qquad \text{III.44}$$

where

$$\varepsilon_0 = 4JSz , \qquad\qquad \text{III.45}$$

$$\alpha = JS^2\rho z , \qquad\qquad \text{III.46}$$

$$\rho = J'S'/JS - 1 . \qquad\qquad \text{III.47}$$

Since α has the effect of a constant shift of the spectrum by that amount, and does not affect the spectrum in any other way, we ignore it in the following analysis.

The secular determinant $\mathcal{D}(\lambda)$, eqn. III.11 may be integrated analytically if we change the sum to an integral (i.e. if the number of atoms in the crystal is infinite) giving*

$$\mathcal{D}(\lambda) = 1 + i\gamma\left[\left(\varepsilon_0-\lambda\right)\lambda\right]^{-\frac{1}{2}} \qquad\qquad \text{III.48}$$

for

$$\left(\varepsilon_0-\lambda\right)\lambda > 0 \qquad\qquad \text{III.49}$$

i.e. $0 < \lambda < \varepsilon_0$.

If λ lies outside the range III.49, $\mathcal{D}(\lambda)$ is purely real, but inside the range III.49 the real part of $\mathcal{D}(\lambda)$ is a constant. Hence local modes may occur outside the band whose range is eqn. III.49, but there can be no

---

* From eqn. III.36, the magnon sideband will have λ replaced by $\hbar\omega - \varepsilon_2$, that is the range of the sideband is $0 < \lambda-\varepsilon_2 < \varepsilon_0$.

resonance modes inside the band since the derivative of the real part vanishes in this region (see towards the end of this section for a more detailed analysis of resonant modes). Note that $\mathcal{D}(\lambda)$, whose imaginary part is proportional to the pure crystal density of states $g_0(\lambda)$, has square-root singularities at both edges of the band, eqn. III.49.

The change in the density of states due to the impurity is, from eqns. III.43 and III.48,

$$\Delta g(\lambda) = - \frac{c}{\pi} \frac{d\delta}{d\lambda} = - \frac{c}{2\pi} \gamma \frac{\varepsilon_0 - 2\lambda}{\left[(\varepsilon_0 - \lambda)\lambda + \gamma^2\right]\left[(\varepsilon_0 - \lambda)\lambda\right]^{\frac{1}{2}}} \qquad \text{III.50}$$

where from eqn. III.41,

$$\tan \delta = -\gamma\left[(\varepsilon_0 - \lambda)\lambda\right]^{-\frac{1}{2}} \qquad \text{III.51}$$

and c is the concentration of impurity. The pure crystal density of states $g_0(\lambda)$ is obtained from the imaginary part of $\mathcal{D}(\lambda)$, eqn. III.48 (making use of eqn. II.27) as

$$g_0(\lambda) = \frac{1}{\pi} \left[(\varepsilon_0 - \lambda)\lambda\right]^{-\frac{1}{2}} . \qquad \text{III.52}$$

The total density of states is thus

$$g(\lambda) = g_0(\lambda) + \Delta g(\lambda)$$

$$= \frac{1}{\pi} \left[(\varepsilon_0 - \lambda)\lambda\right]^{-\frac{1}{2}}\left\{1 - \frac{c\gamma}{2} \frac{(\varepsilon_0 - 2\lambda)}{(\varepsilon_0 - \lambda)\lambda + \gamma^2}\right\} \qquad \text{III.53}$$

which reduces to $g_0(\lambda)$ when the effect of the impurity, γ goes to zero, as required.

Note that when $\lambda = 0.5\varepsilon_0$, the change of density of states $\Delta g(\lambda)$ is zero for all values of γ . For $\lambda < 0.5\varepsilon_0$ the change of density of states is negative, and for $\lambda > 0.5\varepsilon_0$ it is positive (for $\gamma > 0$) . The effect of the impurity is thus to introduce some skewness to the symmetric pure crystal density of states $g_0(\lambda)$. It will be readily seen, in fact, that $\Delta g(\lambda)$ is antisymmetric about $\lambda = 0.5\varepsilon_0$.

Closer examination of the γ-dependence of the change of density of states reveals that eqn. III.50 as a function of γ is a peaked function, and hence the effect of γ on the density of states is not unique. That is, the amount of skewness introduced by γ for any one value of λ is not a unique function of γ, but there are in general two values of γ for which the density of states will be identical at a given distance from the centre of the band. For a given value of λ, $\Delta g(\lambda)$ will be largest when

$$\gamma = \left[(\varepsilon_0 - \lambda) \lambda \right]^{\frac{1}{2}} .$$

In any event, the change in the density of states within the band will be small because we have assumed the concentration of impurity, c, to be small. This is illustrated in fig. III.2 where we plot the total density of states for $\gamma = 0$ and $\gamma = 0.433\varepsilon_0$, a value of γ for which the overall skewness of the density of states is large.

When λ lies outside the range, eqn. III.49, $\mathcal{D}(\lambda)$ is purely real and the existence of local modes is possible. These will occur when $\mathcal{D}(\lambda)$ is zero for λ outside the band. That is, when

$$1 \mp \gamma \left[(\lambda - \varepsilon_0) \lambda \right]^{-\frac{1}{2}} = 0 \qquad\qquad \text{III.54}$$

i.e.

$$\lambda = \frac{\varepsilon_0}{2} \pm \sqrt{\frac{\varepsilon_0^2}{4} + \gamma^2} \qquad\qquad \text{III.55}$$

(the $-$ sign is for $\lambda > \varepsilon_0$, the $+$ sign for $\lambda < 0$ in eqn. III.55) which lie outside the band since $\gamma^2 > 0$. For γ going to zero, the local modes will both occur at the edges of the band. The situation is illustrated in fig. III.3 where we show the intersection of

$$R(\lambda) = \left[(\lambda - \varepsilon_0) \lambda \right]^{-\frac{1}{2}}$$

with $-1/\gamma$. The points of intersection define the local mode frequencies. Local modes at these frequencies are represented as delta functions whose height is proportional to the concentration c of impurity. Note that for
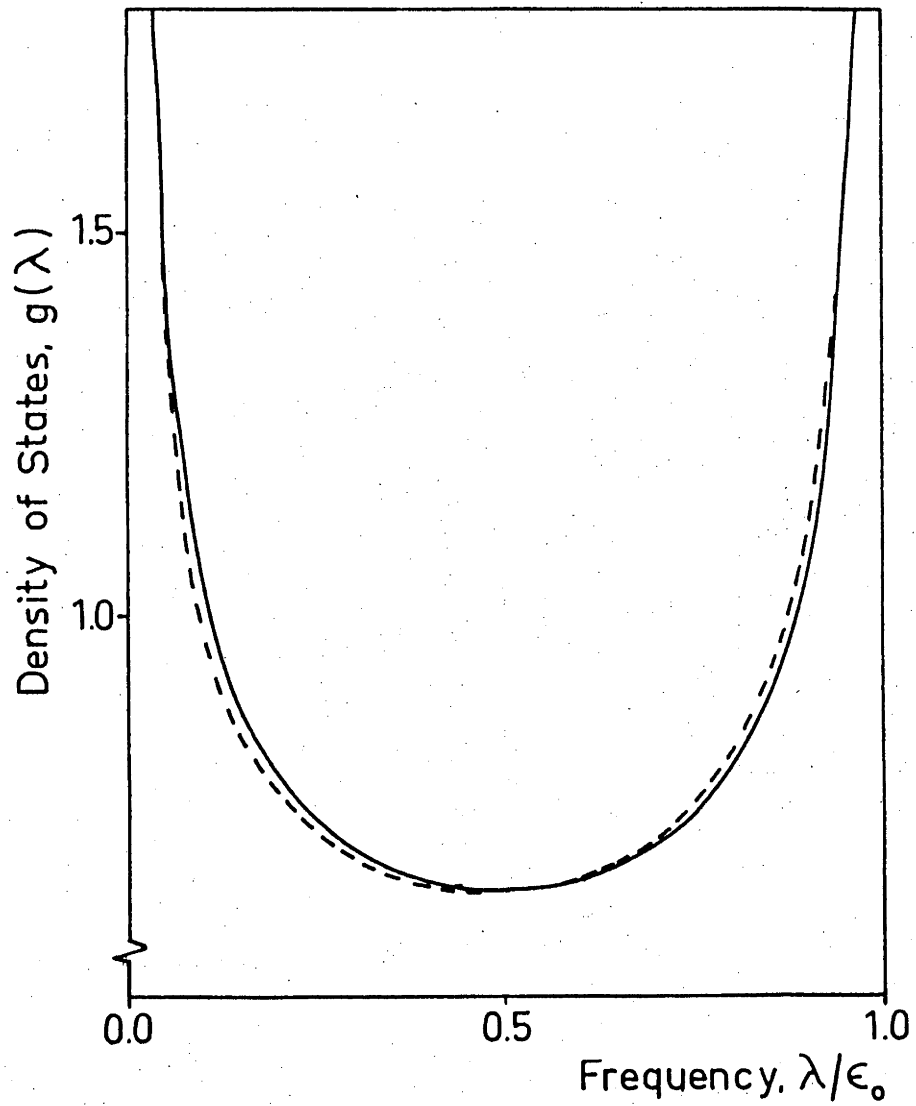
FIGURE III.2. Plot of the pure crystal density of states (solid curve) and impure crystal density of states for $\gamma/\varepsilon_0 = 0.433$ (dashed curve) for a one-dimensional crystal. Note the small amount of skewness introduced by the impurity despite a concentration $c = 0.1$ which is made large to demonstrate the effect.
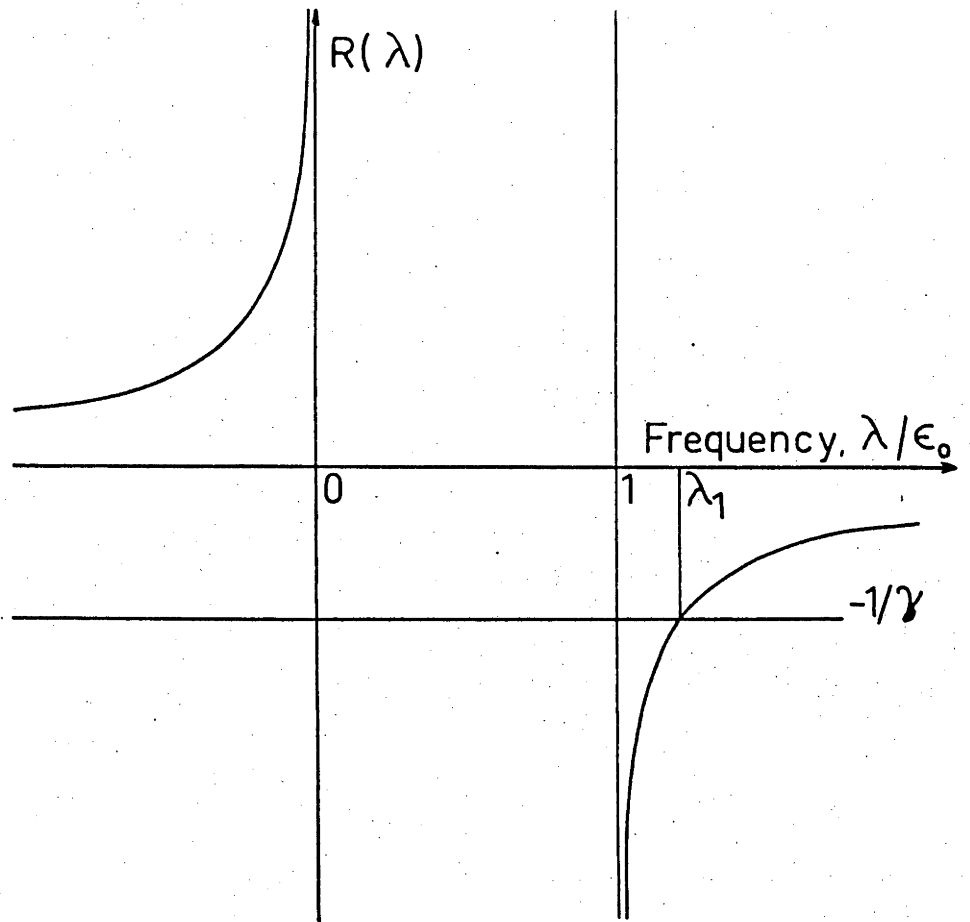
FIGURE III.3. Plot of the real part $R(\lambda)$ of the one-dimensional lattice Green function. The point λ_1 where the curve $-1/\gamma$ intersects $R(\lambda)$ defines the frequency of the local mode.

$\gamma < 0$ the local mode lies on the low energy side of the band, while for $\gamma > 0$ the local mode occurs on the high energy side of the band, both modes are removed from the band by the same amount for the same value of $|\gamma|$.

The effect of an impurity on a one-dimensional magnon sideband is to shift the density of states slightly so that for $\gamma > 0$, for example the magnon excitation modes are shifted from the low energies to higher ones within the band. The effect is small within the band. For all values of γ there will also be local modes which lie on one side of the band or the other depending on the sign of γ , both types of mode separated from the band by the same amount. The removal from the band of the local modes is a function of γ , and they merge with the edges of the band as γ goes to zero. These effects are illustrated in fig. III.1.

As pointed out in chapter I, Mermin and Wagner (1966) have proved that there is no ferromagnetic ground state in a one-dimensional crystal. There are, however, some antiferromagnetic crystals which exhibit one-dimensional ferromagnetic behaviour of their magnetic ions (Sorgen, Cohen and Makovsky 1974, for example) and a calculation such as the above may be useful if the interaction between chains of magnetic ions is small compared with the interaction within a row of the ions.

We now move to a more realistic calculation: that of a three-dimensional ferromagnet with an impurity. We will treat the same crystal as was used in the pure crystal calculation of section II.1, *EuO* . Unfortunately because of the lack of experimental work done on this crystal, there are no reports of the effects of impurities on the sideband. We will therefore study hypothetical cases which cover the various possibilities for the effect of an impurity predicted by the model. The magnon sideband is calculated using eqn. III.36 and so we must calculate the impurity density of states. We begin by writing the secular function $\mathcal{D}(\lambda)$ in its real and imaginary parts, making use of Dirac's relation

$$\lim_{\varepsilon \to 0^+} \frac{1}{x \pm i\varepsilon} = \frac{P}{x} \mp i\pi\delta(x) \qquad\qquad \text{III.56}$$

where P represents the principal part. Then

$$\mathcal{D}(\lambda) = 1 + \gamma R(\lambda) + i\pi\gamma g_0(\lambda) \qquad\qquad \text{III.57}$$

where $g_0(\lambda)$ is the pure crystal density of states, and $R(\lambda)$ is related

to $g_0(\lambda)$ by the Hilbert transform

$$R(\lambda) = \frac{P}{\pi} \int_0^1 \frac{g_0(\lambda')}{\lambda'-\lambda} \, d\lambda' \qquad\qquad \text{III.58}$$

for the density of states normalised to the range $(0, 1)$ *. The properties

of $-R(\lambda)$ have been discussed for a simple cubic ferromagnet by Callaway

(1964).

Calculations of the pure crystal density of states $g_0(\lambda)$ for an *fcc*

crystal have been reported in section II.1. An attempt has been made to

calculate $R(\lambda)$ from these calculations, and to obtain the impure magnon

density of states, eqn. III.37 by making use of the phase factor δ to obtain

the change in the density of states, eqn. III.43. The details of the

numerical analysis are presented in appendix 3.

We begin by considering how, in general, the impurity may affect the

spectrum. The discussion will apply to both the ferromagnetic case and the

antiferromagnetic one presented in the next section. The properties of the

spectra affected by the impurity which we enunciate here are general

properties of the model and will apply to any three-dimensional crystal

which has a Hamiltonian of the form discussed in this work.

The most important feature of the calculation of the change in the

spectrum due to spin impurities is the behaviour of the real part of the

lattice Green function $R(\lambda)$, eqn. III.58 both within and without the

pure crystal absorption band. We will begin by considering the behaviour

---

* $R(\lambda)$ is often defined to be the negative of this, then the sign of $R(\lambda)$
in eqn. III.57 is changed (Callaway 1974).

outside the band, where the imaginary part of the secular determinant, and

hence also the pure crystal density of states, are zero.

For frequencies outside the band, the impure crystal density of states

is zero except possibly for a number of discrete points, where it is

represented as a delta function whose intensity is proportional to the

impurity concentraction, c . Such states outside the band are called

local modes, and will occur at frequencies which are the solutions of the

equation

$$1 + \gamma R(\lambda) = 0 \ , \quad \lambda \ \ \text{outside band.} \qquad \text{III.59}$$

It is not always possible to find values of λ which satisfy eqn.

III.59, and we will now consider when a local mode is likely to occur. The

most straightforward way to determine if there are solutions of eqn. III.59

and what they are, is to consider the intersection of $R(\lambda)$ with $-1/\gamma$,

for λ outside the band. In this region $R(\lambda)$ will be monotonic on each

side of the band and there can be at most one local mode on either side of

the band.

In fig. III.4 we depict the curves $R(\lambda)$ and $-1/\gamma$ for various values

of γ . The calculation is for an *fcc* crystal like *EuO* . For $\gamma > 0$ (curve

①) the curves intersect at a point λ_1 on the high energy side of the band,

and hence there will be a local mode at this point. For γ small, λ_1 will

lie close to the band edge and may not be observable. For $\gamma < 0$ the

situation is interesting. For $1/|\gamma|$ smaller than the value of $R(\lambda)$ at

the lower band edge, R_1 (curve ②) we again find an intersection outside

the band, but this time on the low-energy side of the band. For $1/|\gamma|$

greater than R_1 (curve ③), however, there are no local modes, and the

problem of the existence of resonances arises for $1/|\gamma|$ lying between R_1

and R_2 . For $|\gamma|$ sufficiently small that $1/|\gamma|$ lies above R_2 , there

can be neither resonances nor local modes in the spectrum, which will then
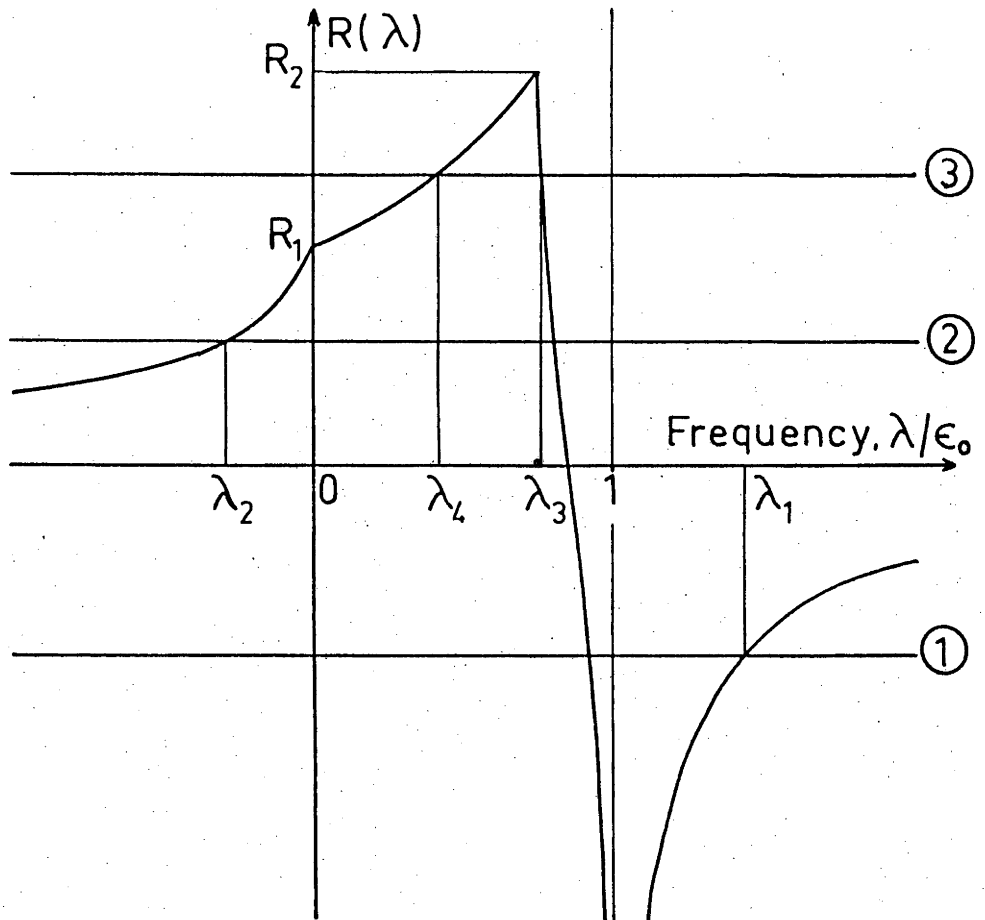
FIGURE III.4. Plot of the real part of the *fcc* lattice Green function both within and without the band $0 < \lambda < \varepsilon_0$. The curves labelled (1), (2) and (3) represent values of $-1/\gamma$ as described in the text.

not have any large changes over any region of the band due to the impurity.

When a local mode is present, since the total number of states of the system is unaltered by the impurity (Wolfram and Callaway 1963) the net change of the spectrum within the band is small in any given region as may be seen for example from fig. III.1 which illustrates that property of Rayleigh's theorems (Maradudin, Montroll, Weiss and Ipatova 1971). Hence when a local mode exists as it does for

$$\gamma > 0$$

and (see fig. III.4)

$$- \infty > \gamma > \frac{-1}{R_1} \qquad\qquad\qquad \text{III.60}$$

the change in the density of states within the band will be everywhere small, because of the small concentration c , and hence the in-band region will have no observable change made to it by the impurity.

When there can be no local modes, there is the possibility of a resonance mode within the band appearing. This may appear for

$$\frac{-1}{R_1} > \gamma > \frac{-1}{R_2} \; . \qquad\qquad\qquad \text{III.61}$$

(see fig. III.4). The resonance will occur at points which satisfy

$$1 + \gamma R(\lambda) = 0 \; , \quad \lambda \; \text{ inside band} \qquad\qquad \text{III.62}$$

if γ satisfies eqn. III.61 and also provided the change in the density of states is positive for λ satisfying eqn. III.62. The width of the resonance must also be small compared to the value of λ satisfying eqn. III.62 so the peak will have a large height and thus be observable despite the small impurity concentration. [Note the comparison with the one-dimensional model where $R(\lambda)$ is zero inside the band, and diverges as the band is approached from outside so that local modes will occur for all γ , fig. III.3.]

The nature of a resonance may be determined as follows: in appendix 4 we express the change in the density of states due to the impurity in the form

$$\Delta g(\lambda) = \gamma\pi \frac{g_0'(\lambda)\left(1+\gamma R(\lambda)\right)-\gamma\pi g_0(\lambda)R'(\lambda)}{\left(1+\gamma R(\lambda)\right)^2+\left(\pi\gamma g_0(\lambda)\right)^2} \qquad \text{III.63}$$

where the prime denotes differentiation with respect to λ. If $1 + \gamma R(\lambda)$ is small we may expand it in a Taylor series and retain only the first term, so

$$1 + \gamma R(\lambda) \simeq \gamma\left|\lambda - \lambda_0\right|R'(\lambda)$$

where the maximum value of the resonance occurs at $\lambda = \lambda_0$.

Then eqn. III.63 becomes, near a resonance,

$$\Delta g(\lambda) \simeq -\pi c \left(\frac{g_0(\lambda)}{R'(\lambda)}\right)_{\lambda=\lambda_0} \left[\left(\lambda-\lambda_0\right)^2+\left(\frac{\pi g_0(\lambda)}{R'(\lambda)}\right)^2_{\lambda=\lambda_0}\right]^{-1}$$

$$= - \frac{c\;\Gamma/2}{\left(\lambda-\lambda_0\right)^2+\Gamma^2/4} \qquad \text{III.64}$$

where the width of the resonance is described by (Callaway 1974)

$$\Gamma = 2\pi\;g_0(\lambda)/R'(\lambda)\big|_{\lambda=\lambda_0}\;. \qquad \text{III.65}$$

So near $\lambda = \lambda_0$, $\Delta g(\lambda)$ has a Lorentzian lineshape with a width determined by Γ, eqn. III.65. The change $\Delta g(\lambda)$ near λ_0 will be large only if Γ is small so that $\Delta g(\lambda)$ has a large narrow peak near $\lambda = \lambda_0$. The change in density of states must be positive (or one can have an "antiresonance") which will occur only if Γ is negative, from eqn. III.64. The conditions for a resonance near $\lambda = \lambda_0$ are then given by

$$\left|\Gamma\right| = 2\pi g_0(\lambda)/R'(\lambda) \ll 1\;,$$

$$\Gamma < 0\;. \qquad \text{III.66}$$

Of the two possible positions of a resonance λ_3 and λ_4 shown in fig. III.4 only at $\lambda = \lambda_3$ does $R(\lambda)$ have a negative slope thus permitting the second of the conditions eqn. III.66 to be satisfied. Thus only values of λ_3 which are greater than the cusp point (at $0.75\epsilon_0$ in fig. III.4) may

be considered for the position of a possible resonance.

For *fcc* crystals such as *EuO* we have plotted the mode lifetime $|\frac{1}{\Gamma}|$ vs $|\gamma|$ in fig. III.5 for γ satisfying eqn. III.61. For there to be a resonance we require the first of the inequalities III.66 to be satisfied, and hence $|\frac{1}{\Gamma}|$ must be much greater than unity. To the accuracy of the present calculations we find from fig. III.5 that a resonance is most likely to occur near where $R(\lambda) = R_2$ (fig. III.4). Since the lifetime in this region is only about 1.2 which is not much greater than unity, however, we therefore conclude that there will not appear a resonance mode in the magnon sideband of an *fcc* crystal even when γ satisfies eqn. III.61, under the assumptions of the present model and to within the accuracy of the numerical work. It is unlikely that the numerical differentiation is in error by orders of magnitude and the conclusion that a local mode will not occur is made with some confidence.

To summarise the results we expect from observations of the effect of a substitutional spin impurity on the *fcc* ferromagnet *EuO* , we expect that for $\gamma > 0$, that is, for the impurity-host exchange integral J' greater than the host-host exchange integral J in absolute magnitude* there will be a local mode on the high-energy side of the band whose separation from the band will be large for large γ and small for small γ . For γ negative but sufficiently large so that

$$1/|\gamma| < R_1 \hspace{4cm} \text{III.67}$$

(see fig. III.4) a local mode will appear on the low energy side of the band, approaching the band as $1/|\gamma|$ approaches R_1 . When local modes appear on either side of the band the density of states and hence the magnon sideband

---

* Note that antiferromagnetic coupling of the impurity is also possible, in which case γ will be negative for all possible values of J' .
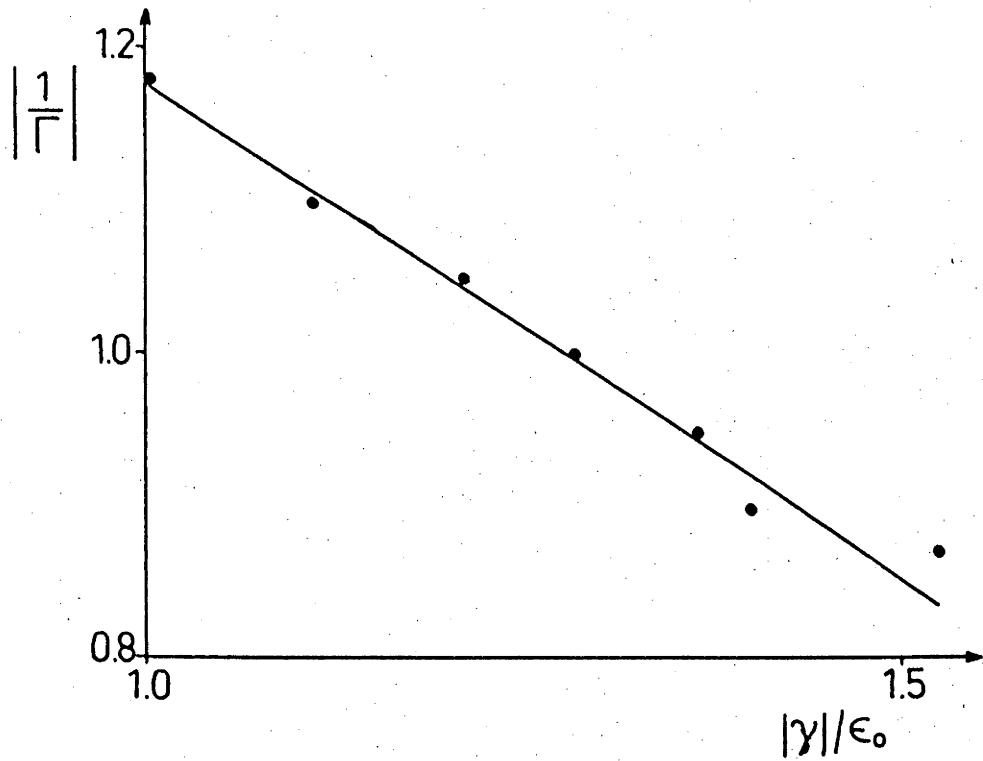
FIGURE III.5. Plot of possible resonant mode lifetimes for the *fcc* crystal

for various values of γ satisfying eqn. III.61. The range

of γ/ϵ_0 shown is from -1.05 to -1.53 while the range of

γ/ϵ_0 satisfying condition III.61 is from -1.05 to -1.75.

lineshape, will be affected only slightly in any one region of the band, and the change is unlikely to be observable for the small concentration of impurities considered by the model.

For γ negative and satisfying the condition III.61 it is possible for resonance modes to appear when γ approaches $-1/R_2$, but numerical calculations suggest that the width of the mode for these values of γ is too large for the resonance to be observable.

When γ is negative and smaller in magnitude than $1/R_2$ there will be no dramatic changes in the magnon sideband lineshape and it is expected that the effect of the impurity will be unobservable.

III.2 Substitutional Impurity in an Antiferromagnet: Magnon Sidebands

Calculations of the effect of a substitutional spin impurity in an antiferromagnet having magnon sidebands in its absorption spectrum have been made by Parkinson (1969a, 1969b), discussing several crystals, but in particular the appearance of local modes that will occur from Ni^{2+} impurities in $RbMnF_3$. The work follows directly from the pure crystal magnon sideband study of Parkinson and Loudon (1968). In this section we will consider the general theory of substitutional impurity effects which result from our model and then consider the specific effects an impurity might have on an antiferromagnetic perovskite such as $RbMnF_3$.

The model calculation is very similar to that of section III.1 for the ferromagnet. The main difference is the degeneracy which results from the existence of two sublattices, as discussed in section II.2. For the model Hamiltonian including impurity, which we use in the present calculation, eqn. I.40, we have ignored any effect of the impurity scattering excitations from one branch to another, an effect which is small $\left(\text{i.e. } \hat{M}_2 = \hat{M}_3 = 0\right.$

from eqn. I.37 as discussed in section I.3), and hence the impurity will not cause the degeneracy to be split. The Hamiltonian, eqn. I.40 is

$$H^{(AF)} = \sum_k \varepsilon(k) \left(\alpha_k^+\alpha_k + \beta_k^+\beta_k\right) + \varepsilon_2 \sum_k \left(A_k^+A_k + B_k^+B_k\right)$$

$$+ g \sum_k \left(\alpha_k^+A_k + A_k^+\alpha_k + \beta_k^+B_k + B_k^+\beta_k\right) + \gamma \sum_{k,k'} \left(\alpha_k^+\alpha_{k'} + \beta_k^+\beta_{k'}\right) . \quad \text{III.68}$$

The calculation proceeds as in section III.1. The Hamiltonian which perturbs the system is given by equation I.9 as

$$H_{\text{pert}}^{(AF)} = \lambda \sum_k \left(\alpha_k^+A_k^+ + \alpha_kA_k + \beta_k^+B_k^+ + \beta_kB_k\right) . \quad \text{III.69}$$

The magnon dispersion in eqn. III.68 is given by

$$\varepsilon(k) = 2JSz\left[1-\gamma_k^2\right]^{\frac{1}{2}} + JS^2\rho z , \quad \text{III.70}$$

$$\gamma_k = \frac{1}{z} \sum_{[\Delta]} e^{ik\cdot\Delta} \quad \text{III.71}$$

and

$$\rho = (J'S'-JS)/JS \quad \text{III.72}$$

where J' and S' are the exchange integral and spin of the impurity and J and S the corresponding values for the host ions. The operators α_k, A_k are annihilation operators for magnons and excitons on sublattice A, respectively, and β_k and B_k those for sublattice B. The sum over k is over the first Brillouin zone of a crystal whose unit cell has one ion from each sublattice in it.

The shift in the ground state energy due to the impurity, $JS^2\rho z$ in eqn. III.70 is independent of k, and will merely cause a shift of the entire spectrum without affecting the lineshape. For this reason it may be ignored in the calculations which follow.

We begin the calculation by again writing the Hamiltonian in matrix form, now as,

$$H^{(AF)} = [\alpha^+ \beta^+ A^+ B^+] \begin{bmatrix} \hat{M}_1 & 0 & \hat{M}_2 & 0 \\ 0 & \hat{M}_3 & 0 & \hat{M}_4 \\ \hat{M}_5 & 0 & \hat{M}_6 & 0 \\ 0 & \hat{M}_7 & 0 & \hat{M}_8 \end{bmatrix} \begin{bmatrix} \alpha \\ \beta \\ A \\ B \end{bmatrix} \qquad \text{III.73}$$

where the notation is that of section II.2 with the exception that now

$$\left(M_1\right)_{ij} = \left(M_3\right)_{ij} = \varepsilon\left(k_i\right)\delta\left(k_i, k_j\right) + \gamma . \qquad \text{III.74}$$

We therefore diagonalise the submatrix

$$\begin{bmatrix} \hat{M}_1 & 0 \\ 0 & \hat{M}_3 \end{bmatrix} \qquad \text{III.75}$$

before we may proceed to diagonalise the entire matrix. Each of the submatrices $\hat{M}_1 = \hat{M}_3$ has been diagonalised in section III.1. The secular equation for III.75 then becomes (from eqn. III.11)

$$\mathcal{D}(\lambda) = \left[1 + \gamma \sum_k \frac{1}{\varepsilon(k) - \lambda}\right]^2 = 0 . \qquad \text{III.76}$$

The matrix which diagonalises III.75 is block diagonal, the diagonal blocks having identical matrices with $\left(\lambda, k_i\right)$th element (eqn. III.13)

$$T_\lambda\left(k_i\right) = \frac{1}{N_\lambda} \frac{1}{\varepsilon\left(k_i\right) - \lambda} \qquad \text{III.77}$$

for

$$N_\lambda^2 = \sum_k \left(\frac{1}{\varepsilon(k) - \lambda}\right)^2 . \qquad \text{III.78}$$

Eqn. III.76 reveals immediately the two-fold degeneracy of the eigenvalues of the impurity part of the Hamiltonian, which are the result of the unit cell having one ion from each sublattice.

The matrix $\hat{T}$ whose columns are the eigenvectors T of eqn. III.77 will diagonalise each of the matrices $\hat{M}_1, \hat{M}_3$. Hence the Hamiltonian in block diagonal form is

$$H^{(AF)} = \begin{bmatrix} \alpha^+ \beta^+ A^+ B^+ \end{bmatrix} \quad \hat{T} \begin{bmatrix} \hat{\Lambda}_1 & 0 & \hat{M}_2 & 0 \\ 0 & \hat{\Lambda}_2 & 0 & \hat{M}_4 \\ \hat{M}_5 & 0 & \hat{M}_6 & 0 \\ 0 & \hat{M}_7 & 0 & \hat{M}_8 \end{bmatrix} \hat{T}^+ \begin{bmatrix} \alpha \\ \beta \\ A \\ B \end{bmatrix} \qquad \text{III.79}$$

where

$$\left(\Lambda_1 \right)_{ij} = \lambda_i \delta(i, j)$$

$$= \left(\Lambda_2 \right)_{ij} \qquad \text{III.80}$$

and

$$\hat{T} = \left[\begin{array}{cc|cc} \hat{T} & 0 & 0 & 0 \\ 0 & \hat{T} & 0 & 0 \\ \hline 0 & 0 & \hat{T} & 0 \\ 0 & 0 & 0 & \hat{T} \end{array} \right] . \qquad \text{III.81}$$

The diagonalisation of III.79 may now proceed as if the matrix were a 2×2 matrix. This is a result of the fact that $\hat{M}_2 = \hat{M}_4$, $\hat{M}_5 = \hat{M}_7$, $\hat{M}_6 = \hat{M}_8$ and all these matrices are scalar. The matrix in eqn. III.79 is then diagonalised by the matrix

$$\hat{U} = \begin{bmatrix} \hat{u}_1 & 0 & \hat{u}_2 & 0 \\ 0 & \hat{u}_1 & 0 & \hat{u}_2 \\ \hat{u}_3 & 0 & \hat{u}_4 & 0 \\ 0 & \hat{u}_3 & 0 & \hat{u}_4 \end{bmatrix} \qquad \text{III.82}$$

where the matrices $\hat{u}_i$, $i = 1, 4$ are given by eqns. III.19 to III.22. We may thus define new operators for which the Hamiltonian $H^{(AF)}$ is diagonal. That is,

$$H^{(AF)} = \sum_\lambda \left[\lambda^-(\lambda) \left(\Phi_\lambda^+ \Phi_\lambda + X_\lambda^+ X_\lambda \right) + \lambda^+(\lambda) \left(\Psi_\lambda^+ \Psi_\lambda + \Omega_\lambda^+ \Omega_\lambda \right) \right] \qquad \text{III.83}$$

where

$$\Phi_\lambda = \frac{1}{N_\lambda} \left[2Y(Y-X) \right]^{-\frac{1}{2}} \sum_k \frac{\alpha_k}{\varepsilon(k)-\lambda} - \frac{1}{N_\lambda} \left[\frac{Y-X}{2Y} \right]^{\frac{1}{2}} \sum_k \frac{A_k}{\varepsilon(k)-\lambda} , \qquad \text{III.84}$$

$$X_\lambda = \frac{1}{N_\lambda} \left[2Y(Y-X)\right]^{-\frac{1}{2}} \sum_k \frac{\beta_k}{\varepsilon(k)-\lambda} - \frac{1}{N_\lambda} \left[\frac{Y-X}{2Y}\right]^{\frac{1}{2}} \sum_k \frac{B_k}{\varepsilon(k)-\lambda} \, , \qquad \text{III.85}$$

$$\Psi_\lambda = \frac{1}{N_\lambda} \left[2Y(Y+X)\right]^{-\frac{1}{2}} \sum_k \frac{\alpha_k}{\varepsilon(k)-\lambda} + \frac{1}{N_\lambda} \left[\frac{Y+X}{2Y}\right]^{\frac{1}{2}} \sum_k \frac{A_k}{\varepsilon(k)-\lambda} \, , \qquad \text{III.86}$$

$$\Omega_\lambda = \frac{1}{N_\lambda} \left[2Y(Y+X)\right]^{-\frac{1}{2}} \sum_k \frac{\beta_k}{\varepsilon(k)-\lambda} + \frac{1}{N_\lambda} \left[\frac{Y+X}{2Y}\right]^{\frac{1}{2}} \sum_k \frac{B_k}{\varepsilon(k)-\lambda} \qquad \text{III.87}$$

and

$$\lambda^\pm(\lambda) = \frac{\varepsilon_2+\lambda}{2} \pm \left[\left(\frac{\varepsilon_2-\lambda}{2}\right)^2 + g^2\right]^{\frac{1}{2}} \, , \qquad \text{III.88}$$

$$X(\lambda) = \left(\varepsilon_2-\lambda\right)/2g \, , \qquad \text{III.89}$$

$$Y(\lambda) = \left[X(\lambda)^2+1\right]^{\frac{1}{2}} \, . \qquad \text{III.90}$$

As $g \to 0$, $\lambda^+ \to \varepsilon_2$ and $\lambda^- \to \lambda$, so that we recover the exciton

energy and the magnon energy which is perturbed by the impurity, λ being

given by the solutions of eqn. III.76. Both exciton and magnon states are

still doubly degenerate. Hence for g non-zero we have two (degenerate)

branches, one exciton-like and one magnon-like, represented by the operators

Φ_λ, X_λ and Ψ_λ, Ω_λ respectively.

In section III.1 we presented some discussion of the existence of local

modes which may be inferred from the secular determinant, eqn. III.11. The

same considerations apply in the present work, though any local modes of

eqn. III.76 which may exist will also be doubly degenerate. As in the last

section, the frequency of local modes may be determined from the solution of

eqn. III.76 outside the band, where it is purely real. For three-dimensional

cubic crystals this is most simply done numerically after the manner of

section III.1.

The operators Φ, X, Ψ and Ω can be readily shown to satisfy boson

commutation rules and to commute with each other. This last fact emphasises

that the impurity Hamiltonian we have chosen does not cause any scattering

of excitations from one sublattice to another.

The magnon sideband lineshape may now be calculated along similar lines to the previous examples. We express the perturbation Hamiltonian, eqn. III.69 in the new operators for which the crystal Hamiltonian is diagonal. After the usual manipulations we obtain

$$H_{pert}^{(AF)} = \imath \sum_{\lambda} \left\{ \frac{1}{2Y(\lambda)} \left[\Psi_{\lambda}^{+}\Psi_{\lambda}^{+} + \Omega_{\lambda}^{+}\Omega_{\lambda}^{+} + \Psi_{\lambda}\Psi_{\lambda} + \Omega_{\lambda}\Omega_{\lambda} - \left(\Phi_{\lambda}^{+}\Phi_{\lambda}^{+} + X_{\lambda}^{+}X_{\lambda}^{+} + \Phi_{\lambda}\Phi_{\lambda} + X_{\lambda}X_{\lambda} \right) \right] \right.$$

$$\left. + \frac{X(\lambda)}{Y(\lambda)} \left[\Phi_{\lambda}^{+}\Psi_{\lambda}^{+} + X_{\lambda}^{+}\Omega_{\lambda}^{+} + \Phi_{\lambda}\Psi_{\lambda} + X_{\lambda}\Omega_{\lambda} \right] \right\} \quad \text{III.91}$$

which has a similar form to the pure crystal perturbation Hamiltonian, eqn. II.57.

The optical absorption is given from section I.4 by Green functions of the time-independent part of eqn. III.91. The commutation rules for the operators Φ, X, Ψ, Ω, and use of the diagonal form of the crystal Hamiltonian, eqn. III.83 give us the following non-zero Green functions:

$$\langle\langle \Phi_{\lambda}\Phi_{\lambda}, \Phi_{\lambda'}^{+}\Phi_{\lambda'}^{+} \rangle\rangle = \frac{\delta(\lambda,\lambda')}{\hbar\omega - 2\lambda^{-}(\lambda)}$$

$$= \langle\langle X_{\lambda}X_{\lambda}, X_{\lambda'}^{+}X_{\lambda'}^{+} \rangle\rangle , \quad \text{III.92}$$

$$\langle\langle \Psi_{\lambda}\Psi_{\lambda}, \Psi_{\lambda'}^{+}\Psi_{\lambda'}^{+} \rangle\rangle = \frac{\delta(\lambda,\lambda')}{\hbar\omega - 2\lambda^{+}(\lambda)}$$

$$= \langle\langle \Omega_{\lambda}\Omega_{\lambda}, \Omega_{\lambda'}^{+}\Omega_{\lambda'}^{+} \rangle\rangle , \quad \text{III.93}$$

$$\langle\langle \Phi_{\lambda}\Psi_{\lambda}, \Phi_{\lambda'}^{+}\Psi_{\lambda'}^{+} \rangle\rangle = \frac{\delta(\lambda,\lambda')}{\hbar\omega - (\lambda^{+}+\lambda^{-})}$$

$$= \frac{\delta(\lambda,\lambda')}{\hbar\omega - (\varepsilon_{2}+\lambda)}$$

$$= \langle\langle X_{\lambda}\Omega_{\lambda}, X_{\lambda'}^{+}\Omega_{\lambda'}^{+} \rangle\rangle . \quad \text{III.94}$$

The Green functions III.92 and III.93 again give the two-magnon and two-exciton absorptions, and the Green function III.94 gives the magnon sideband. The optical absorption in the region of the sideband is therefore given by

$$\alpha(\omega) \sim -4\pi\omega \frac{\left(2\varepsilon_2-\hbar\omega\right)^2}{\left(2\varepsilon_2-\hbar\omega\right)^2+4g^2} g\left(\hbar\omega-\varepsilon_2\right) \qquad\qquad \text{III.95}$$

which is identical in form to the pure crystal result, eqn. II.63 with the

difference that $g(\varepsilon)$ is now the impure crystal density of states, given by

$$g(\lambda) = -\frac{1}{\pi N} \operatorname{Im} \frac{d}{d\lambda} \ln D(\lambda) \qquad\qquad \text{III.96}$$

and

$$D(\lambda) = D_0(\lambda)\mathcal{D}(\lambda) \qquad\qquad \text{III.97}$$

for $\mathcal{D}(\lambda)$ given by eqn. III.76, and $D_0(\lambda)$ is the pure crystal density of

states, given for example by the square of eqn. III.39. In eqn. III.96, N

is the number of unit cells in the lattice.

The density of states, eqn. III.96 may be evaluated in a similar

manner to that for the ferromagnet (section III.1). We make use of the

expression III.41

$$\tan \delta = -\frac{\operatorname{Im} \mathcal{D}(\lambda)}{\operatorname{Re} \mathcal{D}(\lambda)} \qquad\qquad \text{III.98}$$

to write the change in density of states from the pure crystal value as

(eqn. III.43)

$$\Delta g(\lambda) = -\frac{c}{\pi} \frac{d\delta}{d\lambda} \qquad\qquad \text{III.99}$$

where c is the (small) concentration of impurities within the crystal.

Following the discussion in section II.1 of the dependence of the magnon

sideband lineshape on the exciton-magnon interaction strength g , we expect

the effect to be small, and ignore the term

$$\left(2\varepsilon_2-\hbar\omega\right)^2 / \left[\left(2\varepsilon_2-\hbar\omega\right)^2+4g^2\right] \qquad\qquad \text{III.100}$$

in what follows. Hence from eqn. III.95, if ε_2 is large compared with the

maximum magnon energy ε_0 , the magnon sideband will be closely approximated

in shape to the impure magnon density of states $g\left(\hbar\omega-\varepsilon_2\right)$ and we must thus

consider the changes of this which are due to the impurity. The effects of

an impurity on the density of states were discussed in section III.1 in a

general way, and we will consider here only the situation as it affects an

antiferromagnetic crystal, taking a perovskite structure as our example, as

was done for the pure crystal case in section II.2.

Johnson, Dietz and Guggenheim (1966) have reported on the effects of

Ni^{2+} impurities on the emission spectra of MnF_2, $KMnF_3$ and $RbMnF_3$.

Unfortunately the spectrum taken in emission is complicated because of the

possibility of different coupling of the excitons and magnons with each

other and with the radiation field. Therefore it is likely that the model

Hamiltonians we have chosen specifically to study absorption effects may not

describe the situation very well. This is confirmed by the occurrence of

sidebands lower in energy than the parent excitons, and for energies of

separation much larger than $\varepsilon_0 \sim 70$ cm^{-1} in the case of $RbMnF_3$, as

expected from the discussion of section II.2. The sidebands at lower energy

than the parent are probably the highly temperature dependent "hot-bands"

mentioned briefly in the introduction. We therefore conclude that we are

unable to describe the phenomena observed by Johnson and others (1966) with

the present model calculations. We take note, however of the value of the

impurity-host exchange integral. J' determined by the authors to be given

in terms of the pure crystal value J as

$$\frac{J'}{J} = 3.5 \qquad \qquad III.101$$

for Ni^{2+} in a host of Mn^{2+} ions. Since from eqn. I.36a, γ is

approximated by

$$\gamma \sim 2JSz\varepsilon$$

$$= 2JSz\left(\frac{J'}{J} - 1\right) . \qquad \qquad III.102$$

This value of J'/J (eqn. III.101) gives γ a positive value of

$2.5\varepsilon_0$, for ε_0 , and the magnon dispersion energy given by eqns. II.65 as

$$\varepsilon(k) = \varepsilon_0\left[1 - \frac{1}{9}\left(\cos k_x a + \cos k_y a + \cos k_z a\right)^2\right]^{\frac{1}{2}},$$

$$\varepsilon_0 = 12JS \qquad\qquad\qquad \text{III.103}$$

for the perovskite structure.

In fig. III.6 we present the curve of $R(\lambda)$ for the perovskite structure which has the magnetic ions arranged antiferromagnetically on a simple cubic lattice. $R(\lambda)$ is the Hilbert transform of the pure crystal density of states $g_0(\lambda)$ shown in fig. II.4. Following the discussion of section III.1 a local mode will occur whenever γ is positive, or for γ negative and sufficiently large that

$$0 < -1/\gamma < R_1 . \qquad\qquad\qquad \text{III.104}$$

In the former case the local mode is on the high energy side of the band, and for condition III.104 it lies on the low energy side.

There is also the possibility of resonant modes appearing for the range

$$R_1 < -1/\gamma < R_2 \qquad\qquad\qquad \text{III.105}$$

as explained in section III.1. For resonance modes to occur the conditions III.66 must be met for γ satisfying eqn. III.105. The second of these conditions will apply if λ is greater than the cusp point of fig. III.6 at $\sqrt{8/9}$. We must thus examine the first criterion of eqn. III.66 for

$$1.0 > \lambda > \sqrt{8/9} \qquad\qquad\qquad \text{III.106}$$

and γ satisfying eqn. III.105.

We have plotted the lifetimes $\left|\frac{1}{T}\right|$ for possible resonance modes of the perovskite structure in fig. III.7. We again find that the largest lifetime occurs for $-1/\gamma$ very close to R_2, but again also the lifetime of about 2.1 is not sufficiently larger than unity for the resonance to be observable, though the lifetime for this structure is longer than that for the ferromagnetic fcc structure. Another complication in this case is the greater proximity of points of possible resonance to the divergence of the
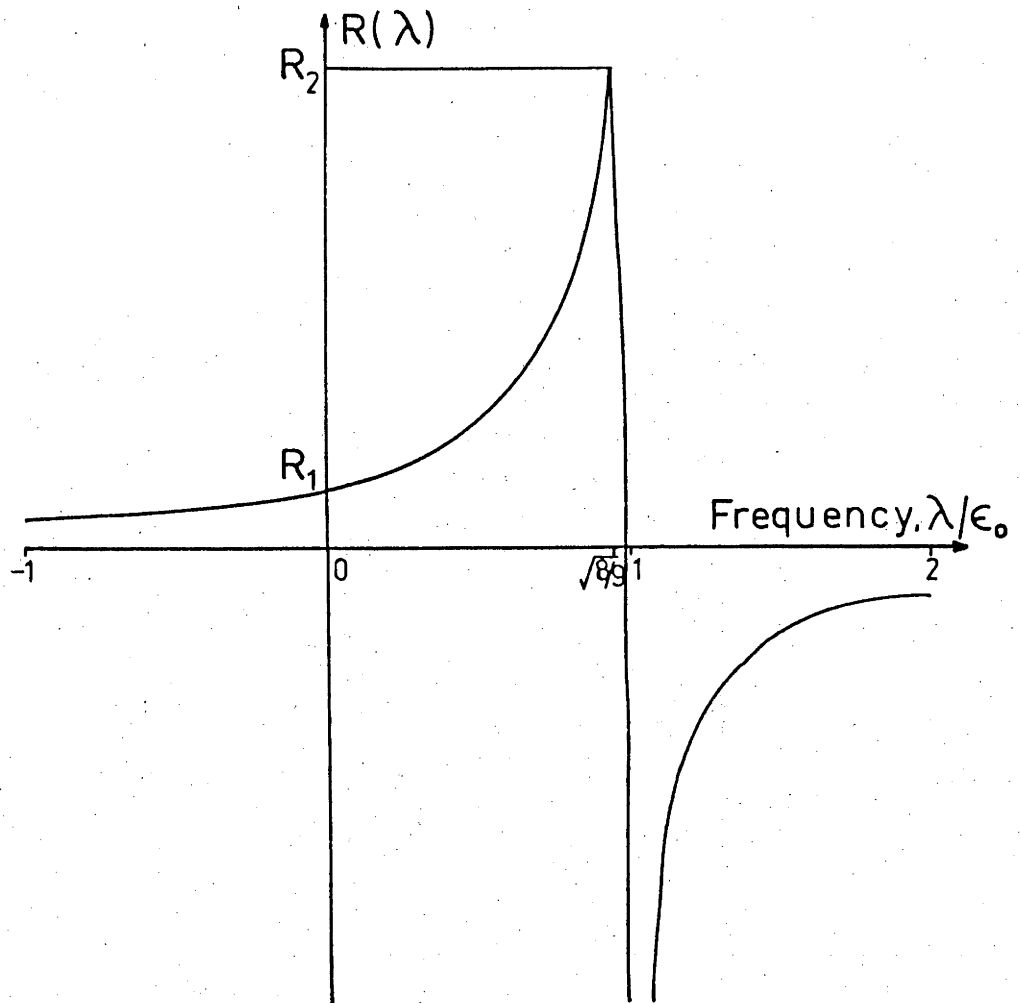
FIGURE III.6. Plot of the real part of $R(\lambda)$ of the lattice Green function

for a perovskite structure crystal such as $RbMnF_3$. The

energy has been normalised so that the pure absorption band

lies between 0 and 1 .
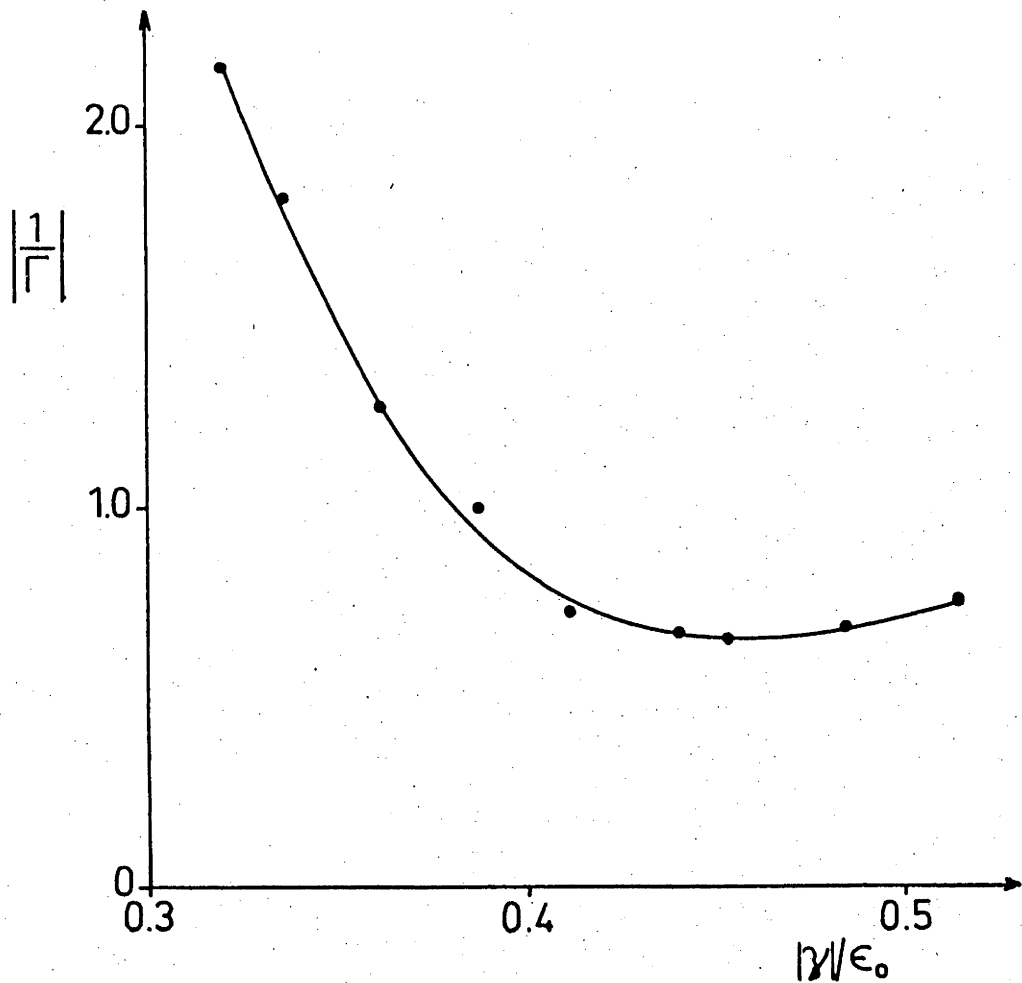
FIGURE III.7. Values of the lifetimes of possible resonant modes for the perovskite crystal for γ satisfying condition III.105 and λ satisfying condition III.106. Values shown are for γ/ε_0 in the range -0.32 to -0.515 where the lifetime is largest. The range of γ/ε_0 satisfying condition III.105 is -0.32 to -2.7. Data for $\gamma \lesssim -0.4$ are highly inaccurate.

density of states at the band edge (fig. II.4) which will make any other

close maximum in the density of states difficult to resolve.

We therefore summarise the expected effects of a substitutional spin

impurity on a perovskite structure crystal like $RbMnF_3$ as follows. Local

modes will occur for γ positive, and for negative values of γ sufficiently

large to satisfy condition III.104*. When local-modes exist there will be

only small and probably unobservable changes to the in-band region of the

spectrum. For the Ni^{2+} impurity studied by Johnson and others (1966) there

will be a local mode at an energy approximately 0.71 times the bandwidth

higher than the top of the band in the absorption spectrum.

In the region of the spectrum satisfied by condition III.106 and for γ

satisfying condition III.105 the possibility of the appearance of resonance

modes was explored, and it was found that although the lifetime of states in

this region is longer than that for the ferromagnetic fcc structure studied

in section III.1, the lifetimes are not sufficiently long for a resonance to

become observable. Hence for all values of γ such that

$$- 1/\gamma > R_1 \qquad\qquad\qquad III.107$$

it is expected that the impurity will not have any observable effect on the

magnon sideband lineshape.

Parkinson (1969a, 1969b) has also studied impurity effects on the magnon

sidebands of $RbMnF_3$ and concludes that local modes (for s_0 symmetry

modes localised on the impurity) will occur above the band for $\varepsilon > 0$, i.e.

in our case for $\gamma > 0$ (eqn. III.102) apart from any effect of anisotropy

fields (small in $RbMnF_3$). He does not mention any condition for the

appearance of local modes below the band, however. Parkinson (1969b)

---

* Note: The condition that γ is negative may be fulfilled if the impurity
couples ferromagnetically to the host crystal, though in this case interband
scattering of magnons may not be negligible and it may not be reasonable
to ignore the effect of off-diagonal sub-matrices $\hat{M}_2$ and $\hat{M}_3$ of
eqn. I.34.

discusses resonance modes within the band but does not give any strong

arguments for their existence, or otherwise. It would thus appear that the

present simple model is capable of explaining many of the impurity phenomena

discussed by Parkinson (1969a, 1969b) with his more sophisticated model, but

also permits a discussion of the existence of resonant modes within the band

in a semi-qualitative manner.

CHAPTER IV

CONCLUSION

In this work we have presented a simple model for the exciton-magnon interaction for describing magnon sidebands in absorbtion spectra in an ideal crystal and a Koster-Slater type model for describing the effect of a substitutional spin impurity on the system.

Despite the simplicity of the model, we are able to describe the essential features of the pure crystal magnon sideband and give an account of the effect of an impurity which allows consideration of both local mode and resonant mode phenomena. It is this aspect which justifies the chosen form of the phenomenological Hamiltonians.

One short-coming of the model is the small effect that the exciton-magnon interaction strength g has on the resultant magnon sideband line-shape whose shape is closely approximated by the magnon density of states. This is contrary to the calculation of Parkinson and Loudon (1968) who found for their model that a non-zero exciton-magnon interaction in perovskite $RbMnF_3$ causes the sideband shape to change from the perovskite density of states with a singularity at the high energy edge of the band (fig. II.4) so that the singularity is removed and the band has a maximum which lies inside the band rather than at the edge. As discussed in appendix 1 this arises from a more sophisticated effective exciton-magnon Hamiltonian, leading to the lattice Green function (Parkinson and Loudon 1968, their eqn. (47))

$$G_{P-L} = G / \left(1 - \frac{\varepsilon_0 \rho}{z} G \right) \qquad\qquad IV.1$$

where G is approximately the lattice Green function we have used and

$$\rho = \frac{J'S'}{JS} - 1 \qquad\qquad IV.2$$

where J' and S' are the excited state (*not* impurity) values of the exchange integral and spin for the exciton interaction. The Green function G used by Parkinson and Loudon (1968) is given by

$$G(\omega) = \frac{1}{N} \sum_k \frac{2\sin^2(k_x a) l_2(k)^2}{\hbar\omega - \varepsilon_2 - \varepsilon(k)} \qquad \text{IV.3}$$

where $l_2(k)$ is given by eqn. I.25. The Green function considered in the present work was

$$G(\omega) = \frac{1}{N} \sum_k \frac{1}{\hbar\omega - \varepsilon_2 - \varepsilon(k)} . \qquad \text{IV.4}$$

The additional factor in eqn. IV.3 has little effect in the region where $G(\omega)$ is large, i.e. at the edge of the Brillouin zone and therefore the Green functions may be considered approximately equivalent.

In the present model our results therefore obtain from considering ρ in eqn. IV.1 to be zero. With a more realistic treatment of the exciton-magnon interaction Hamiltonian we would expect to obtain a Green function like that of eqn. IV.1 (appendix 1) and hence get a more significant contribution from the interaction to the magnon sideband lineshape.

Any explanation of a shift of the magnon maximum of the magnon sideband must take into account a more realistic expression for the magnon dispersion $\varepsilon(k)$. For example, a shift of the maximum of the sideband in a ferromagnetic *fcc* crystal could be effected by inclusion of some simple cubic next nearest neighbour interaction, as discussed by Swendsen and Callen (1972) and Loly and Buchheit (1972). The amount of shift due to this effect will depend on the relative magnitudes of the nearest neighbour to next nearest neighbour interactions. Such an improvement to the expression for $\varepsilon(k)$ is readily included in the present model calculation, and will not alter the form of the expressions for the magnon sidebands derived here. It is thus also possible to at least partially explain the shift of the sideband maximum by effects which do not depend on any exciton-magnon interaction.

Local modes are found to occur in the model when the equation

$$1 + \gamma R(\lambda) = 0 \qquad\qquad IV.5$$

for $R(\lambda)$ the real part of the lattice Green function, eqn. IV.4, has

solutions for λ outside the band of frequencies, where the imaginary part

of eqn. IV.4 is zero. For such solutions where γ is positive the local

mode lies on the high-energy side of the band, and where γ is negative it

lies on the low-energy side. Since $R(\lambda)$ is monotonic outside the band,

only one local mode can occur for any given value of γ. Near the edge of

the band, $R(\lambda)$ will be large if there is a large singularity in the density

of states just within the edge of the band, and so for γ small the local

mode will be very close to the edge and may be unobservable.

For the three-dimensional crystals studied there are certain values of

the impurity parameter γ for which there will be no local mode, and the

possibility of resonances appearing within the band must be considered.

Resonances will occur in the absence of local modes if there are solutions

of eqn. IV.5 for λ lying within the band provided the width in the peak of

the change of density of states is small. This was found not to be the case

(to within the accuracy of the numerical calculations) for either of the

crystals studied, though the width was smaller for the perovskite structure

than the *fcc* structure for the value of γ such that the width was

smallest.

For the particular model we have studied, the resonance (if it occurs)

will occur at exactly the solutions of eqn. IV.5 inside the band. This is

because the solutions lie at the point of inflexion of the function δ

(eqn. III.41) whose negative derivative gives the change of the density of

states (eqn. III.43). [This may be seen by substituting $\gamma\left(\lambda-\lambda_0\right)R'(\lambda)$ for

$R(\lambda)$ near λ_0 into the expression for δ and noting that δ has a maximum of

$\pi/2$ at λ_0 and its derivative has zero slope at $\lambda = \lambda_0$ from the change

in sign of the slope at $\lambda = \lambda_0$.] We illustrate these points in

figures IV.1 and IV.2 where we have plotted the function δ of eqn. III.41 in the former and the change in the density of states

$$\Delta g(\lambda) \sim -\frac{d\delta}{d\lambda} \qquad\qquad IV.6$$

in the latter, for the *fcc* structure considered in sections II.1 and III.1 (for which the calculations of $R(\lambda)$ were most accurate - appendix 3). At the higher energy point λ_0 for which eqn. IV.5 is satisfied within the band, the function δ undergoes a change in the sign of its slope. If the slope at this point is large enough, a resonance will occur because the excitation mode at this point will be sufficiently narrow in width to be observed (section III.1). As illustrated in fig. IV.2 there is a peak in the change of density of states at $\lambda = \lambda_0$ but it is not sufficiently large to account for the small factor c, the concentration of impurities which multiplies the derivative confirming the conclusion made in section III.1 to this effect. The same consideration also means that the increase in Δg near the edges of the band will also be too small to have an observable effect on the shape of the total density of states.

In the perovskite structure studied in sections II.2 and III.2 one further feature becomes important. This is the fact that as resonance modes will lie to the high energy side of the cusp point at $\sqrt{8/9}$, if they exist, the resonance lies very close to the large singularity at the edge of the band and hence may be difficult to resolve.

Parkinson (1969b) remarks that the resonant mode frequency will be shifted from $\lambda = \lambda_0$ satisfying eqn. IV.5 within the band due to the strong energy dependence of $g_0(\lambda)$. However, for a resonance to appear, the condition for a narrow resonance width must be satisfied (eqn. III.66) and this can only be so if $g_0(\lambda)$ does not have a strong energy dependence at this point. Therefore, for the present model we cannot support the assertion of Parkinson (1969b) and expect any resonance to occur exactly at the
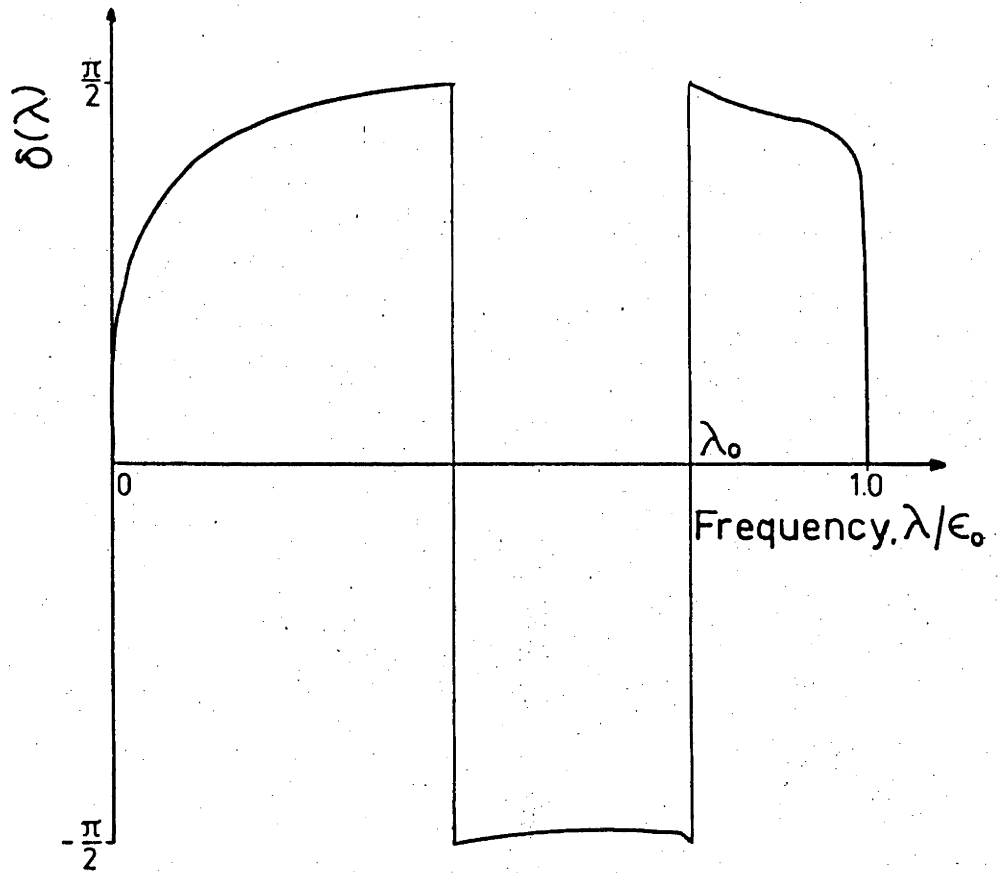
FIGURE IV.1. Plot of the function $\delta(\lambda)$ vs λ/ε_0 for the *fcc* crystal with

γ chosen so that $R(\lambda)$ has a large slope. $\gamma = -1.3\varepsilon_0$.
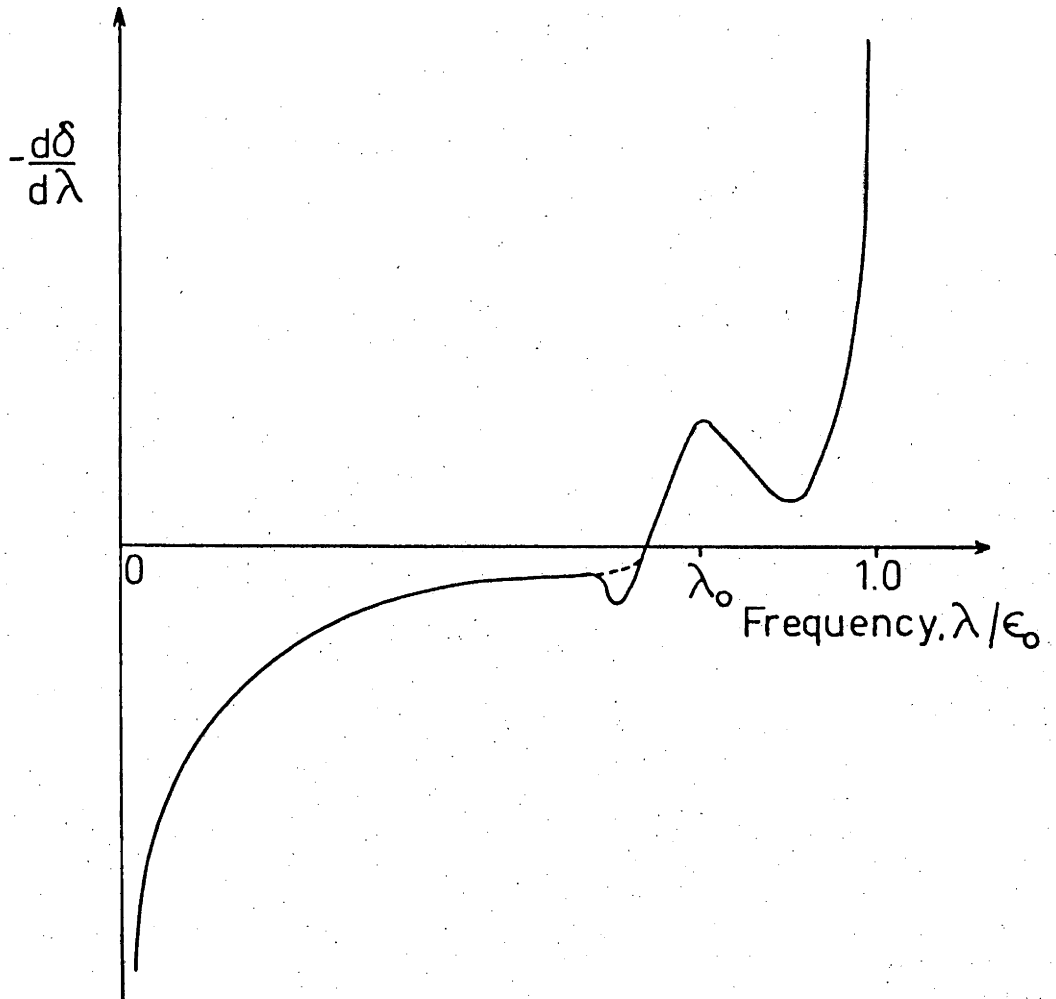
FIGURE IV.2. Plot of the derivative of $\delta(\lambda)$ of fig. IV.1 vs λ/ε_0 , which

is proportional to the change of the density of states, for

$\gamma = -1.3\varepsilon_0$. The derivative is obtained numerically and is

not considered to be very accurate, particularly near the ends

of the interval, though it does indicate the features of

interest. The negative kink just below λ_0 is due to a

numerical problem.

frequency $\lambda = \lambda_0$.

Unfortunately very little experimental work has been done to date on ferromagnetic insulators which might have magnon sidebands in their absorption spectra, and also little work has been done on the effects of impurities on the spectra of either ferro- or antiferromagnetic insulators. It would be interesting to see how the results of such experiments compare with the predictions of the present model, particularly for values of γ such that local modes may occur, but also for γ in the region where a resonant mode may occur to test the prediction that resonant modes will not occur within the band. It is to be hoped that the effect of impurities on magnon sidebands will receive more attention from experimenters in the near future.

We conclude with a final remark on the model. As pointed out in section I.4, use of the lattice Green functions calculated in the present work may also be made to predict other phenomena of the crystals treated here. From this point of view, the approach indicated by this model will have much wider application in solid state calculations than indicated by the magnon sideband calculations. It should also be noted that predictions of two-magnon and two-exciton lineshapes as affected by the exciton-magnon interaction and the impurity arise naturally from the calculation leading to the magnon sideband absorption band, and such predictions may also be of value in interpreting the spectra near where these phenomena are likely to occur.

Although the model used in this work has treated the exciton energy ε_2 and the exciton-magnon interaction strength g as independent of wavenumber, it is also possible to solve the problem exactly when these are dependent on wavenumber. We give a brief indication of how this may be done in appendix 5. Apart from the important effect that g as a function of wavenumber has on the spectrum (appendix 1), the treatment of a finite exciton dispersion is necessary to accurately describe some experimentally observed sidebands.

APPENDIX 1

DISCUSSION OF THE FORM OF THE EXCITON-MAGNON HAMILTONIANS

We present in this appendix, a discussion of the form of the perturbation Hamiltonian for interaction of radiation with a crystal having both exciton and magnon excitations. The problem is treated from the form of the crystal wavefunctions (unperturbed) and the allowed matrix elements which are obtained from them. The discussion is not intended to be a rigorous derivation of the form of the perturbation but is presented to give some insight into the significance of the perturbation Hamiltonian chosen for the model discussed in the main text, eqns. I.8 and I.9.

It is sufficient to discuss the ferromagnetic crystal Hamiltonian for the pure crystal. Though the other Hamiltonians used in the present work are more complicated, the argument presented here applies equally well to them. We thus consider the pure crystal Hamiltonian, eqn. I.28,

$$H^{(F)} = \sum_k \epsilon(k) a_k^+ a_k + \epsilon_2 \sum_k b_k^+ b_k + g \sum_k \left(a_k^+ b_k + b_k^+ a_k \right) \qquad \text{A.1}$$

where the symbols have the same meaning as in the main text.

We have chosen the third term of eqn. A.1 to represent the exciton-magnon interaction as it may be considered as a simple approximation to the rigorous form eqn. I.1. This may be seen by considering the equation of motion of a Green function, G, eqn. I.54. We may proceed in one of two ways. We may differentiate the Green function G n times and then take some approximation to the resultant Green function on the right hand side by, for example, taking part of the Green function as a statistical average, so that the remainder gives the same G as the left hand side. The resultant solution for G may therefore also be obtained directly from a simpler effective crystal Hamiltonian H_0. For the present case where G

is quadratic in the exciton and magnon operators, the effective Hamiltonian may be reduced from the four-operator form of eqn. I.1 to a two-operator form of the type we have chosen by the above procedure.

The other method of solving the equation of motion for G is to take the equation of motion of the new Green function on the right hand side of eqn. I.54, and so on until one obtains a Green function on the right hand side which may be approximated by the original one, thus leaving a system of linear equations to be solved. Such a procedure is equivalent to the first one but may account for many more terms than by truncating the series obtained by taking higher order derivatives of G directly, because of the algebraic complexity of taking a large number of terms.

Our approximate exciton-magnon interaction Hamiltonian might be considered to arise from use of the first of the above procedures, and its small overall effect on the shape of the magnon sideband (section II.1) may be explained by the fact that we have rejected too many terms of the series of Green functions. The analysis of Parkinson and Loudon (1968) on the other hand was made using the second of these procedures and therefore the Green function they obtain, eqn. IV.1, may be a more accurate represent-ation of an exact Green function found using the complete exciton-magnon interaction Hamiltonian eqn. I.1. This is reflected in the greater effect of the exciton-magnon interaction on the magnon sideband found by these authors. It can be shown, however, in the case of a pure crystal, that if we give g some k-dependence then the result will be a weighted Green function depending on $g(k)$ which may have a large effect on the Green function for some values of k. In this way it would also be possible to explain the shift of the maximum as described by Parkinson and Loudon (1968) within the framework of the present model. In principle at least this is also possible with the impurity present. Hence the difference between the form of exciton-magnon Hamiltonian chosen in the present work and

the effective Hamiltonian used by Parkinson and Loudon (1968) is not as great as it may at first appear.

The diagonalisation of the Hamiltonian A.1 has been given in section II.1 and has the form (eqn. II.15)

$$H^{(F)} = \sum_k (\lambda_k^- \eta_k^+ \eta_k + \lambda_k^+ \nu_k^+ \nu_k)$$

A.2

where η_k and ν_k are harmonic-oscillator-like annihilation operators. They satisfy boson commutation rules, and commute with each other. As discussed in section II.1 one may consider the Hamiltonian A.2 as describing a system with two new types of excitation, one represented by η_k and the other by ν_k. These excitations may be described by wavefunctions $|n_\eta\rangle$ and $|n_\nu\rangle$. Hence the wavefunctions of the entire system will be given by products of the individual excitation wavefunctions. The wave equation for the system is then given by

$$H^{(F)} |n_\eta\rangle |n_\nu\rangle = \left(n_\eta \lambda_k^- + n_\nu \lambda_k^+\right) |n_\eta\rangle |n_\nu\rangle$$

A.3

since, for example

$$\lambda_k^- \eta_k^+ \eta_k |n_\eta\rangle = \lambda_k^- \eta_k^+ \sqrt{n_\eta} \; |n_\eta - 1\rangle$$

$$= \lambda_k^- n_\eta |n_\eta\rangle \; .$$

A.4

The wavefunctions $|n_\eta\rangle$ and $|n_\nu\rangle$ for which the Hamiltonian is diagonal may be written as a unitary transformation of the original exciton and magnon wavefunctions $|n_e\rangle$ and $|n_m\rangle$ by making use of the unitary matrix $\hat{S}$, eqns. II.13 and II.14. The relationship between the wavefunctions is (Schiff 1968)

$$|n_\eta\rangle = \frac{|n_m\rangle}{\sqrt{2y(y-x)}} - \sqrt{\frac{y-x}{2y}} \, |n_e\rangle \; ,$$

$$|n_\nu\rangle = \frac{|n_m\rangle}{\sqrt{2y(y+x)}} + \sqrt{\frac{y+x}{2y}} \, |n_e\rangle$$

A.5

where the symbols $x(k)$ and $y(k)$ are defined in eqns. II.11 and II.12.

We now consider the system to be perturbed by a time-dependent perturbation of the form $H_1 = Bf(t)$ where B is independent of time. The Green function representing the linear response of an observable $A(t)$ to the perturbation is given e.g. by Mahanty (1974) and at $T = 0K$ becomes (Richardson 1975)

$$G_{AB}(\omega) = \frac{-1}{\hbar\sqrt{2\pi}} \sum_n \left\{ \frac{\langle 0|A|n\rangle\langle n|B|0\rangle}{\omega-\omega_{0n}} - \frac{\langle n|A|0\rangle\langle 0|B|n\rangle}{\omega+\omega_{0n}} \right\} . \qquad \text{A.6}$$

For the present problem we require the imaginary part of the Green function eqn. A.6 (see section I.4) which is given by

$$\text{Im } G_{AB}(\omega) = \frac{-\pi}{\hbar\sqrt{2\pi}} \sum_{n\neq0} \left\{ \langle 0|A|n\rangle\langle n|B|0\rangle\delta\left(\omega-\omega_{0n}\right) - \langle n|A|0\rangle\langle 0|B|n\rangle\delta\left(\omega+\omega_{0n}\right) \right\} . \qquad \text{A.7}$$

In eqns. A.6 and A.7, $|n\rangle$ represents the nth excited state of the unperturbed system and $\omega_{0n} = \left(E_0-E_n\right)/\hbar$ where

$$H^{(F)}|n\rangle = E_n|n\rangle .$$

From eqn. A.7 the optical absorbtion is obtained from evaluation of the matrix elements $\langle 0|A|n\rangle$ and $\langle 0|B|n\rangle$. In section I.4 it was shown that for optical absorption, A and B are both dipole moment operators.

We may now study the possible forms of A or B in terms of the exciton and magnon operators a_k and b_k. From eqn. A.5,

$$|0\rangle = |0_e\rangle|0_m\rangle = \{|0_\eta\rangle|0_\eta\rangle+|0_\nu\rangle|0_\nu\rangle\}/2y + |0_\eta\rangle|0_\nu\rangle x/y , \qquad \text{A.8}$$

$$|n\rangle = |n_e\rangle|n_m\rangle = \{|n_\eta'\rangle|n_\eta\rangle+|n_\nu'\rangle|n_\nu\rangle\}/2y + \{|n_\eta'\rangle|n_\nu\rangle+|n_\eta\rangle|n_\nu'\rangle\}x/2y . \qquad \text{A.9}$$

Then for the matrix elements of A to be non-zero, operations like the one shown in eqn. A.4 reveal that A must contain some or all of the operators

$$\eta^+, \eta, \nu^+, \nu, \eta^+\eta^+, \eta\eta, \nu^+\nu^+, \nu\nu, \eta^+\nu^+, \eta\nu, \text{ etc.} \qquad \text{A.10}$$

while terms like $\eta^+\eta, \eta^+\nu$, etc. will not contribute. Making use of eqn. II.16, A may have terms like

$$\left(a_k^++a_k\right), \left(b_k^++b_k\right), \left[1 + \frac{1}{2y}\right]\left(a_k^+a_k^++a_ka_k\right), \left[1 - \frac{1}{2y}\right]\left(b_k^+b_k^++b_kb_k\right) ,$$

$$\frac{x}{y} \left(a_k^+ b_k^+ + a_k b_k \right) \ , \ \text{etc.} \qquad\qquad \text{A.11}$$

giving non-zero matrix elements in eqn. A.7. Since magnon sidebands only

involve combinations of excitons and magnons, only the last term shown in

eqn. A.11 will contribute to the calculation of magnon sidebands. Richardson

(1974) has attempted to calculate magnon sidebands using the second term of

eqn. A.11 stating that the exciton-magnon interaction in the crystal

Hamiltonian $H^{(F)}$ will cause the correct coupling between excitations.

This is not strictly true, and the lineshapes predicted by that theory

represent changes to the pure magnon and pure exciton transitions due to the

exciton-magnon interaction. In a real crystal the exciton and its associated

magnon sideband do not, in general, both couple to the electric component of

the radiation. From a phenomenological point of view, the theory given by

Richardson (1974) is a "zeroth-order" estimation of magnon sideband behaviour.

The present work represents some improvement on that.

APPENDIX 2

CONSIDERATION OF A k-DEPENDENT FUNCTION $\gamma(k, k')$

The main feature of the model presented in this work is the fact that the crystal Hamiltonian chosen to describe the system can be diagonalised exactly. The key to this diagonalisation is the fact that the four submatrices of the Hamiltonian in matrix representation commute (eqn. II.6). For the case of an impurity, however, one further requirement is made. For advantage to be taken of the commutation of the submatrices, one must be able to diagonalise the impurity part of the Hamiltonian without affecting the other submatrices, that is, the other submatrices must commute with the transformation matrix which diagonalises the impurity part (for example submatrix $\hat{A}$ in eqn. III.6). This problem is taken care of in the present calculation by taking matrices $\hat{B}$ and $\hat{D}$ (eqn. III.6 for example) as scalar matrices. The methods would still be useful more generally for any matrices $\hat{B}$ and $\hat{D}$ which commute with the matrix $\hat{T}$ which diagonalises submatrix $\hat{A}$. This problem is quite complex, depending on the form of $\hat{T}$ which in turn is a function of the impurity Hamiltonian under consideration. We will not discuss this complex problem, but rather will consider the possibility of diagonalising the impurity part of the Hamiltonian when the more rigorous form eqn. I.31 is considered, so that the impurity contribution γ is a function of k , eqn. I.32, that is

$$\gamma(k, k') = 2|J|S_z e^{i(k'-k)\cdot 1}\left[\varepsilon+\rho\gamma_{k'-k}-\gamma\left(\gamma_{k'}+\gamma_{k}\right)\right] \qquad \text{B.1}$$

for the impurity at site 1 in the crystal. We demonstrate in this appendix that the matrix $\hat{A} - \lambda\hat{I}$, such that

$$(A-\lambda)_{ij} = \left(\varepsilon\left(k_i\right)-\lambda\right)\delta\left(k_i, k_j\right) + \gamma\left(k_i, k_j\right) \qquad \text{B.2}$$

may be diagonalised exactly, though the calculation is rather lengthy.

We write eqn. B.1 in matrix form as follows, taking the impurity at the origin, for convenience,

$$\gamma(k, k') = 2|J|S\left[z\epsilon\xi\cdot\tilde{\xi} + \sum_j \{\rho p_j\cdot\tilde{p}_j - \gamma(p_j\cdot\tilde{\xi}+\xi\cdot\tilde{p}_j)\}\right]$$

$$= 2|J|S\left[\xi\cdot\tilde{\mu} + \sum_j p_j\cdot\tilde{\eta}_j\right] \qquad \text{B.3}$$

where

$$\xi = \begin{bmatrix} 1 \\ 1 \\ \vdots \\ 1 \end{bmatrix}, \quad p_j = \begin{bmatrix} e_1^{(j)} \\ \vdots \\ e_N^{(j)} \end{bmatrix} \qquad \text{B.4}$$

for $e_i^{(j)} = e^{ik_i\cdot\Delta_j}$ and

$$\mu = z\epsilon\xi - \gamma\sum_j p_j \,,$$

$$\eta_j = \rho p_j^* - \gamma\xi \,, \qquad \text{B.5}$$

p_j^* being the complex conjugate of p_j and $\tilde{p}$ is the transpose of p.

The sum over j is over the number z of nearest neighbours. We consider only the case where the lattice vectors Δ are orthogonal (e.g. cubic crystals).

From eqn. B.2 the eigenvalue equation may be written as

$$\left\{\hat{A}' + \left(\xi\cdot\tilde{\mu} + \sum_j p_j\cdot\tilde{\eta}_j\right)\right\}u = 0 \qquad \text{B.6}$$

where u are the eigenvectors and $\hat{A}'$ is the matrix with elements

$$(\hat{A}')_{ij} = \frac{\epsilon(k_i)-\lambda}{2|J|S}\,\delta(k_i, k_j) \,. \qquad \text{B.7}$$

We now write eqn. B.6 as

$$\hat{A}'^{-\frac{1}{2}}\left[\hat{A}' + \xi\cdot\tilde{\mu} + \sum_j p_j\cdot\tilde{\eta}_j\right]\hat{A}'^{-\frac{1}{2}}(\hat{A}'^{\frac{1}{2}}u) = 0$$

or

$$\left[\hat{I}+\hat{A}'^{-\frac{1}{2}}\left(\xi\cdot\tilde{\mu} + \sum_j p_j\cdot\tilde{\eta}_j\right)\hat{A}'^{-\frac{1}{2}}\right]X = 0 \qquad \text{B.8}$$

where

$$X = \hat{A}'^{\frac{1}{2}}u \,. \qquad \text{B.9}$$

We now define vectors

$$f = \hat{A}'^{-\frac{1}{2}}\xi \quad , \quad g = \tilde{\mu}\hat{A}'^{-\frac{1}{2}} \quad , \tag{B.10}$$

$$h_j = \hat{A}'^{-\frac{1}{2}}p_j \quad , \quad 1_j = \tilde{\eta}_j\hat{A}'^{-\frac{1}{2}} \quad , \quad j = 1, z \tag{B.11}$$

so eqn. B.8 is written as

$$\left[\hat{I}+fg + \sum_j h_j 1_j\right]X = 0 \quad , \quad j = 1, z \quad ,$$

or

$$f(g.X) + \sum_j h_j(1_j.X) = -X \quad , \quad j = 1, z \quad . \tag{B.12}$$

The vector X may now be written as an expansion in the orthogonal functions f and h_j , $j = 1, z$ (for cubic crystals the primitive lattice vectors are orthogonal) as

$$X = af + \sum_j b_j h_j \quad . \tag{B.13}$$

We therefore solve for a and b_j , $j = 1, z$ by substituting eqn. B.13 into eqn. B.12 so we have

$$f\left(g.\left(af + \sum_j b_j h_j\right)\right) + \sum_j h_j\left(1_j.\left(af + \sum_{j'} b_{j'} h_{j'}\right)\right) = -af - \sum_j b_j h_j \quad . \tag{B.14}$$

Equating coefficients gives the following $(z+1) \times (z+1)$ system of equations

$$\begin{bmatrix} g.f-1 & g.h_1 & g.h_2 & \cdots & g.h_z \\ 1_1.f & 1_1.h_1-1 & 1_1.h_2 & \cdots & 1_1.h_z \\ \vdots & & & & \\ 1_z.f & 1_z.h_1 & & \cdots & 1_z.h_z-1 \end{bmatrix} \begin{bmatrix} a \\ b_1 \\ \vdots \\ b_z \end{bmatrix} = 0 \tag{B.15}$$

which may be solved to yield a, b_j , $j = 1, z$ to give the eigenvectors of the system, making use of eqn. B.9. The eigenvalues may be obtained from the secular determinant of eqn. B.15.

It is thus clear that the Hamiltonian with $\gamma(k, k')$ included as a

function of the wavenumbers may be diagonalised exactly, though the algebra involved is tedious. For the model calculation we present in this thesis, it is considered sufficient to treat γ as independent of wavenumber, since the phenomenological effects of an impurity are still predicted by the simpler form. Similar considerations also apply to the even more complicated form of $\gamma(k, k')$ in an antiferromagnetic crystal.

APPENDIX 3

NUMERICAL CALCULATIONS OF LATTICE GREEN FUNCTIONS AND DENSITIES OF STATES

In this appendix we discuss the various numerical calculations that have been performed throughout the text. We begin by describing the calculation of the pure crystal density of states for the *fcc* and perovskite crystals we have studied. The impure crystal density of state calculations are then presented, and finally we consider the estimation of local mode frequencies in the impure crystals. As pointed out in section III.1 the one-dimensional density of states may be evaluated analytically and will not be treated here. We present in this appendix only the calculations for three-dimensional crystals.

i) Pure crystal density of states

There have been many and varied attempts to evaluate numerically the pure crystal density of states

$$g_0(\lambda) = \frac{1}{N} \sum_k \delta\left(\varepsilon(k)-\lambda\right) \qquad\qquad \text{C.1}$$

of magnons in three-dimensional crystals. Attempts have been made to obtain analytic expressions with limited success. For example Joyce (1971) has given an expression for the *fcc* crystal Green function (from which the density of states may be obtained) in terms of complete elliptic integrals of the first kind.* The most common method of estimation until recently has been to attempt to calculate series approximations for the integrals involved. Mahanty (1966) and Ra (1971) for example have given a Fourier series method for calculating lattice Green functions, while Byrnes, Podgor and Zachary (1969) have given a calculation for *bcc* Green functions in which they expand the integrand into a geometric series. Chadi and Cohen (1973)

---

* Such expressions are usually very complicated and of little practical value, unfortunately. Jelitto (1969) has, however, given useful approximate analytic expressions for $g_0(\lambda)$ for the cubic crystals.

and Morita (1975) have made use of the special symmetries present in the Brillouin zone of cubic crystals to enable accurate averages over the zone to be made, and to predict values of the lattice Green function at any point in the zone, given its value at certain special points.   All the methods described so far have the restriction that they must be rederived for each particular crystal of interest, and often there is no guarantee that a method which is successful for one crystal structure will be tractable for any other structure.

Recently, however, a new procedure for evaluating lattice Green functions has become available.   This method involves the use of Monte-Carlo type integration using random numbers generated over the first Brillouin zone.   A good description of the simplest form of the method is given by Buchheit and Loly (1972).   Other Monte-Carlo calculations using various types of interpolations with improved accuracy for a given computation time have been described by Mueller, Garland, Cohen and Bennemann (1971), Gilat and Raubenheimer (1966) and Cooke and Wood (1972).

In the present work we have evaluated the magnon density of states in the manner of Buchheit and Loly (1972).   The procedure is as follows:

For an infinite crystal, the sum of eqn. C.1 may be replaced by an integral over the wavevector k , the volume of integration being the first Brillouin zone.   For cubic crystals the volume is obtained from a basic cube which facilitates the calculation.   For example, the fcc Brillouin zone is shown in fig. C.1 where we illustrate the irreducible zone, 1/48 th part of the entire zone, any point of which may be transformed to other equivalent points of the Brillouin zone (completely covering the entire zone by so doing) by crystal group operations.   Such a zone is common to all cubic crystals and greatly simplifies integration over the entire zone, as the total integral will be simply 48 times the integral over this volume. For the Monte-Carlo calculation we generate points throughout the cube of side ΓX in the first quadrant.   This cube contains 12 irreducible zones,
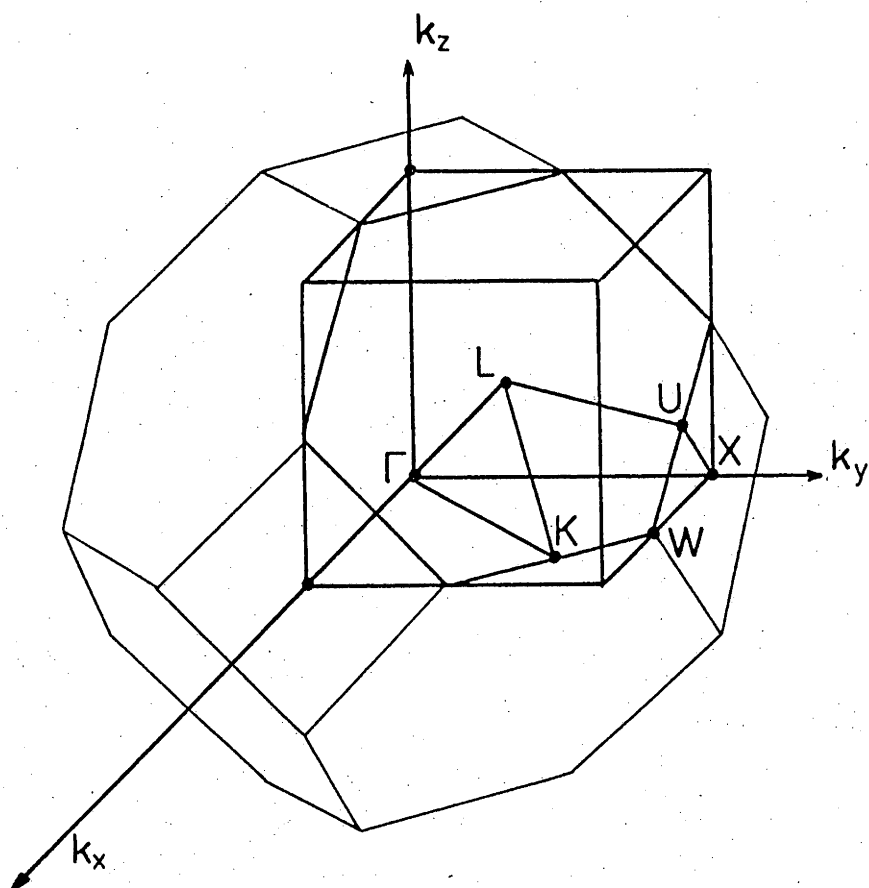
FIGURE C.1. Illustration of the first Brillouin zone of the *fcc* crystal.
The irreducible zone is bounded by $\Gamma LKWXU$ and is 1/48 th
of the entire zone. The cube for the numerical integration
described in appendix 3 is that in the positive octant with a
side ΓX. It contains 12 equivalent irreducible zones.

and the integral will be multiplied by 4 to give the correct value for $g_0(\lambda)$.

The Monte-Carlo method involves generating triplets of random numbers between 0 and 1, multiplying each by π, and evaluating $\varepsilon(k)$ for the triplet. The range of energies (λ) is divided up into a set of histograms and unity is added to the histogram corresponding to the magnitude of $\varepsilon(k)$. This is done until sufficient smoothness of the curve is obtained, the accuracy of the result being inversely proportional to the square root of the number of points generated in the Brillouin zone. This simple procedure gives better than 5% accuracy after 10^6 values of k , in the cubic crystals studied.

As also pointed out by Buchheit and Loly (1972) an estimate of the energy at which van Hove singularities occur in the density of states may be made from evaluating the minimum of the group velocity at the energy of each histogram. The group velocity is given by the expression

$$\nu_g = \nabla_k \varepsilon(k) \ . \qquad\qquad\qquad C.2$$

We find the minimum of the modulus of ν_g , which goes to zero at any van Hove singularity, but is non-zero elsewhere. This procedure is highly sensitive, and is valuable for determining singularities near the edges of the zone, or where there is only a slight change in slope of the density of states at the singularity.

ii) Impure crystal density of states

The impure crystal density of states was given by equation III.37 or III.40. The impurity density of states requires evaluation of the integral (for an infinite crystal - see appendix 4)

$$I(\lambda) = \int_{BZ} \frac{d^3k}{\varepsilon(k)-\lambda} \qquad\qquad\qquad C.3$$

which for $0 < \lambda < \varepsilon(k)_{max}$ is complex. The imaginary part is just the pure

crystal density of states $g_0(\lambda)$, using Dirac's relation, eqn. III.56,

and the real part is the Hilbert transform of $g_0(\lambda)$, eqn. III.58,

$$R(\lambda) = \frac{P}{\pi} \int_0^1 \frac{g_0(\lambda')}{\lambda'-\lambda} \, d\lambda' \qquad \qquad \text{C.4}$$

for P signifying the principal part of the integral and $g_0(\lambda)$ normalised

so that it is non-zero between 0 and 1 .

As described in section III.1 the impure crystal density of states is

given by

$$g(\lambda) = g_0(\lambda) + \Delta g(\lambda) \qquad \qquad \text{C.5}$$

where

$$\Delta g(\lambda) = -\frac{c}{\pi} \frac{d\delta}{d\lambda} , \qquad \qquad \text{C.6}$$

$$\tan \delta = -\gamma\pi g_0(\lambda)/\bigl(1+\gamma R(\lambda)\bigr) \qquad \qquad \text{C.7}$$

the impurity having a (small) concentration of c .

$R(\lambda)$ may be evaluated using the Monte-Carlo method as for the pure

density of states $g_0(\lambda)$, but instead of only one histogram having a weight

of unity for each value of k , all histograms have a weight for each k .

The ith histogram has weight

$$W_i = -\ln\left|\frac{w_{i+1}-w_m}{w_i-w_m}\right| \qquad \qquad \text{C.8}$$

where w_i is the energy of the ith histogram, w_m is the energy of the

histogram in which $\varepsilon(k)$ lies, for that particular k , and $W_m = 0$.

The expression C.8 for W_i is just the Hilbert transform of a step function

which is unity between w_i and w_{i+1} and zero elsewhere. As a consequence

of the weight function C.8, the numerical calculation takes almost an order

of magnitude longer in time to achieve the same accuracy as the calculation

of $g_0(\lambda)$. It was thus considered desirable to find an alternative means of

evaluating $R(\lambda)$.

The method used follows from combining the Monte-Carlo calculation of Buchheit and Loly (1972) with the Fourier sine series calculation of Mahanty (1966). The pure crystal density of states $g_0(\lambda)$ is evaluated using the Monte-Carlo method to the desired accuracy. Use is then made of a numerical fast Fourier transform procedure (Gentleman and Sande 1966) to evaluate the Fourier coefficients a_n of $g_0(\lambda)$. This enables the real part $R(\lambda)$ to be readily calculated since (Mahanty 1966)

$$R(\lambda) = \frac{1}{\pi} \sum_n a_n \left\{ \cos(n\pi\lambda) \left[Si(n\pi\lambda) + Si\left(n\pi(1-\lambda)\right) \right] \right.$$

$$\left. - \sin(n\pi\lambda) \left[Ci(n\pi\lambda) - Ci\left(n\pi(1-\lambda)\right) \right] \right\} \quad \text{C.9}$$

where Si and Ci are sine and cosine integrals (Abramowitz and Stegun 1965). From the nature of the calculation, the accuracy of $R(\lambda)$ is less than that of $g_0(\lambda)$, particularly near the singularities where high frequency terms of the Fourier series may be required, but which will have poor accuracy due to the statistical noise present in the evaluation of $g_0(\lambda)$.

It is felt, however, that the accuracy is adequate for describing the essential features of the change in density of states due to the impurity.*

The next stage is to evaluate the derivative of δ with respect to energy, eqn. C.6. The differentiation numerically is very difficult because of the large amount of noise, particularly on $g_0(\lambda)$. The method used was developed by Anderssen and Bloomfield (1974a, 1974b) whose papers give the details of the computation. Because of the high level of noise the data is smoothed considerably when differentiated, and there is some distortion of

---

* For the perovskite structure the Fourier coefficients gave fairly poor values of $R(\lambda)$ between the cusp point at $\sqrt{8/9}$ and the upper edge of the band, because of the small range of this interval, i.e. the small number of points in this interval compared to the total, and it was found better to use the Monte-Carlo method in this region, though the computation time for the desired accuracy of approx. 5% was over an order of magnitude greater than the series method.

the differentiated value of $\tan \delta$, particularly near the singularities. One way to improve this situation is to reduce the noise by calculating a more accurate value for $g_0(\lambda)$, but for the present purposes the expense of computation time was considered too great. It is felt, however, that the results obtained are qualitatively accurate in describing the effect of the impurity, a situation which is adequate for the exemplary nature of the calculations.

iii) Local mode frequencies

The frequencies at which local modes occur were discussed in section III.1. The energy of the local mode is given as a solution of

$$1 + \gamma R(\lambda) = 0 \qquad\qquad\qquad C.10$$

where $R(\lambda)$ is given by eqn. C.4 and γ is a parameter dependent on the impurity. The range of λ for which C.10 gives local modes is that for which $g_0(\lambda)$ is zero, i.e. outside the main absorption band.

There are several ways that solutions of eqn. C.10 may be found. Since λ lies outside the main band, there are no singularities in $R(\lambda)$ (except at the band edge), and the direct analytic integration of $R(\lambda)$ may be possible. For the *fcc* crystal model used in sections II.1 and III.1 to describe *EuO* , the integral has been done analytically by Joyce (1971) and is given in terms of complete elliptic integrals of the first kind. The integral for the perovskite structure is not known, however.

Values of $R(\lambda)$ outside the band may also be estimated by the procedure for finding $R(\lambda)$ described in part ii) of this appendix. It is found, however, that the inaccuracy of the determination of Fourier coefficients from $g_0(\lambda)$ limits the accuracy for which the value of $R(\lambda)$ may be calculated as λ moves away from the band. For example, for the ferromagnetic *fcc* crystal the curve for $R(\lambda)$ is limited to cases where λ is less than about 1.5 times the width of the band. Hence the method is good when the local

mode is close to the band (i.e. γ is small) but fails for a strong impurity effect, where the analytic expressions are more likely to be accurate.

The simplest method of calculating $R(\lambda)$ outside the band is to use the Monte-Carlo method described in part ii) of this appendix, with each histogram having the weight given by eqn. C.8. The accuracy of the calculation may be made as good as desired, with increasing computer time, and the accuracy will not vary greatly over the range of the calculation, unless it is far removed from the main absorption band when the differences in eqn. C.8 may become large. Because of the smoothness of the curve and the absence of singularities in the region of interest, the calculation of $R(\lambda)$ outside the band gives far better accuracy for the same number of random numbers than the same calculation inside the band. It is this method which has been used to discuss the local modes in chapter III.

Although some of the methods mentioned in this appendix give greater accuracy of calculating the magnon density of states and local modes, the methods chosen for use in this work were selected on the grounds of the ease with which they may be applied to any cubic crystal, and many other crystals as well. Because of this it is felt that the methods selected have much wider application than the uses made of them here.

APPENDIX 4

SOME LIMITS FOR THE INFINITE CRYSTAL

In this appendix we indicate explicitly the limiting behaviour of certain expressions in the case when the crystal is infinite, that is, the number of unit cells in the crystal is infinite. To simplify the analysis slightly we will consider a ferromagnet, with the Hamiltonian eqn. I.39,

$$H^{(AF)} = \sum_k \epsilon(k) a_k^+ a_k + \epsilon_2 \sum_k b_k^+ b_k + g \sum_k \left(a_k^+ b_k + b_k^+ a_k \right) + \frac{\gamma}{N} \sum_{kk'} a_k^+ a_{k'} , \qquad D.1$$

where the sums over k are now infinite sums, as for an infinite crystal the Brillouin zone is dense. That is we replace the sum over k by

$$\frac{1}{N} \sum_k \to \frac{\Omega}{(2\pi)^3} \int d^3k = \frac{1}{V^*} \int d^3k \qquad D.2$$

where Ω is the volume of a primitive cell and V^* the volume of the first Brillouin zone of the crystal.

With an impurity present the magnon part of the Hamiltonian D.1 is written in the form

$$(\hat{A}+\hat{P})_{kk'} = \left(\epsilon(k)-\lambda \right) \delta(k-k') + \gamma . \qquad D.3$$

The general expression for an eigenvector is

$$S_\lambda = \delta(\hat{A}+\hat{P}-\lambda\hat{I}) X \qquad D.4$$

for arbitrary X .

Making use of the fact that

$$\delta(\hat{A}+\hat{P}-\lambda\hat{I}) = \frac{\text{Im}}{\pi} [\hat{A}+\hat{P}-(\lambda-i\epsilon)\hat{I}]^{-1} \qquad D.5$$

we define a Green function matrix

$$\hat{G}(\lambda) = [\hat{A}+\hat{P}-\lambda\hat{I}]^{-1} . \qquad D.6$$

For the pure crystal, consider

$$\hat{G}_0(\lambda) = [\hat{A}-\lambda\hat{I}]^{-1}$$

with components

$$G_0(k-k'; \lambda) = \frac{\delta(k-k')}{\epsilon(k)-\lambda} .$$ D.8

Then we may write eqn. D.6 as

$$\hat{G}(\lambda) = \hat{G}_0(\lambda) - \hat{G}_0(\lambda)\hat{P}\hat{G}(\lambda)$$

$$= [\hat{I}+\hat{G}_0(\lambda)\hat{P}]^{-1}\hat{G}_0(\lambda) .$$ D.9

In the first line of eqn. D.9 the first term represents the pure crystal Green function and the second the change of the Green function due to the impurity.

We obtain an expression for $\hat{G}(\lambda)$ of eqn. D.9 in component form by the following procedure which we show here for the infinite crystal though the method is identical for a finite crystal if we make use of eqn. D.2.

Eqn. D.9 may be written

$$G(k, k'; \lambda) = \frac{\delta(k-k')}{\epsilon(k)-\lambda} - \frac{\gamma}{V^{*2}} \iint \frac{\delta(k-k'')}{\epsilon(k)-\lambda} G(k''', k'; \lambda)dk''dk'''$$

$$= \frac{\delta(k-k')}{\epsilon(k)-\lambda} - \frac{\gamma}{V^*} \frac{1}{\epsilon(k)-\lambda} \int G(k''', k'; \lambda)dk''' .$$ D.10

Multiply both sides by $1/V^*$ and integrate over k , giving

$$\frac{1}{V^*} \int dk G(k, k'; \lambda)\left[1 + \frac{\gamma}{V^*} \int \frac{dk''}{\epsilon(k'')-\lambda}\right] = \frac{1}{\epsilon(k')-\lambda}$$ D.11

so

$$\frac{1}{V^*} \int G(k, k'; \lambda)dk = \frac{1}{\epsilon(k')-\lambda} \mathcal{D}(\gamma, \lambda)$$ D.12

for

$$\mathcal{D}(\gamma, \lambda) = \gamma\left[1 + \frac{\gamma}{V^*} \int \frac{dk'}{\epsilon(k')-\lambda}\right]^{-1} .$$ D.13

It may be noted by comparison with eqn. III.11 that eqn. D.13 is related to the secular determinant of $\hat{A} + \hat{P}$.

Therefore the Green function for the infinite crystal may be written from eqn. D.10 using eqn. D.12 as

$$G(k, k'; \lambda) = \frac{\delta(k-k')}{\epsilon(k)-\lambda} - \frac{1}{\epsilon(k)-\lambda} \mathcal{D}(\gamma, \lambda) \frac{1}{\epsilon(k')-\lambda} .$$ D.14

The crystal density of states is obtained from the diagonal part of eqn. D.5, as

$$g(\lambda) = \frac{\text{Im}}{\pi} \frac{1}{N} \sum_{\mathbf{k}} G(\mathbf{k}, \mathbf{k}; \lambda) \qquad \text{(finite crystal)}$$

$$= \frac{\text{Im}}{\pi} \frac{1}{V^*} \int_{BZ} G(\mathbf{k}, \mathbf{k}; \lambda) d\mathbf{k} \quad \text{(infinite crystal)} \qquad \text{D.15}$$

for integration over the volume of the first Brillouin zone.

We make use of Dirac's relation

$$\lim_{\varepsilon \to 0^+} \frac{1}{x \pm i\varepsilon} = P\left(\frac{1}{x}\right) \mp i\pi\delta(x) \qquad \text{D.16}$$

where P represents the principal part of the integral, in obtaining the imaginary part of eqn. D.15. The first term of eqn. D.14 gives the pure crystal density of states as

$$g_0(\lambda) = \frac{1}{V^*} \int_{BZ} \delta\left(\varepsilon(\mathbf{k}) - \lambda\right) d^3k \ . \qquad \text{D.17}$$

The impurity part of the density of states is given by the second term of eqn. D.14 in eqn. D.15,

$$\Delta g(\lambda) = \frac{1}{V^*} \int_{BZ} d^3k \cdot \frac{\text{Im}}{\pi} \left[\frac{\mathcal{D}(\gamma, \lambda)}{\left(\varepsilon(\mathbf{k}) - \lambda\right)^2} \right] \ . \qquad \text{D.18}$$

Now we write

$$\frac{1}{V^*} \int_{BZ} \frac{d^3k}{\left(\varepsilon(\mathbf{k}) - \lambda\right)^2} = \frac{d}{d\lambda} \frac{1}{V^*} \int_{BZ} \frac{d^3k}{\varepsilon(\mathbf{k}) - \lambda}$$

$$= \frac{d}{d\lambda} \left[R(\lambda) + i\pi g_0(\lambda) \right] \qquad \text{D.19}$$

making use of eqns. D.16 and D.17 and defining the function

$$R(\lambda) = \frac{P}{V^*} \int \frac{d^3k}{\varepsilon(\mathbf{k}) - \lambda} \ . \qquad \text{D.20}$$

Hence from eqn. D.13 we write

$$\mathcal{D}(\gamma, \lambda) = \gamma \left(1 + \gamma R(\lambda) + i\pi\gamma g_0(\lambda) \right)^{-1} \ . \qquad \text{D.21}$$

So that eqn. D.18 becomes

$$\Delta g(\lambda) = \frac{\text{Im}}{\pi} \frac{\gamma\left(R'(\lambda) + i\pi g_0'(\lambda)\right)}{1 + \gamma R(\lambda) + i\pi\gamma g_0(\lambda)} \qquad \text{D.22}$$

where primes denote differentiation with respect to λ .

Now define a function $\delta(\lambda)$ (Callaway 1974) such that

$$\tan \delta(\lambda) = -\frac{\pi\gamma g_0(\lambda)}{1 + \gamma R(\lambda)} . \qquad \text{D.23}$$

Then from eqn. D.22,

$$\Delta g(\lambda) = \pi\gamma \frac{g_0'(\lambda)\left(1 + \gamma R(\lambda)\right) - R'(\lambda)\gamma g_0(\lambda)}{\left(1 + \gamma R(\lambda)\right)^2 + \left(\pi\gamma g_0(\lambda)\right)^2}$$

$$= -\frac{1}{\pi}\frac{d\delta}{d\lambda} \qquad \text{D.24}$$

since

$$\frac{d\tan\delta}{d\lambda} = -\frac{\pi\gamma\left[g_0'(\lambda)\left(1 + \gamma R(\lambda)\right) - \gamma g_0(\lambda)R'(\lambda)\right]}{\left(1 + \gamma R(\lambda)\right)^2} \qquad \text{D.25}$$

and

$$\frac{d\delta}{d\lambda} = \cos^2\delta \, \frac{d\tan\delta}{d\lambda} . \qquad \text{D.26}$$

Hence use of eqn. III.43 is still valid for an infinite crystal. For a concentration c of impurity, the change in density of states for each impurity may be added if c is sufficiently small, so the total effect is c times $\Delta g(\lambda)$ of eqn. D.24 as used in eqn. III.43.

The rest of the calculation leading to the magnon sideband lineshape is straightforward for the infinite crystal, with the sum over λ replaced by an integral over λ and the density of states given by eqns. D.17 and D.24 rather than their discrete values.

The analysis of the antiferromagnet will follow similar lines to those given here, with the same conclusions obtained concerning the changes in formulae for an infinite crystal.

APPENDIX 5

THE MODEL WITH k-DEPENDENT EXCITON ENERGY AND

EXCITON-MAGNON INTERACTION STRENGTH

We treat the ferromagnetic crystal for simplicity.

For the situation where

$$g = g(k) \ ,$$

$$\varepsilon_2 = \varepsilon_2(k)$$

the submatrices of eqn. III.6 no longer commute, and we must diagonalise the Hamiltonian matrix directly. This may be done using operations on the rows and columns of the determinant to give the secular equation for the eigen-values of the *complete* Hamiltonian matrix as

$$D(\lambda) = \prod_k \left(\varepsilon(k)-\lambda\right) \prod_{k'} \left[\varepsilon_2(k') - \lambda - \frac{g(k')^2}{\varepsilon(k')-\lambda}\right]$$

$$\cdot \left[1 + \gamma \sum_{k''} \frac{1}{\varepsilon(k'') - \lambda - \frac{g(k'')^2}{\varepsilon_2(k'')-\lambda}}\right] \cdot \quad \text{E.1}$$

The change in the density of states due to the impurity is now given by the imaginary part of the logarithmic determinant of

$$\mathcal{D} = 1 + \gamma \sum_k \frac{1}{\varepsilon(k) - \lambda - \frac{g(k)^2}{\varepsilon_2(k)-\lambda}} \qquad \text{E.2}$$

while the first two terms of eqn. E.1 give the pure crystal density of states. Note the modification of the density of states due to the $g(k)$-dependent term.

A typical eigenvector has the form

$$T_\lambda = \frac{1}{N_\lambda} \begin{bmatrix} \cfrac{1}{\varepsilon(k_1) - \lambda - \cfrac{g(k_1)^2}{\varepsilon_2(k_1)-\lambda}} \\[1em] \vdots \\[0.5em] \cfrac{1}{\varepsilon(k_N) - \lambda - \cfrac{g(k_N)^2}{\varepsilon_2(k_N)-\lambda}} \\[1.5em] \cfrac{-g(k_1)}{\left(\varepsilon_2(k_1)-\lambda\right)\left(\varepsilon(k_1)-\lambda\right)-g(k_1)^2} \\[0.5em] \vdots \\[0.5em] \cfrac{-g(k_N)}{\left(\varepsilon_2(k_N)-\lambda\right)\left(\varepsilon(k_N)-\lambda\right)-g(k_N)^2} \end{bmatrix} \quad , \qquad \text{E.3}$$

$$N_\lambda^2 = \sum_k \left[\left(\cfrac{1}{\varepsilon(k) - \lambda - \cfrac{g(k)^2}{\varepsilon_2(k)-\lambda}} \right)^2 + \left(\cfrac{g(k)}{\left(\varepsilon_2(k)-\lambda\right)\left(\varepsilon(k)-\lambda\right)-g(k)^2} \right)^2 \right] \quad . \qquad \text{E.4}$$

So the matrix, T , formed with eigenvectors T_λ of eqn. E.3 as columns

will diagonalise the Hamiltonian matrix. We may therefore define new

operators for which the Hamiltonian is diagonal, and then proceed to

calculate the magnon sideband lineshape, as described in section III.1. The

result in this case will not be exactly like the magnon density of states,

but will be a modified density of states, depending on the k-dependence of

g and ε_2 . The lineshape of the sideband may be calculated by the Monte-

Carlo method of appendix 3.

BIBLIOGRAPHY

Abramowitz, M. and Stegun, I.A., 1965, "Handbook of Mathematical Functions",

    Chapter 5 (New York: Dover).

Abrikosov, A.A., Gorkov, L.P. and Dzyaloshinski, I.E., 1963, "Methods of

    Quantum Field Theory in Statistical Physics" (Englewood Cliffs:

    Prentice-Hall).

Allen, S.J., Loudon, R. and Richards, P.L., 1966, Phys. Rev. Lett. 16,

    463-466.

Anderssen, R.S. and Bloomfield, P., 1974a, Technometrics 16, 69-75.

Anderssen, R.S. and Bloomfield, P., 1974b, Numer. Math. 22, 157-182.

Barak, J., Gabai, A. and Kaplan, N., 1974, Phys. Rev. B9, 4914-4919.

Berlin, T.H. and Kac, M., 1952, Phys. Rev. 86, 821-835 (appendix).

Bhandari, R. and Falicov, L.M., 1972, J. Phys. C 5, 1445-1460.

Bloch, F., 1930, Z. Phys. 61, 206-219.

Born, M. and Von Kármán, T., 1912, Physik. Z. 13, 297-309.

Buchheit, M. and Loly, P.D., 1972, Am. J. Phys. 40, 289-293.

Byrnes, J.S., Podgor, S. and Zachary, W.W., 1969, Proc. Camb. Phil. Soc. 66,

    377-380.

Callaway, J., 1963, Phys. Rev. 132, 2003-2009.

Callaway, J., 1964, J. Math. Phys. 5, 783-798.

Callaway, J., 1974, "Quantum Theory of the Solid State", part B (New York:

    Academic).

Chadi, D.J. and Cohen, M.L., 1973, Phys. Rev. B8, 5747-5753.

Cooke, J.F. and Wood, R.F., 1972, Phys. Rev. B5, 1276-1283.

Cowley, R.A. and Buyers, W.J.L., 1972, Rev. Mod. Phys. 44, 406-450.

Dexter, D.L., 1962, Phys. Rev. 126, 1962-1967.

Dietz, R.E., Meixner, A.E. and Guggenheim, H.J., 1970, J. Luminescence 1,

    279-298.

Dietz, R.E. and Misetich, A., 1968, in "Localised Excitations in Solids",
     ed. R.F. Wallis, pp. 366-378 (New York: Plenum).

Dietz, R.E., Misetich, A. and Guggenheim, H.J., 1966, Phys. Rev. Lett. 16,
     841-844.

Elliott, R.J., Krumhansl, J.A. and Leath, P.L., 1974, Rev. Mod. Phys. 46,
     465-543.

Elliott, R.J., Thorpe, M.F., Imbusch, G.F., Loudon, R. and Parkinson, J.B.,
     1968, Phys. Rev. Lett. 21, 147-150.

Eremenko, V.V. and Belyaeva, A.I., 1969, Sov. Phys. Usp. 12, 320-343.

Eremenko, V.V., Novikov, V.P. and Petrov, E.G., 1974, J. Low   Temp. Phys.
     16, 431-454.

Freeman, S. and Hopfield, J.J., 1968, Phys. Rev. Lett. 21, 910-913.

Fujiwara, T., Gebhardt, W., Petanides, K. and Tanabe, Y., 1972, J. Phys. Soc.
     Japan 33, 39-48.

Gaididei, Yu.B. and Loktev, V.M., 1974, Phys. Stat. Sol. (b) 62, K29-K32.

Gentleman, W.M. and Sande, G., 1966, AFIPS Conf. Proc. 29, 563-578.

Ghosh, D.K., 1973, Phys. Rev. B8, 392-405.

Gilat, G. and Raubenheimer, L.J., 1966, Phys. Rev. 144, 390-395.

Glass, S.J. and Lawson, J.O., 1973, Phys. Lett. 46A, 234-236.

Gondiara, K. and Tanabe, Y., 1966, J. Phys. Soc. Japan 21, 1527-1548.

Halley, J.W., 1966, Phys. Rev. 149, 423-433.

Halley, J.W., 1967, Phys. Rev. 154, 458-470.

Halley, J.W. and Silvera, I., 1965, Phys. Rev. Lett. 15, 654-656.

Heller, W.R. and Marcus, A., 1951, Phys. Rev. 84, 809-813.

Hone, D., Callen, H. and Walker, L.R., 1966, Phys. Rev. 144, 283-295.

Hulin, D., Benoit à la Guillaume, C. and Hanus, J., 1971, AIP Conf. Proc.
     no 5, part 2, 850-854.

Hulin, D., Hanus, J., Benoit à la Guillaume, C. and Reed, T.B., 1970, Sol.
     St. Commun. 8, 1525-1528.

Imbusch, G.F. and Guggenheim, H.J., 1968, Phys. Lett. 26A, 625-626.

Ishii, H., Kanamori, J. and Nakamura, T., 1965, Prog. Theor. Phys. 33, 795-811.

Jelitto, R.J., 1969, J. Phys. Chem. Solids. 30, 609-626.

Johnson, L.F., Dietz, R.E. and Guggenheim, H.J., 1966, Phys. Rev. Lett. 17, 13-15.

Joyce, G.S., 1971, J. Phys. C 4, L53-L56.

Keffer, F., 1966, "Spin Waves" in Handbuch der Physik XVIII/2.

Kittel, C., 1963, "Quantum Theory of Solids" (New York: Wiley).

Knox, R.S., 1963, "Theory of Excitons", Sol. State Phys. Supp. 5.

Kubo, R., 1957, J. Phys. Soc. Japan 12, 570-586.

Landau, L.D. and Lifshitz, E.M., 1958, "Quantum Mechanics" (London: Pergamon).

Loly, P.D. and Buchheit, M., 1972, Phys. Rev. B5, 1986-1993.

Loudon, R., 1968, Adv. Phys. 17, 243-280.

Lovesey, S.W., 1968a, J. Phys. C 1, 102-117.

Lovesey, S.W., 1968b, J. Phys. C 1, 118-124.

McClure, D.S., 1968, in "Excitons, Magnons and Phonons", ed. Zahlan, p. 135-152.

McGuire, T.R., Argyle, B.E., Shafer, M.W. and Smart, J.J., 1963, J. Appl. Phys. 34, 1345-1346.

Mahanty, J., 1966, Proc. Phys. Soc. 88, 1011-1014.

Mahanty, J., 1974, "The Green Function Method in Solid State Physics" (New Delhi: East-West Press).

Maradudin, A.A., Montroll, E.W. and Weiss, G.H., 1963, Solid State Physics Supplement 3 (New York: Academic).

Maradudin, A.A., Montroll, E.W., Weiss, G.H. and Ipatova, I.P., 1971, Solid State Physics Suppl. 3, 2nd ed. (New York: Academic).

Meltzer, R.S., 1972, AIP Conf. Proc. no 10, part 2, 1704-1708.

Meltzer, R.S., Lowe, M. and McClure, D.S., 1969, Phys. Rev. 180, 561-578.

Mermin, N.D. and Wagner, H., 1966, Phys. Rev. Lett. 17, 1133-1136.

Misetich, A., Dietz, R.E. and Guggenheim, H.J., 1968, in "Localised

    Excitations in Solids", ed. R.F. Wallis, pp. 379-385 (New York:

    Plenum).

Morita, T., 1975, J. Phys. A 8, 478-489.

Moriya, T., 1966, J. Phys. Soc. Japan 21, 926-932.

Moriya, T., 1968, J. Appl. Phys. 39, 1042-1049.

Moriya, T., 1970, in "Optical Properties of Solids", ed. E.D. Haidemenakis,

    Chapter XXI (New York: Gordon and Breach).

Moriya, T. and Inoue, M., 1968, J. Phys. Soc. Japan 24, 1251-1264.

Mueller, F.M., Garland, J.W., Cohen, M.H. and Bennemann, K.H., 1971, Ann.

    Phys. 67, 19-57.

Parkinson, J.B., 1969a, J. Appl. Phys. 40, 993-994.

Parkinson, J.P., 1969b, J. Phys. C 2, 2003-2011.

Parkinson, J.P.,and Loudon, R., 1968, J. Phys. C 1, 1568-1583.

Petrov, E.G., 1971, Phys. Stat. Sol. (b) 48, 367-379.

Petrov, E.G. and Gaididei, Yu.B., 1971, Phys. Stat. Sol. (b) 46, 103-116.

Ra, O., 1971, Zeit. fur Natur. 26, 111-123.

Reeh, H., 1973, Nuovo Cimento 17B, 7-12.

Richards, P.M. and Brya, W.J., 1974, Phys. Rev. B9, 3044-3052.

Richardson, D.D., 1974, Aust. J. Phys. 27, 457-470.

Richardson, D.D., 1975, J. Phys. A (in press).

Schiff, L.I., 1968, "Quantum Mechanics", 3rd ed., Chapter 23 (New York:

    McGraw-Hill).

Sell, D.D., 1968, J. Appl. Phys. 39, 1030-1035.

Sell, D.D., Greene, R.L. and White, R.M., 1967, Phys. Rev. 158, 489-510.

Shah, M.N., Umezawa, H. and Vitiello, G., 1974, Phys. Rev. B10, 4724-4736.

Sobel'man, I.I., 1972, "Introduction to the Theory of Atomic Spectra"

    (Oxford: Pergamon).

Sorgen, A., Cohen, E. and Makovsky, J., 1974, Phys. Rev. B10, 4643-4649.

Srivastava, V.C. and Stevenson, R., 1972, Sol. St. Commun. 11, 41-46.

Srivastava, V.C., Stevenson, R. and Linz, A., 1973, Sol. St. Commun. 13, 873-876.

Stevenson, R., 1966, Phys. Rev. 152, 531-535.

Stokowski, S.E., Sell, D.D. and Guggenheim, H.J., 1971, Phys. Rev. B4, 3141-3152.

Sugano, S. and Tanabe, Y., 1963, in "Magnetism", Vol. 1, ed. G.T. Rado and H. Suhl, pp. 243-267 (New York: Academic).

Swendsen, R.H., 1973, J. Phys. C 6, 3763-3773.

Swendsen, R.H., 1975, Phys. Rev. B11, 1935-1942.

Swendsen, R.H. and Callen, H., 1972, Phys. Rev. B6, 2860-2875.

Takeno, S., 1963a, Prog. Theor. Phys. 30, 565-566.

Takeno, S., 1963b, Prog. Theor. Phys. 30, 731-742.

Tanabe, Y. and Gondiara, K.-I., 1967, J. Phys. Soc. Japan 22, 573-581.

Tanabe, Y., Gondiara, K.-I. and Murata, H., 1968, J. Phys. Soc. Japan 25, 1562-1575.

Tanabe, Y., Moriya, T. and Sugano, S., 1965, Phys. Rev. Lett. 15, 1023-1025.

Tonegawa, T., 1968, Prog. Theor. Phys. 40, 1195-1226.

Tonegawa, T. and Kanamori, J., 1966, Phys. Lett. 21, 130-131.

White, R.M., 1970, "Quantum Theory of Magnetism", (New York: McGraw-Hill).

Wolfram, T. and Callaway, J., 1963, Phys. Rev. 130, 2207-2217.

Wortis, M., 1963, Phys. Rev. 132, 85-97.

Zubarev, D.N., 1960, Sov. Phys. Usp. 3, 320-345.